Endoplasmic reticulum-mitochondria associations and amyotrophic lateral sclerosis

Stoica, Radu

Awarding institution:
King's College London

ENDOPLASMIC RETICULUM-MITOCHONDRIA ASSOCIATIONS AND AMYOTROPHIC LATERAL SCLEROSIS

Radu Stoica MBBS

Thesis submitted in fulfilment of the degree of Doctor of Philosophy,

King's College London, Institute of Psychiatry (University of London)

February 2013

ABSTRACT

Damage to both mitochondria and the endoplasmic reticulum (ER) involving ER stress and the unfolded protein response (UPR) are characteristic features in amyotrophic lateral sclerosis (ALS). However, how these two pathological features might be linked in a common disease pathway is unclear. Approximately 5-20% of the mitochondrial surface is closely apposed to ER and tethers linking the two organelles can be visualised via electron microscopy. These regions mediate a number of physiological processes including Ca^{2+} and phospholipid exchange between ER and mitochondria, ER and mitochondrial stress responses and apoptosis. Moreover, defects in ER-mitochondria associations are now known to contribute to neurodegenerative diseases. To properly investigate the role of ER-mitochondria associations in physiological processes and disease situations, the identity of the molecular tethers that physically link ER with mitochondria needs to be established. Previous work from our research group identified the outer mitochondrial membrane protein, protein tyrosine phosphatase-interacting protein 51 (PTPIP51) as a binding partner for the resident ER protein vesicle-associated membrane protein-associated protein-B (VAPB). As such, VAPB and PTPIP51 represent plausible candidates for mediating ER-mitochondria associations. In order to test this possibility, ER and mitochondria associations were quantified following the experimental manipulation of VAPB and/or PTPIP51 expression. The results strongly support a role for VAPB and PTPIP51 in controlling ER-mitochondria associations.

TAR DNA-binding protein-43 (TDP-43) is strongly linked to ALS and mutations in *TARDBP*, the gene encoding TDP-43, are the cause of some familial forms of the disease. The effects of TDP-43 expression on ER-mitochondria associations and

binding of VAPB to PTPIP51 were investigated. The results showed that both wild-type and ALS mutant TDP-43 disrupt ER-mitochondria associations and that this is accompanied by decreased binding of VAPB to PTPIP51. Mutations in the genes encoding fused in sarcoma (FUS) and Cu/Zn superoxide dismutase-1 (SOD1) also cause some familial forms of ALS and preliminary investigations revealed that FUS but not SOD1 also decreases VAPB-PTPIP51 interactions.

Finally, the mechanisms that regulate binding of VAPB to PTPIP51 were investigated. Phosphorylation is known to influence protein-protein interactions and phosphorylation sites in VAPB and PTPIP51 were identified by mass spectrometry. However, mutation of these sites did not influence VAPB-PTPIP51 binding.

ACKNOWLEDGEMENTS

I wish to thank my supervisor Chris Miller for giving me the opportunity to work in his laboratory and for all the guidance and encouragement throughout, my second supervisor Kurt De Vos for his valuable feedback and constructive science conversations. I would also like to thank everyone in the department who helped me all these years one way or another.

My grateful thanks are extended to Gema Vizcay (Centre for Ultrastructural Imaging, King's College London) for embedding and sectioning the electron microscopy specimens, Winston Vetharoy (Rayne Institute, King's College London) for assisting with the cell sorting procedure and Steven Lynham (Institute of Psychiatry) for performing the mass spectrometry analyses.

Finally, a special thank you goes to my family and close friends for their patience and continuous support. This thesis is dedicated to my father who always encouraged me to pursue my career goals no matter how far; he is sorely missed.

This work was funded by the European Union's 7th Framework Programme (MitoTarget Project) and also supported by the Medical Research Council, the Wellcome Trust and Alzheimer's Research UK.

TABLE OF CONTENTS

ABSTRACT…….2

ACKNOWLEDGEMENTS……....4

TABLE OF CONTENTS……....5

LIST OF FIGURES AND TABLES……10

ABBREVIATIONS……...13

CHAPTER 1: INTRODUCTION..... 20

1.1 Motor neuron diseases and amyotrophic lateral sclerosis.....21

1.1.1 Epidemiology 21

1.1.2 Clinical aspects and current treatments.....22

1.1.3 Pathology of ALS.....24

1.2 ALS genetics –overview 28

1.2.1 SOD1 and ALS 30

1.2.2 TDP-43 and ALS 32

1.2.3 FUS and ALS 34

1.2.4 VAPB and ALS.....36

1.3 Neurodegeneration mechanisms in ALS.....42

1.3.1 Excitotoxicity.....42

1.3.2 Oxidative stress 44

1.3.3 Pathological protein aggregation.....46

1.3.4 Mitochondrial dysfunction.....48

1.3.5 Axonal transport dysfunction.....50

1.3.6 Damage to mRNA metabolism 52

1.3.7 ER stress and the unfolded protein response (UPR).....54

1.4 The ER-mitochondria axis and neurodegenerative diseases.....58

1.4.1 Neurodegenerative diseases and alterations to ER-mitochondria associations..60

1.4.2 ER-mitochondria tethering proteins.....61

1.5 Aims of the thesis.....64

CHAPTER 2: MATERIALS AND METHODS 65

2.1 Materials 67

2.1.1 Stock solutions 67

2.1.2 General molecular biology reagents.....69

2.1.2.1 Plasmids 69

2.1.2.2 Oligonucleotides 70

2.1.2.3 Growth of *E. coli* for DNA purification: media.....71

2.1.2.4 Plasmid DNA preparation from *E. Coli*.....72

2.1.2.5 Agarose gel electrophoresis of nucleic acids 72

2.1.2.6 Site-directed mutagenesis 73

2.1.3 Protein analysis 74

2.1.3.1 Protein sample preparation.....74

2.1.3.2 Sodium dodecyl sulphate-polyacrylamide gel electrophoresis (SDS-PAGE) 75

2.1.3.3 Immobilisation of proteins on nitrocellulose membranes.....76

2.1.3.4 Antibody probing of membrane-bound proteins.....76

2.1.3.5 Protein staining 77

2.1.4 Immunoprecipitation reagents.....77

2.1.5 Antibodies 78

2.1.5.1 Primary antibodies 78

2.1.5.2 Secondary antibodies 80

2.1.6 Fluorescence microscopy 80
2.1.7 Duolink® *in situ* Proximity Ligation Assay (PLA) 81
2.1.8 Electron microscopy 82
2.1.9 Mammalian cell culture 82
2.2 Methods 84
2.2.1 General microbiology methods 84
2.2.1.1 Storage and growth of *E. coli* for DNA purification 84
2.2.1.2 Preparation of plasmid DNA 84
2.2.1.3 Quantitation of nucleic acids 85
2.2.1.4 Restriction enzyme digestion of plasmid DNA 85
2.2.1.5 Agarose gel electrophoresis of plasmid DNA 86
2.2.1.6 PCR-based site-directed mutagenesis 86
2.2.1.7 Digesting the PCR product 89
2.2.1.8 Transformation into XL10-Gold® ultracompetent cells 89
2.2.2 Protein analysis 90
2.2.2.1 Protein concentration determination (Bradford Assay) 90
2.2.2.2 SDS-PAGE of protein samples 90
2.2.2.3 Immunoblotting (Western Blotting) 91
2.2.2.4 Antibody probing of membrane-bound proteins 91
2.2.2.5 Immunoprecipitation 93
2.2.2.6 Mass spectrometry studies 94
2.2.3 Microscopy 96
2.2.3.1 Immunofluorescence 96
2.2.3.2 *In situ* Proximity Ligation Assay™ (PLA™) 98
2.2.3.3 Transmission electron microscopy 99

2.2.4 Mammalian cell culture and transfection methods 100
2.2.4.1 NSC34, CV-1, CHO and HEK293 cell culture 100
2.2.4.2 Transient transfection 100
2.2.4.3 Delivery of siRNA to cell cultures 102
2.2.5 Treatment of HEK293 cells with the tyrosine phosphatase inhibitor pervanadate 104
2.2.6 Fluorescence-activated cell sorting (FACS) of NSC34 cells 104
CHAPTER 3: VAPB AND PTPIP51 MEDIATE ER-MITOCHONDRIA ASSOCIATIONS 106
3.1 Introduction 107
3.2 Results 110
3.2.1 VAPB and PTPIP51 mediate ER-mitochondria associations in electron microscopy studies using NSC34 cells 110
3.2.2 VAPB and PTPIP51 mediate ER-mitochondria co-localization in confocal light microscopy studies using CV1 cells 112
3.3 Discussion 124
CHAPTER 4: BOTH WILD-TYPE AND ALS MUTANT TDP-43 REDUCE ER-MITOCHONDRIA ASSOCIATIONS 128
4.1 Introduction 129
4.2 Results 132
4.2.1 Expression of wild-type and ALS mutant TDP-43 disrupt ER-mitochondria associations in electron microscopy studies using NSC34 cells 132
4.2.2 TDP-43 disrupts ER-mitochondria co-localization in confocal microscopy studies using CV1 cells 133
4.2.3 TDP-43 does not affect expression of VAPB, PTPIP51 or mitofusin-2 133

4.2.4 TDP-43 induced disruption of ER-mitochondria associations is accompanied by changes in VAPB-PTPIP51 interaction 134

4.2.5 ALS associated FUS but not SOD1 disrupts VAPB binding to PTPIP51 in immunoprecipitation assays 136

4.3 Discussion 147

CHAPTER 5: VAPB AND PTPIP51 PHOSPHORYLATION AS A REGULATORY MECHANISM FOR CONTROLLING THEIR INTERACTION 151

5.1 Introduction 152

5.2 Results 154

5.2.1 Purification of PTPIP51 by immunoprecipitation and separation on SDS-PAGE 154

5.2.2 Identification of phosphorylation sites in PTPIP51 by mass spectrometry 155

5.2.3 PTPIP51 is phosphorylated on tyrosine residue(s) 155

5.2.4 Purification of VAPB by immunoprecipitation and separation on SDS-PAGE 157

5.2.5 Identification of phosphorylation sites in VAPB by mass spectrometry 157

5.2.6 Mutation of the PTPIP51 and VAPB phosphorylation sites does not affect the PTPIP51-VAPB interaction 158

5.3 Discussion 176

CHAPTER 6: SUMMARY AND FUTURE DIRECTIONS 179

6.1 Summary 180

6.2 Future directions 182

REFERENCES 185

LIST OF FIGURES AND TABLES

Figures

Figure 1.1 The Awaji-shima diagnosis criteria (de Carvalho et al., 2008) 24

Figure 1.2 Pathological protein aggregates in sporadic and familial ALS 28

Figure 1.3 Schematic representation of VAPB structure showing protein domains and the localization of ALS-associated pathogenic mutations within the MSP domain 37

Figure 1.4 The vertebrate UPR 57

Figure 3.1 siRNA knockdown of VAPB or PTPIP51 114

Figure 3.2 siRNA knockdown of VAPB or PTPIP51 reduces ER-mitochondria associations 115

Figure 3.3 FACS post-sorting analyses demonstrating high purity of ECFP/AcGFP positive samples 116

Figure 3.4 Confirmation of cell sorting purification of ECFP-VAPB and PTPIP51-HA expressing cells. 118

Figure 3.5 Overexpression of VAPB and/or PTPIP51 increases ER-mitochondria associations 119

Figure 3.6 siRNA knockdown of VAPB or PTPIP51 reduces co-localization of ER and mitochondria 121

Figure 3.7 Overexpression of VAPB, PTPIP51 and VAPB with PTPIP51 all increase co-localization of ER and mitochondria 122

Figure 4.1 FACS post-sorting analyses demonstrating purification of EGFP positive samples 137

Figure 4.2 Expression of wild type and ALS mutant TDP-43 reduce ER-mitochondria associations 138

Figure 4.3 Expression of wild type or ALS mutant TDP-43 reduce ER-mitochondria co-localization 139
Figure 4.4 Overexpression of wild-type or ALS associated mutant TDP-43 do not alter expression of VAPB, PTPIP51 or mitofusin-2 (MFN2) 140
Figure 4.5 Specificity of the Duolink proximity ligation assay for VAPB and PTPIP51 141
Figure 4.6 Expression of wild-type or ALS associated mutants of TDP-43 all reduce the interaction of VAPB with PTPIP51 in proximity ligation assays 142
Figure 4.7 Expression of wild-type or ALS associated mutants of TDP-43 (TDP-43 Q331K, TDP-43 M337V, TDP-43 G348C and TDP-43 A382T) reduce the binding of VAPB to PTPIP51 in immunoprecipitation assays 144
Figure 4.8 Expression of wild-type or ALS associated mutants of FUS (FUS R521C, FUS R521G, FUS R521H and FUS R518K) reduce the binding of VAPB to PTPIP51 in immunoprecipitation assays 145
Figure 4.9 Expression of wild-type or ALS associated mutants of SOD1 (SOD1 G93A, SOD1 A4V) do not influence the binding of VAPB to PTPIP51 in immunoprecipitation assays 146
Figure 5.1 Purification of PTPIP51-HA by immunoprecipitation 161
Figure 5.2 Phosphorylation sites identified in PTPIP51 162
Figure 5.3 Identification of PTPIP51 S44 as a phosphorylation site by LC/MS/MS ... 163
Figure 5.4 Identification of PTPIP51 S46 as a phosphorylation site by LC/MS/MS ... 164
Figure 5.5 Identification of PTPIP51 S50 as a phosphorylation site by LC/MS/MS ... 165
Figure 5.6 Identification of PTPIP51 S212 as a phosphorylation site by LC/MS/MS . 166
Figure 5.7 Schematic representation of PTPIP51 structure showing positions of phosphorylation sites identified by mass spectrometry 167

Figure 5.8 PTPIP51 is phosphorylated on tyrosine residue(s) 168
Figure 5.9 Purification of myc-VAPB by immunoprecipitation 169
Figure 5.10 Phosphorylation sites identified in VAPB 170
Figure 5.11 Identification of VAPB T150 as a phosphorylation site by LC/MS/MS ... 171
Figure 5.12 Identification of VAPB S158 as a phosphorylation site by LC/MS/MS ... 172
Figure 5.13 Schematic representation of VAPB structure showing positions of phosphorylation sites identified by mass spectrometry 173
Figure 5.14 Mutation of PTPIP51 residues to alanine to preclude phosphorylation and aspartate to mimic permanent phosphorylation do not affect PTPIP51 binding to VAPB 174
Figure 5.15 Mutation of VAPB residues to alanine to preclude phosphorylation and aspartate to mimic permanent phosphorylation does not affect VAPB binding to PTPIP51 175

Tables

Table 1.1 Classification of motor neuron diseases 22
Table 2.1 Vectors 69
Table 2.2 Mammalian expression plasmids 69
Table 2.3 Mutagenic primers 70
Table 2.4 Primary antibodies 79
Table 2.5 Secondary antibodies 80
Table 2.6 PCR-based site-directed mutagenesis cycling parameters 88
Table 2.7 Amounts of reagents for ExGen 500 based transient transfection 101
Table 2.8 Delivery of human VAPB and PTPIP51 siRNA to CV1 cells 103
Table 2.9 Delivery of mouse VAPB and PTPIP51 siRNA to NSC34 cells 104

ABBREVIATIONS

Amino acids: single letter code and abbreviations

Single letter code	Abbreviation	Amino Acid
A	Ala	Alanine
C	Cys	Cysteine
D	Asp	Aspartic acid
E	Glu	Glutamic acid
F	Phe	Phenylalanine
G	Gly	Glycine
H	His	Histidine
I	Ile	Isoleucine
K	Lys	Lysine
L	Leu	Leucine
M	Met	Methionine
N	Asn	Asparagine
P	Pro	Proline
Q	Gln	Glutamine
R	Arg	Arginine
S	Ser	Serine
T	Thr	Threonine
V	Val	Valine
W	Trp	Tryptophan
Y	Tyr	Tyrosine

Other abbreviations

Aβ	amyloid β
ADP	adenosine diphosphate
Amp	ampicillin
ALS	amyotrophic lateral sclerosis
AMPA	alpha-amino-3-hydroxy-5-methylisoxazole-4-propionic acid
ANOVA	analysis of variance
APP	amyloid precursor protein
APS	ammonium persulphate
ASK1	apoptosis signal-regulating kinase 1
ATF	activating transcription factor
ATP	adenosine triphosphate
Bcl-2	B-cell lymphoma-2
BiP/GRP78	binding immunoglobulin protein/glucose-regulated protein 78
bp	nucleotide base pair
BSA	bovine serum albumin
C. elegans	*Caenorhabditis elegans*
C-terminus	carboxyl-terminus
C9ORF72	chromosome 9 open reading frame 72 gene
Ca^{2+}	calcium
Caspase-12	cysteinyl aspartate-specific protease-12
CHO	Chinese hamster ovary cell line
CHOP	CCAAT/enhancer binding protein homologous protein
CLR-1	caterpillar-like receptor-1
COPI/COPII	coat protein I/II

CSF	cerebrospinal fluid
CTRL	control
Cu	copper
ddH_2O	double distilled water
DH5α	Douglas Hanahan bacterial strain 5α
DMSO	dimethyl sulfoxide
DNA	deoxyribonucleic acid
dNTP	deoxyribonucleotide triphosphate
DTT	dithiothreitol
EAAT2	excitatory amino acid transporter 2
ECFP	enhanced cyan fluorescent protein
ECL	enhanced chemiluminescence
E. coli	*Escherichia coli*
EDTA	ethylenediaminetetraacetic acid
EGFP	enhanced green fluorescent protein
EGTA	ethyleneglycol-bis (β-aminoethylether) N,N,N′,N′-tetraacetic acid
EM	electron microscopy
EphR	ephrin receptors
ER	endoplasmic reticulum
ERAD	ER-associated protein degradation
ERGIC	ER Golgi intermediate compartment
ERMES	ER-mitochondria encounter structure
FBS	fetal bovine serum
FFAT	two phenylalanines (FF) in acidic tract
FTD	frontotemporal dementia

FTLD	frontotemporal lobar degeneration
FUS	fused in sarcoma
GluR2	glutamate receptor 2
GRIP1	glutamate receptor interacting protein 1
HA	hemagglutinin
HDAC6	histone deacetylase 6
HEK293	human embryonic kidney 293
HIV-1	human immunodeficiency virus type 1
HRP	horseradish peroxidase
HSP	hereditary spastic paraplegia
IB	immunoblot
ICA	intensity correlation analysis
ICQ	intensity correlation quotient
IF	immunofluorescence
IgG	immunoglobulin gamma
IP3R	inositol-1,4,5-triphosphate receptor
IRE1	inositol requiring enzyme 1
IRES	internal ribosome entry site
kb	kilobase
kDa	kiloDalton
Lar	leukocyte common antigen-related-like
LB	Luria Bertani
LMN	lower motor neuron
MAM	mitochondria-associated ER membranes
Mfn2	mitofusin-2

mRNA	messenger RNA
MSP	major sperm protein
N-terminus	amino-terminus
NADPH	nicotinamide adenine dinucleotide phosphate
Nir	N-terminal domain-interacting receptor
NMDA	N-methyl-D-aspartate
NRF2	nuclear factor (erythroid derived 2)-related factor 2
OD	optical density
PACS-2	phosphofurin acidic cluster sorting protein 2
PBS	phosphate buffered saline
PCR	polymerase chain reaction
PDI	protein disulphide isomerase
PERK	protein kinase RNA-like endoplasmic reticulum kinase
PFA	paraformaldehyde
pH	inverse log of hydrogen ion concentration
PLA	proximity ligation assay
PLS	primary lateral sclreosis
PML	promielocytic leukemia protein
pmol	picomole
PMSF	phenylmethyl sulphonyl fluoride
PtdSer	phosphatidylserine
PtdEtn	phosphatidylethanolamine
PTP1B	protein tyrosine phosphatase-1B
PTPIP51	protein tyrosine phosphatase-interacting protein 51
RIDD	regulated IRE1-dependent decay

RMD	required for meiotic nuclear division
RNA	ribonucleic acid
RNase	ribonuclease
Robo	roundabout receptor
ROS	reactive oxygen species
rpm	revolutions per minute
RyR	ryanodine receptor
SAX-3	sensory axon guidance-3 receptor
SDS	sodium dodecyl sulphate
SDS-PAGE	sodium dodecyl sulphate-polyacrylamide gel electrophoresis
SEM	standard error of mean
SERCA	sarco/endoplasmic reticulum Ca^{2+} ATP-ase
siRNA	small interfering RNA
SMA	spinal muscular atrophy
SNARE	soluble N-ethylmaleimide-sensitive factor-attached protein receptor
SOD1	Cu/Zn superoxide dismutase 1
TAE	tris-acetate-EDTA
TARDBP	TAR DNA binding protein gene
TBS	tris-buffered saline
TDP-43	transactive response (TAR) DNA binding protein 43
TE	Tris-EDTA
TEM	transmission EM
TEMED	N,N,N',N'-Tetramethylethylenediamine
TLS	translated in liposarcoma

TOM20	translocase of the outer mitochondrial membrane protein-20
Tris	tris(hydroxymethyl)aminomethane
Tween-20	polyoxyethylene-sorbitan monolaurate
UBQLN2	ubiquilin 2
UMN	upper motor neuron
UPR	unfolded protein response
UV	ultraviolet
VAMP	vesicle associated membrane protein
VAPB	vesicle-associated membrane protein-associated protein B
VCP	valosin-containing protein
VDAC1	voltage-dependent anion channel 1
XBP1	X-box-binding protein 1
xg	centrifugal force

CHAPTER 1: INTRODUCTION

1.1 Motor neuron diseases and amyotrophic lateral sclerosis

Motor neuron diseases are a group of neurological disorders characterized by progressive muscle weakness and/or spasticity that are caused by selective degeneration of lower motor neurons (LMN) and/or upper motor neurons (UMN). These include amyotrophic lateral sclerosis (ALS), spinal muscular atrophy (SMA), spinal bulbar muscular atrophy (SBMA), hereditary spastic paraplegia (HSP), primary lateral sclerosis (PLS) and lethal congenital contracture syndrome (LCCS) (Dion et al., 2009) (Table 1.1).

The most prevalent motor neuron disease is ALS, a devastating adult-onset neurodegenerative disease initially described by the 19th century neurologist Jean-Martin Charcot. The name stems from his observation of a characteristic "myelin pallor" in the lateral portions of the spinal cord, corresponding to the loss of descending UMN axons ("lateral sclerosis"). "Amyotrophy" refers to muscle fibre atrophy after losing the neuronal input from the anterior horn of the spinal cord. The disease affects both LMN and UMN and is usually fatal within 3 years from symptom onset when denervation of respiratory muscles occurs (Hardiman et al., 2011).

1.1.1 Epidemiology

ALS incidence averages 2.13 cases per 100,000 population and most reports suggest a uniform distribution across Western countries (Logroscino et al., 2011; Wolfson et al., 2009). The overall lifetime risk of developing the disease is 1:400 and the mean age of onset is around 60 years with a slight male predominance (male:female ratio is approximately 1.5:1) (Alonso et al., 2009; Manjaly et al., 2010).

Disease	Motor neuron involvement	Clinical features
ALS	UMN+LMN	Progressive muscle atrophy and spasticity
HSP	UMN	Progressive spasticity in the lower extremity
PLS	UMN	Spinal and bulbar spasticity
SMA	LMN	Symmetrical muscle weakness and atrophy
SBMA	LMN	Slowly progressive limb and bulbar muscle weakness and muscle atrophy
LCCS	UMN+LMN	Fetal hydrops and akinesia, degeneration of anterior horn motor neurons and skeletal muscle atrophy

Table 1.1 Classification of motor neuron diseases

1.1.2 Clinical aspects and current treatments

Since there is no established biological marker for ALS, the diagnosis is based almost entirely on characteristic clinical findings. In 1994, the World Federation of Neurology developed the "El Escorial" diagnostic criteria (Brooks, 1994) which were revised in 2000 (Brooks et al., 2000) and 2006 to include electrophysiological criteria that facilitate a more secure diagnosis (de Carvalho et al., 2008) (Figure 1.1). Symptom onset is usually asymmetrical and the initial clinical presentation depends on the sites affected first in the neuraxis. The neurological examination usually reveals a combination of UMN and LMN dysfunction, for example spasticity combined with flaccid paralysis and fasciculation. The dysfunctions will spread to contiguous anatomic regions producing increasingly diffuse and symmetrical phenotypes. The progression rate is linear within each individual but it can vary from 1 year to over 10 years between

different patients (Ravits and La Spada, 2009). In addition to motor symptoms, half of the ALS patients develop various levels of cognitive, behavioural or executive function impairment (Lomen-Hoerth et al., 2003). Moreover, it is now recognized that 15% of ALS patients meet criteria for frontotemporal dementia (FTD), a condition characterized by personality change, poor insight and irritability (Ringholz et al., 2005). This is consistent with a long known neuropathological overlap between ALS and FTD (Wightman et al., 1992), a link strengthened by recent key findings (see for reviews (Morris et al., 2012; Rademakers et al., 2012)). These neuropathological findings, discussed in greater detail below (see Section 1.1.3), prompt the need for new diagnostic approaches and disease classification.

Despite significant advances on the understanding of ALS disease mechanisms, the therapeutic options for ALS remain limited. The only approved disease modifying medication is riluzole, a compound with a modest effect on disease progression and survival (Bensimon et al., 1994; Miller et al., 2012). Measures aimed at symptom control and quality of life preservation include pain management, treatment of spasticity, enteral tube feeding and respiratory support for advanced stages (Hardiman et al., 2011). Several therapeutic compounds such as antioxidants, ciliary neurotrophic growth factor, insulin-like growth factor I or more recently lithium carbonate were tested in clinical trials but they have failed so far to show any significant benefits (Aggarwal et al., 2010; Orrell, 2009).

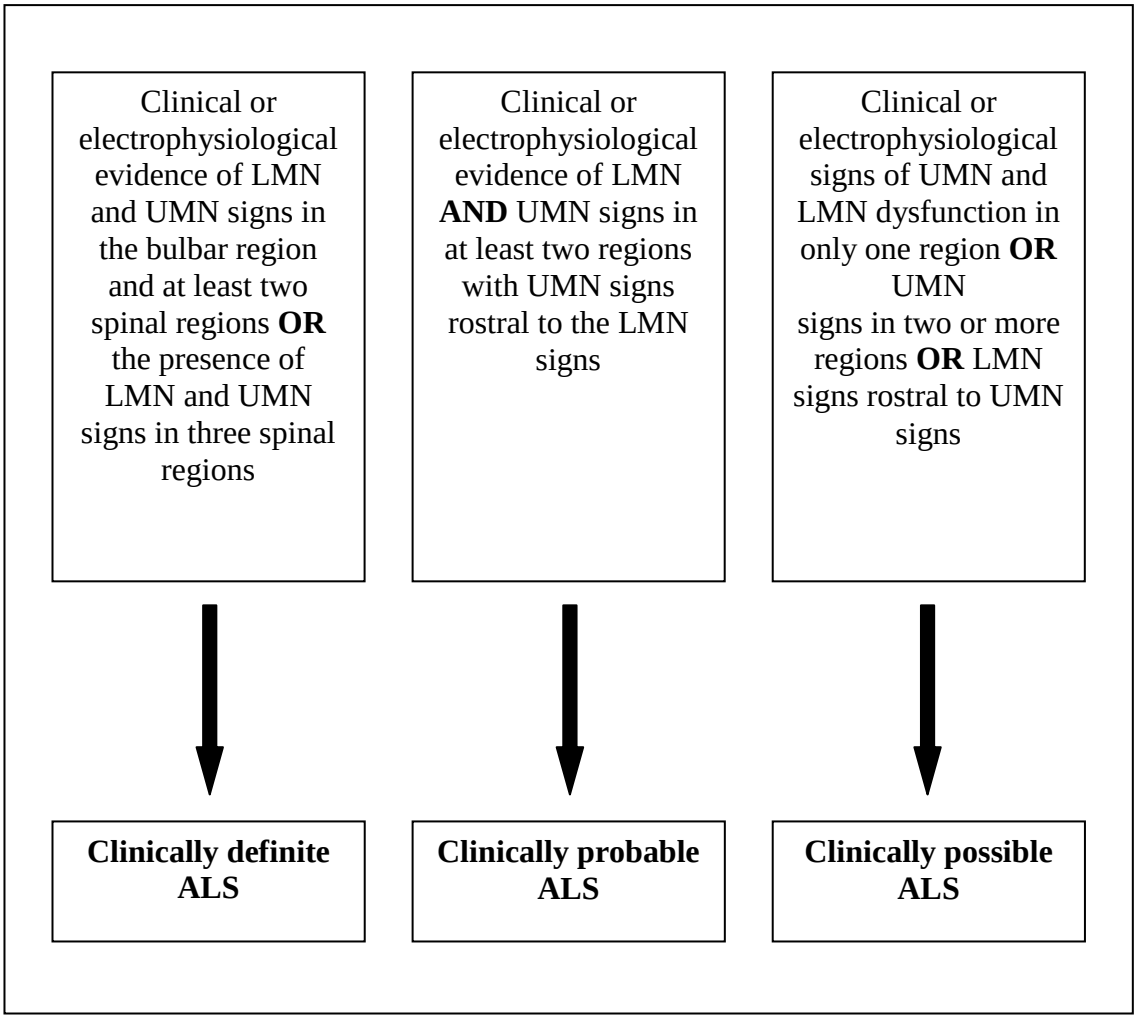

Figure 1.1 The Awaji-shima diagnosis criteria (de Carvalho et al., 2008)

1.1.3 Pathology of ALS

The classic pathological hallmarks of ALS are the degeneration and loss of motor neurons together with astrocytosis and intracellular aggregates in degenerating motor neurons and glia. UMN pathology is characterized by the loss of Betz cells and astrocytosis in the motor cortex accompanied by axonal loss and myelin pallor within the descending pyramidal motor pathway (Hammer et al., 1979; Kamo et al., 1987; Oyanagi et al., 1995). LMN pathology affects the ventral horn of the spinal cord and the motor neurons in the brainstem. Autopsy findings include a reduced number of LMN and reactive astrocytosis (Ekblom et al., 1993; Tsukagoshi et al., 1979). The surviving

neurons are atrophic and contain 3 types of intraneuronal inclusions: Bunina bodies, neurofilament accumulations and ubiquitinated inclusions.

Bunina bodies are cytoplasmic eosinophilic inclusions initially described by the Russian neuropathologist Bunina who suspected them to be the sign of a viral infection (Bunina, 1962). Found mostly in the remaining LMN, Bunina bodies are present in approximately 85% of ALS cases and are generally considered a specific pathologic finding (Piao et al., 2003). They are thought to be of lysosomal origin and are seen more frequently in patients with shorter disease durations and patients with dementia and ALS (Okamoto et al., 2008). Cystatin C, transferrin and more recently peripherin have been identified as major components of these inclusions but despite numerous investigations, their origin and significance are still unclear (Mizuno et al., 2006; Mizuno et al., 2011; Okamoto et al., 1993).

Another long known feature of ALS is the accumulation of phosphorylated neurofilaments and peripherin in affected motor neuron perikarya and their proximal axons (Carpenter, 1968; Corbo and Hays, 1992; Hirano et al., 1984; Munoz et al., 1988). However, these inclusions are not specific to ALS, since aberrant accumulation of neurofilaments occurs in other neurodegenerative diseases including Parkinson's disease, dementia with Lewy bodies, Alzheimer's disease and progressive supranuclear palsy (Al-Chalabi and Miller, 2003). The association with other conditions suggests they might play a role in disease pathogenesis, a hypothesis supported by the finding that point mutations in the light neurofilament subunit gene cause forms of the sensory and motor neuropathy Charcot-Marie-Tooth disease (Mersiyanova et al., 2000). Interestingly, modulation of neurofilament expression in ALS transgenic mice can alter

the disease course and mutations of the neurofilament heavy chain gene have been proposed as risk factors for ALS (Al-Chalabi et al., 1999; Figlewicz et al., 1994; Tomkins et al., 1998). Furthermore, neurofilament accumulations have also been linked with slowed neurofilament transport through axons, which is caused by glutamate-induced phosphorylation and rescued by riluzole (Ackerley et al., 2000; Stevenson et al., 2009).

The third pathological hallmark of ALS is the presence of ubiquitin-positive inclusions in affected motor neurons (see Figure 1.2). These probably indicate the cell's effort to label damaged proteins for proteasomal degradation (Leigh et al., 1988; Lowe et al., 1989). Interestingly, ubiquitinated inclusions are also a common finding in tau-negative frontotemporal lobar degeneration (FTLD), a condition clinically overlapping with ALS, suggesting a common underlying pathophysiology (Shi et al., 2005). This link remained unknown until recently, when transactive response DNA binding protein 43 (TDP-43) was identified as a major component of these inclusions in most ALS and FTLD cases (Arai et al., 2006; Neumann et al., 2006). This seminal discovery prompted the reconsideration of these disorders as a clinicopathological spectrum and led to the development of a new classification system for FTLD and ALS (Mackenzie et al., 2010). Interestingly, TDP-43 pathology has also been detected in Alzheimer's disease cases (Amador-Ortiz et al., 2007) and in disorders such as Huntington disease, corticobasal degeneration and dementia with Lewy bodies, suggesting it might play a more general role in the neurodegenerative process (Chen-Plotkin et al., 2010).

However, a notable exception from TDP-43 pathology is familial ALS caused by mutations in the Cu/Zn superoxide dismutase 1 (SOD1) gene, characterized by ubiquitin

inclusions that are largely negative for TDP-43 but positive for SOD1, possibly indicating a different pathogenic mechanism (Mackenzie et al., 2007). TDP-43 inclusions are also absent in a subset of familial ALS cases associated with mutations in the fused in sarcoma (FUS) gene, where intracytoplasmic FUS aggregates are observed (Kwiatkowski et al., 2009; Vance et al., 2009). FUS inclusions have subsequently been detected in many non-SOD1 ALS cases, indicating an involvement in the pathogenic cascade (Deng et al., 2010).

Optineurin, another protein recently linked to ALS was reported to form inclusions in TDP-43, FUS and SOD1 cases and in several other neurodegenerative disorders (Ito et al., 2011b; Maruyama et al., 2010; Osawa et al., 2011). However, a different group identified it in only a minority of TDP-43 positive cases (Hortobagyi et al., 2012) making its significance difficult to assess.

Finally, recent studies have shown that a large proportion of familial ALS and related FTLD are caused by a GGGGCC repeat expansion within the C9ORF72 gene (DeJesus-Hernandez et al., 2011; Renton et al., 2011). Although ubiquitin and p62 positive TDP-43 inclusions have been identified in these cases, some of the ubiquitin/p62 inclusions do not label for TDP-43, thus suggesting the presence of another pathological protein (Al-Sarraj et al., 2011; Cooper-Knock et al., 2012; Stewart et al., 2012).

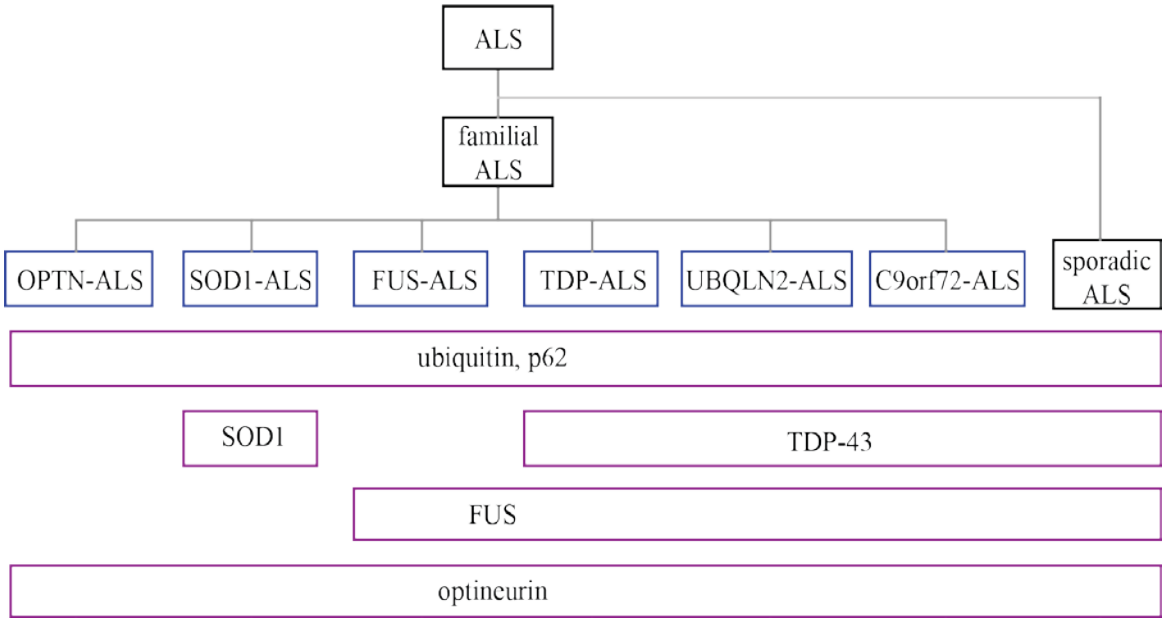

Figure 1.2 Pathological protein aggregates in sporadic and familial ALS

1.2 ALS genetics –overview

Although the cause of ALS is unknown, it is likely the result of a complex interplay between genetic and environmental factors. Most cases occur in an apparently random manner and are termed sporadic ALS, while around 5-10% of patients have a family history and show a Mendelian pattern of inheritance (Byrne et al., 2011). Familial ALS is genetically heterogeneous and a complete list of the causative mutations identified to date is available in the ALS Online Database (http://alsod.iop.kcl.ac.uk/). Interestingly, most mutations are also found in a subset of the apparently sporadic cases, indicating an underestimation of the genetic involvement in ALS (Andersen and Al-Chalabi, 2011). Since sporadic and familial ALS are clinically indistinguishable, motor neuron demise likely occurs through common molecular pathways and insights into the known gene mutations are believed to advance the understanding of sporadic disease.

The number of known ALS-associated mutations has increased dramatically since the first reports of families carrying pathogenic variants of SOD1 almost two decades ago (Rosen et al., 1993). Interestingly, mutations in C9ORF72, TDP-43, FUS, UBQLN2 and valosin-containing protein (VCP) were found to be responsible for both ALS and FTLD cases and this is consistent with the previously documented overlap between the two disorders (Deng et al., 2011; Johnson et al., 2010; Kwiatkowski et al., 2009; Seelaar et al., 2007; Sreedharan et al., 2008; Vance et al., 2009). These compelling clinical, pathological and genetic findings have produced a paradigm shift in the understanding of ALS and FTLD, which are now considered part of a disease continuum. Another piece of the puzzle was the linkage to chromosome 9p observed in a subset families with ALS, FTLD or both (Morita et al., 2006; Valdmanis et al., 2007; Vance et al., 2006). However, the underlying genetic defect remained unknown until two groups identified it as a GGGGCC repeat expansion in a non-coding region of the uncharacterized gene C9ORF72 (DeJesus-Hernandez et al., 2011; Renton et al., 2011). The repeat expansion is accountable for 39% of familial ALS cases and 4-7% of sporadic cases, making it the most prevalent genetic cause of ALS to date (Majounie et al., 2012).

The work in this thesis involves four proteins where mutants have been shown to cause ALS. These are SOD1, TDP-43, FUS and vesicle-associated membrane protein-associated protein B (VAPB). These proteins and their links to ALS are thus described in more detail below.

1.2.1 SOD1 and ALS

The first genetic defects associated with ALS were identified in the Cu/Zn superoxide dismutase (SOD1) gene in 1993 (Rosen et al., 1993). These account for approximately 20% of familial ALS and a small percentage of the sporadic cases (Millecamps et al., 2010) and until recently, SOD1 was believed to be the most common genetic cause for ALS . The identification of mutations in SOD1 facilitated the creation of the first transgenic ALS mouse models, which recapitulate the rapidly progressive motor neuron degeneration seen in human patients (Gurney et al., 1994).

SOD1 is a ubiquitously expressed antioxidant enzyme, which converts superoxide radicals to hydrogen peroxide and molecular oxygen. The protein is encoded by a single gene on chromosome 21 and to date, 166 different mutations have been reported involving most of its 153 amino acids (Andersen and Al-Chalabi, 2011). It was first hypothesised that loss of its dismutase activity might lead to motor neuron degeneration, but a number ALS mutants have been shown to maintain a normal enzymatic activity (Borchelt et al., 1994). Moreover, analyses of transgenic mice that express mutant SOD1 have provided strong evidence that the toxicity is not via a loss of SOD1 activity (Bruijn and Cleveland, 1996). If loss of SOD1 activity was responsible for the observed ALS phenotype, then manipulating this activity would be predicted to alter disease onset and/or progression. However, crossing of mutant SOD1 mice with mice overexpressing wild-type SOD1 or in which the wild-type SOD1 gene has been ablated does not alter disease onset or progression (Bruijn et al., 1998). These results suggest that the toxicity of mutant SOD1 involves a novel toxic gain of function. The nature of this toxicity is still not clear but there is evidence for several mechanisms. These include oxidative damage, accumulation of intracellular aggregates, mitochondrial dysfunction,

growth factor deficiency, astroglial cell pathology, glutamate excitotoxicity, ER stress and damage to axonal transport (see for review (Rothstein, 2009)).

Although SOD1 is ubiquitously expressed, its pathogenic effect was thought to occur strictly within motor neurons. This view was challenged by analyses of transgenic mice with mutant SOD1 expression restricted to neurons or astrocytes, which failed to develop disease (Gong et al., 2000; Pramatarova et al., 2001). Furthermore, pathogenic SOD1 expression in motor neurons surrounded by a wild-type environment prolonged their survival, while normal motor neurons surrounded by mutant SOD1 nonneuronal cells developed ALS pathology (Clement et al., 2003; Yamanaka et al., 2008). These studies have provided evidence that motor neuron degeneration is a non-cell autonomous process or in other words, SOD1 toxicity in nonneuronal cells contributes to the pathogenic cascade. To identify the contributing cells, mice expressing a deletable SOD1 gene were designed. Diminishing mutant SOD1 levels within motor neurons increased survival by delaying disease onset and early progression. Conversely, excising the mutant SOD1 gene in microglia or astrocytes had little effect on the early disease, but sharply slowed disease progression and increased overall survival (Beers et al., 2006; Boillee et al., 2006; Yamanaka et al., 2008). Surprisingly, selective reduction of mutant SOD1 in Schwann cells had the opposite effect, significantly accelerating the late phase of the disease (Lobsiger et al., 2009).

Finally, skeletal muscle pathology in ALS was long considered a secondary event. However, mutant SOD1 expression restricted to skeletal muscle is sufficient to cause muscle atrophy and motor neuron degeneration (Dobrowolny et al., 2008; Wong and Martin, 2010).

Despite the significant progress made since its discovery, the exact pathogenic mechanisms underlying SOD1 toxicity as well as the initial toxic events have yet to be established.

1.2.2 TDP-43 and ALS

Our understanding of ALS pathology was significantly advanced after TDP-43 was identified as the major component of ubiquitin inclusions in most ALS and FTLD cases (Arai et al., 2006; Neumann et al., 2006). This result highlighted a possible role for TDP-43 in disease pathogenesis, confirmed by the finding that missense mutations in *TARDBP*, the gene encoding TDP-43, cause familial forms of ALS (Kabashi et al., 2008; Sreedharan et al., 2008). To date, over 44 mutations in *TARDBP* have been found and these account for approximately 5% of familial ALS cases (Millecamps et al., 2010). These are characterized by earlier, predominantly upper limb onset and longer disease duration compared to sporadic ALS (Corcia et al., 2012).

TARDBP encodes TDP-43, a highly conserved, ubiquitously expressed 414 amino acid protein, initially identified to bind TAR DNA, a regulatory element of HIV-1 (Ou et al., 1995). The protein is predominantly localized to the nucleus and contains two RNA recognition motifs and a glycine rich domain which facilitates binding to nucleic acids and ribonuclear proteins (Wang et al., 2004). The C-terminal glycine-rich domain harbours the majority of ALS associated mutations, which induce fragmentation and mislocalization of TDP-43 to the cytoplasm, where it forms ubiquitinated aggregates (Neumann et al., 2006). Moreover, nuclear TDP-43 depletion in cells with cytoplasmic

aggregates has been observed and lead to the hypothesis that TDP-43 toxicity may be caused by a loss of its nuclear function.

TDP-43 functions include regulation of mRNA alternative splicing and transcription (Ayala et al., 2008; Buratti and Baralle, 2008), mRNA stabilization and transport (Volkening et al., 2009) and formation of RNA stress granules (Colombrita et al., 2009). A recent study characterizing the RNA targets of TDP-43 found several mRNA isoforms that encode proteins relevant for neurological diseases and normal development (Tollervey et al., 2011). TDP-43 knockout mice die early in the embryonic stage and suggest a critical developmental role for this protein (Sephton et al., 2010). To circumvent this, conditional knockout mice have been created and a recent report describes an ALS-like phenotype in mice with post-natal TDP-43 inactivation targeted to the spinal cord motor neurons (Wu et al., 2012).

Overexpression of wild-type TDP-43 has consistently been found to be toxic in most transgenic mouse models (Shan et al., 2010; Tsai et al., 2010; Wils et al., 2010; Xu et al., 2010). The observed phenotypes include motor abnormalities, growth retardation, cognitive impairment or early lethality and can vary greatly according to the promoter used and the TDP-43 expression levels (Da Cruz and Cleveland, 2011). Mice overexpressing ALS-associated TDP-43 mutants have also been created and they exhibit a similar progressive motor phenotype and reduced survival (Stallings et al., 2010; Wegorzewska et al., 2009; Xu et al., 2011b). Both wild-type and mutant transgenic mice are characterized by a selective loss of neurons in the frontal cortex and the anterior horn of the spinal cord, accompanied by ubiquitin aggregates and reactive gliosis (Da Cruz and Cleveland, 2011). Although these clinical and pathological

features are reminiscent of both ALS and FTD, it is difficult to differentiate between mutant and wild-type TDP-43 toxicity. Moreover, it is currently unclear whether TDP-43 is inducing motor neuron degeneration through a loss of function, through a toxic gain of function or both.

1.2.3 FUS and ALS

Shortly after the discovery of TDP-43 involvement in ALS, mutations in the fused in sarcoma (FUS) gene, encoding another RNA/DNA binding protein, were identified in ALS families (Kwiatkowski et al., 2009; Vance et al., 2009). So far, 42 different FUS pathogenic mutations have been reported and these account for 4-6% of familial ALS cases (Andersen and Al-Chalabi, 2011). The associated phenotype is consistent with a predominantly LMN involvement, early disease onset and rapid progression (Millecamps et al., 2010).

FUS, also known as translocated in liposarcoma (TLS), is a ubiquitously expressed 526 amino acid protein originally described as a component of fusion oncogenes in human cancer (Rabbitts et al., 1993). It contains an N-terminal Gln-Gly-Ser-Tyr-rich domain, a Gly-rich domain, an RNA recognition motif, multiple Arg-Gly-Gly repeats and a C-terminal zinc finger motif (Lagier-Tourenne and Cleveland, 2009). Most pathogenic mutations are missense and cluster in the extreme C-terminus of the protein, a highly conserved region functioning as a nuclear localization signal (Mackenzie et al., 2010; Zakaryan and Gehring, 2006). Although the protein resides mainly in the nucleus, analyses of brains and spinal cords from patients with FUS mutations reveals loss of nuclear FUS and ubiquitinated cytoplasmic inclusions positive for FUS, but negative for TDP-43 (Tateishi et al., 2010; Vance et al., 2009).

FUS is an RNA binding protein with structure and functions similar to TDP-43, raising the possibility that RNA misprocessing is a key feature in motor neuron degeneration. The protein shuttles between the nucleus and the cytoplasm (Zinszner et al., 1997) and is involved in cell proliferation, DNA repair, alternative splicing, transcription regulation, RNA and microRNA processing (Janknecht, 2005; Lagier-Tourenne et al., 2010; Law et al., 2006). The FUS gene knockout in inbred mice causes perinatal death accompanied by major B lymphocyte defects (Hicks et al., 2000), while only male sterility was reported in FUS deficient mice on an outbred background (Kuroda et al., 2000).

Transgenic rats overexpressing ALS-associated mutant FUS develop progressive paralysis secondary to axonal degeneration and a significant loss of neurons in the frontal cortex and hippocampus recapitulating features of ALS and FTD (Huang et al., 2011). Similar to TDP-43, expression of human wild-type FUS in rats is sufficient to induce cognitive deficits and mild neuronal loss at a more advanced age (Huang et al., 2011). In both cases, neuronal loss is accompanied by FUS distribution to the cytoplasm, ubiquitin aggregation and reactive gliosis in the brain and spinal cord. Interestingly, a compound blocking glial inflammation managed to preserve the cognitive function of mutant FUS transgenic rats (Huang et al., 2012).

In a recent study, mice expressing wild-type FUS develop progressive paralysis and death in a dose dependent manner and are characterized by loss of spinal motor neurons, muscle atrophy, astrogliosis and ubiquitin-negative cytoplasmic FUS inclusions (Mitchell et al., 2012). Although mutant FUS transgenic mice are not available yet,

these results suggest FUS could induce disease through a toxic gain of function in the cytoplasm.

1.2.4 VAPB and ALS

A dominant missense mutation causing a proline to serine substitution at residue 56 in the VAPB gene was initially identified in eight Brazilian families with phenotypes ranging from typical ALS to late-onset SMA (Nishimura et al., 2004). A further mutation causing a threonine to isoleucine change at position 46 has also been associated with ALS (Chen et al., 2010) (Figure 1.3). Interestingly, transgenic mice expressing VAPB P56S develop cytoplasmic TDP-43 accumulations in the spinal cord, but fail to develop overt motor neuron disease (Tudor et al., 2010).

There are two VAP isoforms in mammals termed VAPA and VAPB that are encoded by different genes and which share approximately 63% sequence identity; both are expressed in most tissues and cell types including the nervous system (Amarilio et al., 2005; Gkogkas et al., 2008; Kim et al., 2010a; Nishimura et al., 1999; Skehel et al., 2000; Teuling et al., 2007). VAPB comprises an N-terminal major sperm protein (MSP) domain, named for its similarity to the nematode MSP, a central coiled-coil domain and a C-terminal transmembrane domain which anchors it in the ER membrane (Nishimura et al., 1999; Skehel et al., 2000; Soussan et al., 1999) (Figure 1.3).

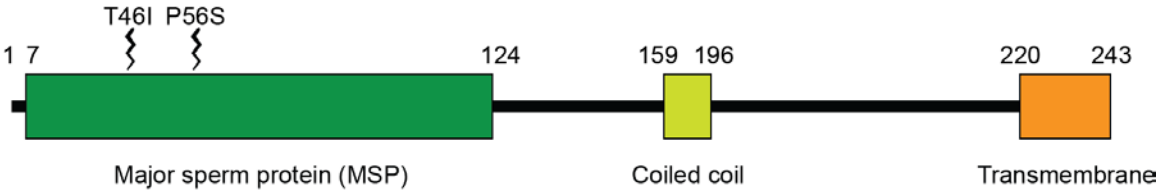

Figure 1.3 Schematic representation of VAPB structure showing protein domains and the localization of ALS-associated pathogenic mutations within the MSP domain

The function of VAPB is not properly understood and it has been implicated in a variety of cellular processes. These include ER to Golgi transport (Amarilio et al., 2005), lipid transport and metabolism (Peretti et al., 2008), bouton formation at the neuromuscular junction and microtubule organisation (Pennetta et al., 2002), the unfolded protein response (UPR) in response to ER stress (Gkogkas et al., 2008; Kanekura et al., 2006; Langou et al., 2010; Suzuki et al., 2009) and signalling via ephrin receptors (Han et al., 2012; Tsuda et al., 2008). Finally, VAPB has recently been shown to play a role in Ca^{2+} homeostasis (De Vos et al., 2012). To carry out these putative functions, VAPB interacts with several proteins including soluble N-ethylmaleimide-sensitive factor-attached protein receptor (SNARE) proteins (Skehel et al., 1995), two phenylalanines (FF) in acidic tract (FFAT) motif-containing proteins (Amarilio et al., 2005), microtubules (Pennetta et al., 2002; Skehel et al., 2000), protein tyrosine phosphatase-interacting protein 51 (PTPIP51) (De Vos et al., 2012), activating transcription factor 6 (ATF6) (Gkogkas et al., 2008) and viral proteins (Hamamoto et al., 2005).

VAPB was originally identified as binding partner for the synaptic vesicle SNARE protein vesicle-associated membrane protein (VAMP)/synaptobrevin in Aplysia californica and this suggests a role in vesicle trafficking (Skehel et al., 1995). Aside from this, several other lines of evidence indicate that VAPB is involved in the transport

of vesicles between ER and Golgi and in intra-Golgi transport. Transport through the Golgi apparatus and from the Golgi to ER is mediated by coat protein I (COPI)-coated vesicles (Letourneur et al., 1994; Orci et al., 1997). Vesicle transport from ER to Golgi is mediated by coat protein II (COPII)-coated vesicles via the ER-Golgi intermediate compartment (ERGIC) (Barlowe et al., 1994; Campbell and Schekman, 1997). VAPB co-localizes with COPI vesicles, ERGIC and the COPII vesicle marker secretion-defective 23 (Sec23) (Moumen et al., 2011; Tran et al., 2012). In addition, VAPB also interacts with the FFAT motif-containing N-terminal domain-interacting receptor (Nir) proteins Nir2 and Nir3 (Amarilio et al., 2005; Loewen et al., 2003), and overexpression of VAPB and Nir2 causes remodelling of the ER and blocks protein export from the ER to the Golgi apparatus (Amarilio et al., 2005). Together, these findings support a role for VAPB in the regulation of vesicle trafficking.

There is also evidence that VAPB is involved in lipid metabolism. Thus, VAPB binds to the FFAT motif-containing lipid transferring, binding and sensing proteins Nir2, oxysterol binding protein and ceramide transfer protein (Amarilio et al., 2005; Kawano et al., 2006; Loewen et al., 2003). The VAPB-FFAT motif interaction is essential for lipid transfer between the ER and Golgi, and also for lipid metabolism (Loewen et al., 2003; Peretti et al., 2008). The VAPB homologue in yeast also binds to the FFAT motif containing protein overproducer of inositol 1 which functions to regulate transcription of genes involved in phospholipid synthesis (Gavin et al., 2002; Loewen et al., 2003).

VAPB has also been implicated in microtubule organisation and in particular, microtubule regulation of bouton formation at the neuromuscular junction. Thus, VAPB interacts either directly or indirectly with microtubules (Amarilio et al., 2005; Pennetta

et al., 2002; Skehel et al., 2000). Via its interaction with microtubules, VAPB influences the neuromuscular junction structure in *Drosophila melanogaster* (Pennetta et al., 2002) and also ER structure in mammals (Amarilio et al., 2005). Also, via its binding to Nir3, VAPB modulates microtubule stability and overexpression of VAPB can induce rearrangement of the ER and microtubule networks (Amarilio et al., 2005).

There is also strong evidence that VAPB plays a role in the UPR following ER stress. Increased protein trafficking through the ER or insults that affect protein folding in the ER lumen can lead to ER stress. To sense ER and respond to ER stress, eukaryotic organisms have evolved the UPR which activates pathways that include transcriptional changes to adjust the ER protein folding capacity and rectify the stress (Bernales et al., 2006; Lin et al., 2008). There are three major branches to the UPR which involve different ER resident proteins. These proteins are inositol-requiring protein 1 (IRE1), double stranded RNA activated protein kinase RNA-like endoplasmic reticulum kinase (PERK) and ATF6 (see Figure 1.3 page 58). These proteins all contain domains that protrude into the ER lumen so as to sense ER stress and also have cytosolic effector domains (Bernales et al., 2006; Lin et al., 2008).

Although a number of lines of evidence suggest that VAPB functions in the UPR, the precise details are unclear. Thus, in some reports overexpression of VAPB promotes UPR and loss of VAPB blocks activation of UPR (Kanekura et al., 2006; Langou et al., 2010; Moumen et al., 2011). Moreover, this role of VAPB in the UPR has been shown to involve IRE1 and X-box binding protein-1 (XBP1) signalling (Kanekura et al., 2006; Suzuki et al., 2009). By contrast, others have shown that VAPB binds to ATF6 and overexpression of VAPB blocks UPR via an effect on ATF6 (Gkogkas et al., 2008).

Studies primarily conducted in *Drosophila* and *C. elegans* have provided evidence that VAPB is cleaved and a region containing the MSP and coiled-coil domains is then secreted to function as a ligand for some growth factor receptors (Han et al., 2012; Tsuda et al., 2008). These secreted VAPB domains function as ligands for ephrin receptors (EphR), sensory axon guidance-3 receptor Roundabout (SAX-3 Robo) receptors and caterpillar-like receptor-1 leukocyte common antigen-related-like (CLR-1 Lar) receptors (Han et al., 2012; Tsuda et al., 2008). EphR, SAX-3 Robo and CLR-1 Lar are located in neuronal growth cones and are involved in axon guidance (Chang et al., 2004; Sun et al., 2000; Wang and Anderson, 1997). Furthermore, Han and co-workers have demonstrated that the secreted MSP domain of VAPB influences mitochondrial localization in striated muscles via SAX-3, Robo and CLR-1 Lar receptors (Han et al., 2012).

Finally, recent work has provided evidence that VAPB is involved in intracellular Ca^{2+} homeostasis (De Vos et al., 2012; Langou et al., 2010). In particular VAPB has been shown to bind to the outer mitochondrial membrane protein PTPIP51 to regulate Ca^{2+} exchange between ER and mitochondria (De Vos et al., 2012). Both ER and mitochondria are Ca^{2+} stores and following release from the ER, Ca^{2+} can be taken up by mitochondria. The VAPB-PTPIP51 interaction has been shown to regulate Ca^{2+} exchange from ER to mitochondria after induction of inositol 1,4,5-trisphosphate receptor (IP3R)-mediated Ca^{2+} release from ER stores (De Vos et al., 2012).

Since the functions of VAPB are not properly understood, the mechanisms by which ALS-associated VAPB P56S causes disease are also not clear. However, VAPB P56S

has been shown to aggregate and induce the formation of abnormal ER-derived inclusions (Fasana et al., 2010; Langou et al., 2010; Nishimura et al., 2004; Teuling et al., 2007; Tudor et al., 2010). The biological consequences of these inclusions and their relationship to the neurodegenerative process are unclear. In particular, the effect of VAPB P56S on UPR has generated conflicting results. Thus, in some reports, expression of VAPB induces UPR and VAPB P56S inhibits this process (Chen et al., 2010; Kanekura et al., 2006; Suzuki et al., 2009). In another, expression of VAPB and VAPB P56S both inhibit UPR but VAPB P56S is more potent in this effect (Gkogkas et al., 2008). Finally, other studies have shown that VAPB and/or VAPB P56S can induce ER stress and UPR (Langou et al., 2010; Tsuda et al., 2008). Studies on the effect of VAPB P56S on Ca^{2+} homeostasis have provided more consistent results with two groups showing that VAPB P56S elevates intracellular Ca^{2+} levels (De Vos et al., 2012; Langou et al., 2010). Whether VAPB P56S induces disease via a loss or gain of function is thus unclear. VAPB P56S may inhibit VAPB function by sequestering wild-type VAPB to the inclusions and preventing its interaction with other proteins (Kanekura et al., 2006; Mitne-Neto et al., 2007; Ratnaparkhi et al., 2008; Suzuki et al., 2009; Teuling et al., 2008). Alternatively, VAPB P56S could be a toxic gain-of-function mutant because VAPB P56S overexpression has been shown to induce the UPR (Gkogkas et al., 2008; Tsuda et al., 2008). Support for a loss of function comes from the finding that VAPB levels are reduced in ALS spinal cord and also in motor neurons derived from induced pluripotent stem cell of patients that harbour the VAPB P56S mutation (Anagnostou et al., 2010; Mitne-Neto et al., 2007).

1.3 Neurodegeneration mechanisms in ALS

Several mechanisms have been proposed to induce motor neuron degeneration in ALS and these have recently been reviewed (Ferraiuolo et al., 2011). They include glutamatergic excitotoxicity, oxidative stress, pathological protein aggregation, mitochondrial dysfunction, damage to RNA processing, axonal transport dysfunction and ER stress. None of these mechanisms are mutually exclusive and it is plausible that they all contribute to the disease process to some extent. In addition, it has become clear that ALS is not just a disease of motor neurons, but that other cell types such as astrocytes and microglia actively participate in the disease process (for review see (Ferraiuolo et al., 2011)). In the following section of this thesis, I discuss the evidence supporting the different pathogenic mechanisms.

1.3.1 Excitotoxicity

Glutamate is the major excitatory neurotransmitter in the central nervous system. After its release from the presynaptic terminal, it binds to and activates ionotropic and metabotropic receptors (Nicoletti et al., 2011; Traynelis et al., 2010). Glutamate is then re-internalized into either glia or neurons by re-uptake systems (Kanai and Hediger, 2004), of which the astroglial excitatory amino acid transporter 2 (EAAT2) is the most common (Danbolt, 2001). Excessive activation of glutamate receptors is capable of inducing neuronal damage through a process called excitotoxicity, which can elicit an excessive Ca^{2+} influx and the activation of cell death programmes (Berliocchi et al., 2005). Excitotoxicity is a well established pathogenic component in many neurological disorders and considerable evidence also points to its involvement in ALS (Foran and Trotti, 2009).

An early hint of glutamate metabolism disruption was the observation of elevated glutamate levels in the cerebrospinal fluid (CSF) of ALS patients (Rothstein et al., 1990). Subsequently, a decreased EAAT2 activity was detected in ALS brain and spinal cord, raising the possibility that the increased glutamate levels reflected defective clearance of glutamate (Rothstein et al., 1992).

Interestingly, the intrinsic properties of motor neurons make them especially vulnerable to alpha-amino-3-hydroxy-5-methylisoxazole-4-propionic acid (AMPA) receptor mediated excitotoxicity (Carriedo et al., 1996; Van Den Bosch et al., 2000). First, motor neurons show a relative deficiency in the glutamate receptor-2 (GluR2) subunit, which normally regulates the AMPA receptor's permeability to Ca^{2+} (Van Damme et al., 2002). Therefore, motor neurons have a high number of Ca^{2+}–permeable AMPA receptors. Second, motor neurons express low levels of Ca^{2+} buffering proteins (Ince et al., 1993), which makes them rely heavily on the mitochondrial Ca^{2+} buffering capacity (Alexianu et al., 1994). Thus, upon repeated AMPA stimulation, mitochondrial Ca^{2+} buffering is saturated, leading to a persistent elevation in baseline cytosolic Ca^{2+} (Grosskreutz et al., 2007). Furthermore, excessive Ca^{2+} entry into motor neurons and mitochondrial Ca^{2+} overload can lead to loss of mitochondrial membrane potential and the generation of reactive oxygen species (ROS) (Carriedo et al., 2000). Finally, there is considerable evidence for altered mitochondrial function in ALS (see Section 1.3.4), which could also increase the susceptibility of motor neurons to excitotoxicity.

Mutations in alsin, a guanine nucleotide exchange factor, cause autosomal recessive juvenile onset ALS, infantile-onset HSP, and juvenile PLS (Eymard-Pierre et al., 2002; Gros-Louis et al., 2003; Otomo et al., 2003). Alsin was found to interact with glutamate

receptor interacting protein 1 (GRIP1), a protein responsible for GluR2 shuttling to the synapse. When deficient, alsin alters the distribution of GRIP1 and reduces the amount of GluR2, rendering motor neurons more vulnerable to excitotoxicity (Lai et al., 2006).

Finally, riluzole, the only disease modifying agent approved for the treatment of ALS has anti-glutamatergic properties. Thus, riluzole blocks presynaptic glutamate release and modulates N-methyl-D-aspartate (NMDA) and AMPA receptors (Albo et al., 2004; Bensimon et al., 1994; Debono et al., 1993; Lacomblez et al., 1996). However, other anti-glutamate compounds such as topiramate and lamotrigine have failed in clinical trials, suggesting the neuroprotective effect of riluzole might also depend on other pathways (Cudkowicz et al., 2003; Ryberg et al., 2003).

1.3.2 Oxidative stress

The aerobic metabolism is constantly generating potentially toxic by-products in the form of reactive oxygen species (ROS). Cellular ROS arise mostly due to an incomplete reduction of molecular oxygen during oxidative phosphorylation. However, under normal conditions the cell's antioxidant mechanisms are constantly scavenging the ROS and preventing or repairing the damage they cause. Oxidative stress occurs when the balance between ROS production and the physiologic antioxidant defence is perturbed (Halliwell, 1994).

Several lines of evidence suggest oxidative stress is involved in ALS pathogenesis. Initially, evidence of oxidative damage was identified in post-mortem ALS spinal cord and motor cortex (Ferrante et al., 1997; Shaw et al., 1995). This was confirmed by biological samples from ALS patients which showed oxidative damage to lipids, DNA

and protein (Bogdanov et al., 2000; Simpson et al., 2004; Smith et al., 1998). The oxidation of mRNA, leading to decreased expression of key proteins is also an important feature in patients and mutant SOD1 mice (Chang et al., 2008). The link between ALS and oxidative stress was strengthened after the discovery of causative ALS mutations in the antioxidant enzyme SOD1 and mutant SOD1 transgenic mice recapitulate the oxidative damage characteristic of human ALS (Andrus et al., 1998; Casoni et al., 2005; Liu et al., 1998; Zimmerman et al., 2007). More recently, ALS mutant TDP-43 has been shown to induce oxidative injury in motor neuron cell lines (Duan et al., 2010). It is now widely accepted that loss of SOD1 dismutase activity does not occurr in all ALS mutants and is not sufficient to cause disease. However, genes involved in the antioxidant response, including nuclear factor erythroid 2-related factor 2 (NRF2) are down-regulated in cells expressing mutant SOD1 (Kirby et al., 2005). NRF2 induces gene expression in response to oxidative stress and also maintains the basal expression of antioxidant enzymes (Nguyen et al., 2009). In addition, decreased levels of NRF2 have been reported in the CNS of ALS patients (Sarlette et al., 2008).

An important source of ROS in ALS is represented by microglia. Activated microglia increase the production of superoxide through the nicotinamide adenine dinucleotide phosphate (NADPH) oxidase as a form of defence against pathogens (Bedard and Krause, 2007). Mutant SOD1 expressed in microglia binds to the NADPH oxidase activator Rac1 and blocks the enzyme in an active state, generating harmful amounts of superoxide ions (Harraz et al., 2008). Moreover, the activation of NADPH oxidase was also detected in the spinal cords of sporadic ALS patients (Wu et al., 2006) and the administration of apocynin, a NADPH oxidase inhibitor, increased survival in SOD1 transgenic mice (Harraz et al., 2008). Interestingly, mutant SOD1 can also induce

activation of microglia following its secretion from neighbouring neurons or astrocytes (Zhao et al., 2010) and extracellular SOD1 has been detected in the CSF of ALS patients and transgenic mice (Turner and Talbot, 2008; Urushitani et al., 2006).

Ageing is an important risk factor for developing ALS and ROS production is known to increase with age. This is unlikely to be the causative event, but in the presence of other pathogenic insults, it could be enough to tip the homeostatic balance and initiate an irreversible cycle of cellular injury. Although antioxidant therapies have extended survival in transgenic animal models (see for review (Turner and Talbot, 2008)), most human trials have failed so far (Barber and Shaw, 2010).

1.3.3 Pathological protein aggregation

The accumulation of ubiquitinated proteins in motor neurons is a hallmark pathology of ALS (see for review (Ince et al., 2011)). The major component of the ubiquitinated inclusions was recently identified as TDP-43, a DNA/RNA binding protein (Neumann et al., 2006). Although TDP-43 resides predominantly in the nucleus in physiological conditions, pathological TDP-43 is cleaved and redistributed to the cytoplasm, where it becomes abnormally phosphorylated and ubiquitinated (Neumann et al., 2006). Since *TARDBP* mutations are capable of causing familial and sporadic ALS (Kabashi et al., 2008; Sreedharan et al., 2008), it has been speculated that abnormal aggregation of TDP-43 contributes to the disease process.

The classical ALS pathology also features accumulations of other proteins. These include phosphorylated neurofilaments, which accumulate in axons and cell bodies and could have detrimental effects on axonal homeostasis (see for review (Al-Chalabi and

Miller, 2003)) and misfolded SOD1 which is also present in ALS spinal cords (Shibata et al., 1996) and in SOD1 transgenic animals (Bruijn et al., 1998). Antibodies selectively detecting misfolded SOD1 have been created (Rakhit et al., 2007) and these label mutant SOD1 inclusions in familial ALS and an oxidized form of wild-type SOD1 in a subset of sporadic ALS cases (Bosco et al., 2010). Finally, mutations in FUS, a nuclear protein, induce its aberrant localization to the cytoplasm, where it forms inclusions (Kwiatkowski et al., 2009; Vance et al., 2009). Recently, the number of FUS inclusions has been shown to increase with disease duration (Suzuki et al., 2012).

Other recently identified causative ALS mutations support a role for abnormal protein aggregation in disease pathogenesis. Mutations in the valosin-containing protein (VCP) gene on chromosome 9 have been found in patients with familial ALS (Johnson et al., 2010). VCP is an abundantly expressed adenosine triphosphate (ATP)ase involved in a wide variety of cellular processes including ER and mitochondrial protein degradation, endosomal sorting, the ubiquitin proteasome system, ER and Golgi reassembly, nuclear envelope formation and the cell cycle (Acharya et al., 1995; Cao et al., 2003; Dai and Li, 2001; Latterich et al., 1995; Rabouille et al., 1995; Ritz et al., 2011; Xu et al., 2011a). Pathogenic VCP mutations have been found to impair the clearance of aggregated proteins (Ju et al., 2008), perturb endolysosomal sorting (Ritz et al., 2011) and induce autophagosome accumulation (Ju et al., 2009). Interestingly, VCP can escort ubiquitinated proteins to the proteasome for degradation by binding to Derlin-1, thus playing a central role in ER-associated protein degradation (ERAD) (Ye et al., 2005).

Mutations in ubiquilin 2 (UBQLN2) cause X-chromosome linked dominantly inherited ALS with or without FTD (Deng et al., 2011). The gene encodes a ubiquitin-like protein

which interacts with polyubiquitin chains and proteasome subunits, and is thought to regulate protein degradation (Ko et al., 2004). Mutant UBQLN2 perturbs the ubiquitin proteasome system suggesting a mechanism linked to impaired protein clearance in ALS (Deng et al., 2011).

1.3.4 Mitochondrial dysfunction

Mitochondria are organelles essential for energy production, Ca^{2+} buffering and mediating apoptosis. Abnormalities in mitochondrial morphology, such as mitochondrial swelling or vacuolization have long been observed in ALS motor neurons (Sasaki and Iwata, 2007). Moreover, these changes correlate with functional alterations such as defects in ATP production and the electron transport chain, and reduced Ca^{2+} buffering capacity (Carrì et al., 1997; Fujita et al., 1996; Siklos et al., 1996; Wiedemann et al., 2002).

Mitochondrial abnormalities and functional deficits have been consistently reported in mutant SOD1 transgenic mice and mutant SOD1 expressing cells (Dal Canto and Gurney, 1995; Kong and Xu, 1998; Liu et al., 2004; Pasinelli et al., 2004; Sotelo-Silveira et al., 2009; Vande Velde et al., 2011; Wong et al., 1995). A proportion of mutant SOD1 is present on the outer mitochondrial membrane, in the intermembrane space and mitochondrial matrix, suggesting that it may directly damage mitochondria (Higgins et al., 2002; Liu et al., 2004; Mattiazzi et al., 2002; Pasinelli et al., 2004; Vande Velde et al., 2008; Vijayvergiya et al., 2005). This abnormal localization of mutant SOD1 is specific for spinal cord mitochondria and is not found in brain or liver, indicating its direct relevance for disease (Mattiazzi et al., 2002; Pasinelli et al., 2004; Vande Velde et al., 2008).

Some specific molecular targets for mutant SOD1 toxicity have been identified. One of them is the outer mitochondrial membrane voltage-dependent anion channel 1 (VDAC1), which directly binds mutant SOD1 (Israelson et al., 2010). VDAC1 regulates the ion and metabolite flux between mitochondria and cytosol and plays a key role in the mitochondrial permeability transition pore apoptotic pathway (McCommis and Baines, 2012). Interaction of mutant SOD1 with VDAC1 impairs channel conductance and adenosine diphosphate (ADP) import across the outer mitochondrial membrane (Israelson et al., 2010). This can lead to reduced ATP production and may explain the perturbation of ATP synthesis observed in mutant SOD1 models (Carrì et al., 1997; Damiano et al., 2006). VDAC1 is involved in Ca^{2+} exchange between ER and mitochondria via its interaction with inositol-1,4,5-triphosphate receptors (IP3R) (Rapizzi et al., 2002; Szabadkai et al., 2006) and mutant SOD1 binding to VDAC1 may also underlie the aberrant Ca^{2+} handling and impaired Ca^{2+} buffering observed in mutant SOD1 models (Grosskreutz et al., 2007; Jaiswal and Keller, 2009). Aberrant mitochondrial Ca^{2+} handling has also been described in VAPB-related ALS (De Vos et al., 2012; Langou et al., 2010) and ALS patients (Siklos et al., 1996) but it is not clear whether this involves VDAC1. Nevertheless, impaired mitochondrial Ca^{2+} handling and increased cytosolic Ca^{2+} are common findings in ALS that could be primary pathogenic events or act indirectly by inducing defects in axonal transport (MacAskill and Kittler, 2010; Wang and Schwarz, 2009) or by rendering motor neurons vulnerable to excitotoxicity (see Section 1.3.1).

Another target of mutant SOD1 is the anti-apoptotic protein B-cell lymphoma-2 (Bcl-2) in spinal cord mitochondria, which is sequestered into SOD1 aggregates (Pasinelli et al.,

2004). Bcl-2 depletion from motor neurons could be the underlying cause of cytochrome c release and caspase activation in mutant SOD1 models (Kirkinezos et al., 2005; Takeuchi et al., 2002).

1.3.5 Axonal transport dysfunction

The proper transport of protein and organelle cargoes along the cytoskeleton is a vital process for virtually all mammalian cells. This process is particularly important in neurons, since they are polarized cells with axons and dendrites usually extending over great distances. Since most neuronal proteins are synthesised in the cell body and then transported to their final destination, neurons require highly efficient transport of cargoes to the distal regions of axons and dendrites to permit functioning of synapses. Likewise, trophic factors need to be shipped from the synapse to the cell body. Transport from cell body to the axon terminal is termed anterograde axonal transport and transport from the axon terminal to the cell body is termed retrograde axonal transport.

Most long range transport through axons is mediated by kinesin and dynein molecular motors that move along microtubules. Within axons, microtubules are mostly orientated with their plus ends (the ends to which tubulin subunits are added) towards the synapse. Most kinesins move towards the plus end of microtubules (anterograde transport) whereas dynein moves towards the minus end of microtubules (retrograde transport) (Hirokawa and Noda, 2008).

A number of lines of evidence suggest that defective axonal transport contributes to neurodegenerative diseases including ALS (for review see (De Vos et al., 2008)).

Firstly, mutations in dynactin, a component of the dynein motor, can cause a familial form of ALS (Munch et al., 2004; Puls et al., 2003) and mutant dynactin damages dynein function (Levy et al., 2006).

Secondly, the presence of protein/organelle accumulations in ALS such as neurofilament and mitochondria in the proximal axon suggest that axonal transport is disrupted (Ackerley et al., 2004; Carpenter, 1968; Hirano et al., 1984; Ince et al., 1998; Sasaki and Iwata, 2007). Thirdly, damage to axonal transport has been described in ALS transgenic animals and cellular models. Defective axonal transport of components of the cytoskeleton, mitochondria and vesicles are observed in mutant SOD1 mice that develop ALS (Bilsland et al., 2010; De Vos et al., 2007; Kieran et al., 2005; Williamson and Cleveland, 1999; Zhang et al., 1997). Also overexpression of neurofilaments can model ALS in mice and damage to axonal transport is seen in these models (Collard et al., 1995; Millecamps et al., 2006).

Finally, disrupting molecular motor function can model ALS in transgenic mice. The Legs-at-odd-angles and Cramping 1 mutant mice develop a progressive locomotor phenotype including motor neuron cell loss, and the genetic defect in these animals has been shown to involve the dynein gene (Hafezparast et al., 2003). Furthermore, overexpression of dynamitin (which disrupts dynein function) causes motor neuron disease in transgenic mice (LaMonte et al., 2002).

In contrast, some evidence suggests that damage to axonal transport of mitochondria might not be mechanistic in the ALS disease process. Syntaphilin is a protein that anchors mitochondria to microtubules in axons and syntaphilin knockout mice show

increased mitochondrial movement (Kang et al., 2008). Crossing mutant SOD1 mice with syntaphilin knockout mice increases axonal transport of mitochondria but it does not slow disease progression (Zhu and Sheng, 2011). However, there is evidence that damage to mitochondrial transport is anterograde specific in ALS (De Vos et al., 2007; Morotz et al., 2012) and loss of syntaphilin increases overall transport so does not properly correct the defect. Others have also reported that SOD1 G85R transgenic mice develop ALS despite having no axonal transport defects (Marinkovic et al., 2012). However, this finding is in disagreement with studies from other groups (Williamson and Cleveland, 1999) and the weight of evidence supports a role for defective axonal transport in ALS.

1.3.6 Damage to mRNA metabolism

Defective splicing of mRNA for the glial glutamate transporter EAAT2 in ALS patients was one of the first pieces of evidence linking RNA processing defects to excitotoxicity and motor neuron degeneration (Lin et al., 1998). Moreover, mRNA oxidation in motor neurons is a common finding in ALS patients and SOD1 transgenic mice (Chang et al., 2008). More recently, the importance of RNA metabolism has been highlighted by the discovery that mutations in genes encoding Senataxin, an RNA helicase, Angiogenin, a ribonuclease and RNA/DNA interacting proteins TDP43 and FUS all cause familial forms of ALS (Chen et al., 2004; Greenway et al., 2006; Kwiatkowski et al., 2009; Sreedharan et al., 2008; Vance et al., 2009).

TDP-43 is a predominantly nuclear protein that regulates mRNA expression, splicing, translation and gene transcription (Cohen et al., 2011). Expression of mutant TDP-43 in cells leads to an abnormal localization to the cytoplasm, particularly in stress granules

(Liu-Yesucevitz et al., 2010). Certain conditions such as oxidative stress or ischemia trigger a global translational silencing and the formation of stress granules, cytoplasmic aggregates which transiently sequester mRNA and RNA binding proteins and can modulate the signalling balance between apoptosis and survival (Thomas et al., 2011). More than 6000 TDP-43 RNA targets have now been identified and these include several that are linked to ALS such as FUS, EAAT1, progranulin and TDP-43 itself (Polymenidou et al., 2011; Sephton et al., 2011; Tollervey et al., 2011).

In a similar manner to TDP-43, ALS mutant FUS shows abnormal cytoplasmic localization and can induce the formation of FUS containing cytoplasmic stress granules (Dormann et al., 2010; Ito et al., 2011a; Kwiatkowski et al., 2009; Vance et al., 2009). FUS is also a component of mRNA transporting granules and might contribute to mRNA shuttling to synapses for local translation (Kanai et al., 2004). Recently, FUS has been shown to facilitate exon 10 skipping in the gene encoding Tau (Ishigaki et al., 2012). This generates 3-repeat Tau, an isoform which is relatively increased in neurodegenerative disorders (Yoshida, 2006). In addition, TDP-43 and FUS interact to regulate mRNA expression of histone deacetylase 6 (HDAC6) (Kim et al., 2010b), a protein involved in autophagy and stress granule formation (d'Ydewalle et al., 2012).

Lastly, a GGGGCC hexanucleotide repeat expansion in a non-coding region of C9ORF72 is currently the most common genetic defect in both ALS and FTD (Cooper-Knock et al., 2012; DeJesus-Hernandez et al., 2011; Majounie et al., 2012; Renton et al., 2011). In one scenario, the expanded hexanucleotide repeats can act through a toxic gain of function at the mRNA level and form intranuclear accumulations that sequester mRNA binding proteins to disrupt mRNA metabolism. Indeed, C9ORF72 RNA foci

have been identified in the spinal cords and frontal cortex of patients carrying the expansion (DeJesus-Hernandez et al., 2011). This toxic mRNA disease mechanism has been described in other forms of neurodegeneration such as myotonic dystrophies and ataxias (Todd and Paulson, 2010).

1.3.7 ER stress and the unfolded protein response (UPR)

In order to survive, all living cells must carry out a quality control programme which regulates protein biosynthesis, folding, translocation, assembly/disassembly, and clearance (degradation). This complex regulatory network requires the coordinated action of chaperones and proteolytic systems and is called protein homeostasis or proteostasis (see for reviews (Bar-Lavan et al., 2012; Hartl et al., 2011)). Molecular chaperones prevent protein aggregation by stabilizing or helping proteins acquire their final conformation (Hartl et al., 2011). When the chaperone machinery is overwhelmed, two major systems mediate the complete degradation of abnormal proteins: the proteasome and the lysosome (Wong and Cuervo, 2010). The proteasome selectively recognizes substrates tagged with ubiquitin, which are mostly short-lived proteins. Autophagy denotes the delivery of cytosolic components and organelles (dubbed mitophagy in case of mitochondria) to the lysosome, where they undergo catalytic degradation.

Under normal conditions, proteins fold in the ER lumen and are prepared for delivery to the cell compartment where they are needed. Finely tuned molecular sensors in the ER lumen are capable of detecting a deficit in the ER folding capacity (i.e. ER stress) and activate signalling pathways collectively termed the UPR (see for reviews (Hetz, 2012; Lin et al., 2008)). The UPR tries to decrease the load of misfolded proteins and restore

proteostasis by (i) attenuation of translation, (ii) induction of chaperones to aid protein folding, and (iii) upregulation of degradation pathways such as ERAD and autophagy to completely remove misfolded proteins (see Figure 1.3). However, if ER stress persists and elicits a prolonged induction of UPR, the cell initiates apoptosis (Nakagawa et al., 2000; Nishitoh et al., 2002).

Several lines of evidence suggest an important role for ER stress in the pathogenic cascade of ALS. Firstly, ER stress and activation of the UPR has been described in mutant SOD1 transgenic mice and in cell lines that express mutant SOD1 (Atkin et al., 2006; Kikuchi et al., 2006; Nishitoh et al., 2008; Saxena et al., 2009; Tobisawa et al., 2003). Furthermore, the induction of UPR stress sensor kinases, chaperones and apoptotic mediators have been detected in the CSF of ALS patients and in postmortem sporadic ALS motor neurons (Atkin et al., 2008; Sasaki, 2010). Interestingly, in mutant SOD1 expressing mice, the upregulation of the ER resident misfolded protein sensor glucose-regulated protein 78/immunoglobulin heavy-chain binding protein (GRP78/BiP), which is indicative of UPR activation, appears to be specific for the fast-fatigable motor neurons, which are most susceptible to disease in ALS and was observed as early as postnatal day 5 (Saxena et al., 2009). It is not clear how mutant SOD1 induces ER stress but there is evidence that mutant SOD1 aggregates accumulate in the ER lumen and on the cytosolic surface of the ER where they interact with BiP and Derlin-1 (Kikuchi et al., 2006; Nishitoh et al., 2008). Binding of mutant SOD1 to Derlin-1 inhibits ERAD and increases ER stress and UPR (Nishitoh et al., 2008). The aberrant interaction between mutant SOD1 and BiP may also lead to an uncontrolled and prolonged UPR by preventing BiP interaction with ER stress sensors (Kikuchi et al., 2006). Mutant SOD1 also upregulates protein-disulfide isomerase (PDI), an ER-

resident chaperone which colocalizes with SOD1 aggregates and is suggested to have a protective role in SOD1 models (Atkin et al., 2006). Prolonged ER stress and UPR have deleterious effects on homeostasis and eventually activate apoptosis via cysteinyl aspartate-specific protease-12 (caspase-12) and apoptosis signal-regulating kinase 1 (ASK1) (Nakagawa et al., 2000; Nishitoh et al., 2002). Both caspase-12 and ASK1 are activated in ALS mutant SOD1 expressing transgenic mice suggesting that UPR dependent apoptosis might contribute to neurodegeneration in ALS (Atkin et al., 2006; Holasek et al., 2005; Wengenack et al., 2004; Wootz et al., 2004).

A second line of evidence implicating ER stress in ALS comes from the finding that mutations in the gene encoding VAPB cause a form of familial ALS; VAPB functions in mediating the UPR in response to ER stress (Gkogkas et al., 2008; Kanekura et al., 2006; Suzuki et al., 2009). However, there are some inconsistencies regarding the role of VAPB in the UPR. Thus, in some reports, expression of VAPB induces UPR and ALS mutant VAPB inhibits this process (Chen et al., 2010; Kanekura et al., 2006; Suzuki et al., 2009). In another, expression of VAPB and ALS mutant VAPB both inhibit UPR but mutant VAPB is more potent in this effect (Gkogkas et al., 2008). Finally, other studies have shown that VAPB and/or mutant VAPB can induce ER stress and UPR (Langou et al., 2010; Tsuda et al., 2008).

Finally, there is evidence that ALS mutant TDP-43 and FUS can induce ER stress and UPR. TDP-43 is cleaved into toxic ubiquitinated hyperphosphorylated 25 kDa fragments (Neumann et al., 2006) and chemical induction of ER stress promotes TDP-43 cleavage via caspase-12 (Suzuki et al., 2011). Also expression of mutant FUS induces ER stress and mutant FUS interacts with and upregulates PDI (Farg et al.,

2012). Together, these findings support a role for ER stress and UPR induction in the ALS pathogenic cascade.

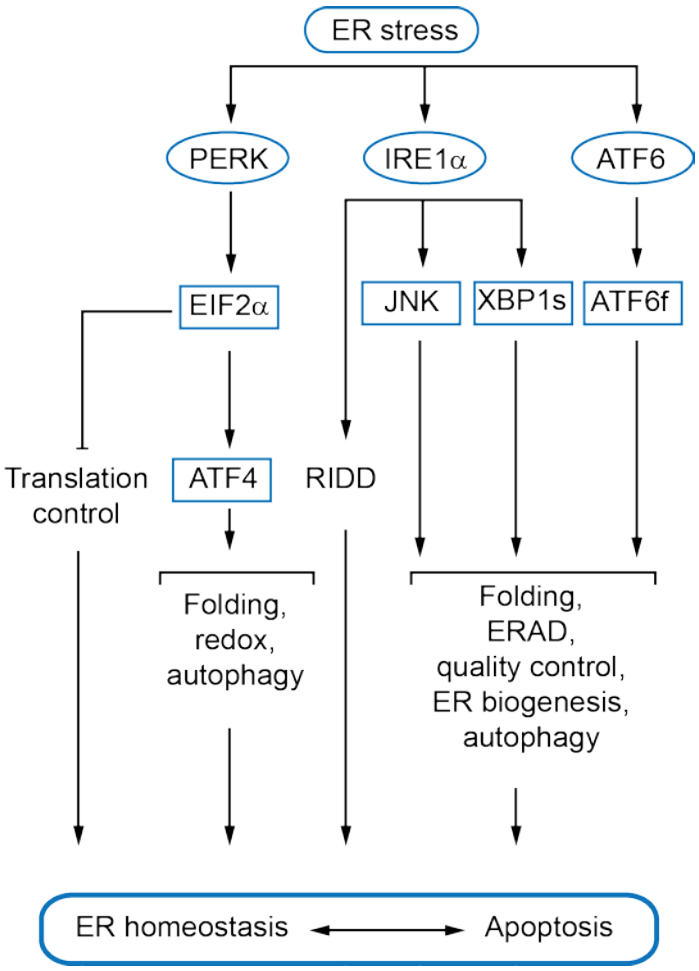

Figure 1.4 The vertebrate UPR

When unfolded proteins accumulate in the ER, the stress sensors PERK, IRE1 and ATF6 initiate signalling cascades known as the UPR. Initially, activated PERK inhibits translation via EIF2α to reduce protein influx in the ER. Subsequently, regulated mRNA splicing and transcriptional activation act on specialized target genes. These genes encode proteins involved in protein folding, autophagy, ERAD and redox mechanisms, in an attempt to re-establish protein homeostasis. If ER homeostasis cannot be restored from the combined action of the three pathways, the cell undergoes apoptosis. RIDD -

Regulated IRE1-dependent decay; ATF4 -Activating transcription factor 4; JNK - c-Jun N-terminal kinase.

1.4 The ER-mitochondria axis and neurodegenerative diseases

As detailed above, defects in a number of apparently disparate cellular functions can be seen in ALS. Understanding how these different pathological changes might be linked in a common pathway remains a major challenge for comprehending ALS disease processes. Recently, several studies have highlighted the role of ER-mitochondria communications in neurodegenerative diseases such as ALS (see for reviews (Cali et al., 2011; Giorgi et al., 2012; Lautenschlaeger et al., 2012; Rowland and Voeltz, 2012; Schon and Area-Gomez, 2012)).

Both ER and mitochondria play pivotal roles in a number of essential cellular functions. Thus, the ER is involved in protein synthesis, lipid metabolism and Ca^{2+} homeostasis, while mitochondria function in energy metabolism, Ca^{2+} homeostasis, lipid synthesis and apoptosis. These functions require a dynamic spatial organization that permits relaying of signals between different organelles. In particular, mitochondria and ER display close associations with between 5 and 20% of the mitochondrial surface closely apposed (10-25 nm distance) to ER membranes (Csordas et al., 2006; Rizzuto et al., 1998). These ER membrane domains are known as mitochondria-associated ER membranes (MAM). A large body of evidence demonstrates that mitochondria communicate directly with ER through MAM to facilitate a number of intracellular signaling processes. These include Ca^{2+} and phospholipid exchange, ER and mitochondrial stress responses, and apoptosis (Giorgi et al., 2009; Hayashi et al., 2009; Pinton et al., 2008; Rowland and Voeltz, 2012).

A number of ALS associated insults are now known to target either MAM proteins, or mitochondrial proteins at the MAM interface. Thus, VAPB is a known MAM protein and ALS mutant VAPB disrupts ER structure and ER to mitochondria Ca^{2+} exchange (De Vos et al., 2012; Fasana et al., 2010; Kim et al., 2010a; Langou et al., 2010; Nishimura et al., 2004; Teuling et al., 2007; Tudor et al., 2010). Also, MAM is involved in ER stress and the UPR (Simmen et al., 2010; Verfaillie et al., 2012) and ALS mutant SOD1, TDP-43 and FUS all induce prolonged UPR (Farg et al., 2012; Saxena et al., 2009; Suzuki et al., 2011; Tong et al., 2012). Likewise, mutant SOD1 damages VDAC1 (Israelson et al., 2010) which is located in the outer mitochondrial membrane and interacts with IP3Rs in MAM via BiP (Rapizzi et al., 2002; Szabadkai et al., 2006).

Such perturbations to ER-mitochondria communications are predicted to induce some of the other pathogenic features of ALS. For example, altered Ca^{2+} exchange between ER and mitochondria is likely to impact on axonal transport of mitochondria since Ca^{2+} regulates this process (Chang et al., 2006; Macaskill et al., 2009; Rintoul et al., 2003; Saotome et al., 2008; Wang and Schwarz, 2009). Indeed, ALS mutant VAPB disrupts axonal transport and this is linked to ER-mitochondria Ca^{2+} exchange (De Vos et al., 2012; Morotz et al., 2012). Thus, a number of ALS associated insults can be linked to the ER-mitochondria axis and damage to this axis is likely to induce some of the pathogenic features of ALS.

Alterations to ER-mitochondria associations are predicted to have particularly detrimental effects to neurons. Tightening of contacts is likely to increase Ca^{2+} signalling between the two organelles, leading to mitochondria Ca^{2+} overload. This in

turn stimulates opening of the mitochondrial permeability transition pore and induction of apoptosis (Csordas et al., 2006; Rowland and Voeltz, 2012). By contrast, loosening of contacts will affect Ca^{2+}-dependent regulation of the tricarboxylic acid cycle and ATP synthesis in mitochondria (Csordas et al., 2006; Rowland and Voeltz, 2012). Mitochondria are enriched in synapses where they are required for generating ATP to maintain ionic potential and for regulating Ca^{2+} homeostasis. Thus, any damage to mitochondria or reduction in their ability to generate ATP is likely to have detrimental effects at the synapse. Synaptic loss is a key and early feature of ALS (Dadon-Nachum et al., 2011; De Vos et al., 2008).

1.4.1 Neurodegenerative diseases and alterations to ER-mitochondria associations

Studies such as those described above which highlight how neurodegenerative disease insults might target MAM and mitochondria proteins at the MAM interface have prompted examinations of ER-mitochondria connections in some disease states. To date, direct studies on the effects of neurodegenerative disease insults on ER-mitochondria contacts are restricted to Alzheimer's disease and Parkinson's disease.

Mutations in the genes encoding presenilins cause some forms of familial Alzheimer's disease. The presenilins (presenilin-1 and presenilin-2) are part of the γ-secretase complex that processes the amyloid precursor protein (APP) to release amyloid β-peptide (Aβ) that is deposited in the brains of Alzheimer's disease patients. Alterations to processing of APP and production of Aβ are believed to be major events in Alzheimer's disease. The presenilins are resident ER proteins (see for reviews (De Strooper and Annaert, 2010; Ho and Shen, 2011; Selkoe and Wolfe, 2007)). Moreover, both presenilin-1 and presenilin-2 are enriched in MAM (Area-Gomez et al., 2009).

Recently, the effects of Alzheimer's disease mutant presenilins on ER-mitochondria contacts have been studied although the results are a little conflicting. In one study, presenilin-2 but not presenilin-1 increases ER-mitochondria contacts whereas in the other, presenilin-1 increases ER-mitochondria contacts (Area-Gomez et al., 2012; Zampese et al., 2011). The presenilin-induced changes to ER-mitochondria contacts have been shown to induce alterations to both Ca^{2+} and lipid metabolism (Area-Gomez et al., 2012; Zampese et al., 2011).

α-synuclein is a major component of Lewy bodies that are a pathological feature of Parkinson's disease and some forms of dementia. Mutations in the *α-synuclein* gene cause familial forms of Parkinson's disease (see for reviews (Goedert et al., 2012; Lee and Trojanowski, 2006)). Damage to mitochondria is strongly linked to Parkinson's disease and some other mutant genes that cause familial Parkinson's disease encode mitochondrial proteins (see for reviews (Exner et al., 2012; Youle and van der Bliek, 2012)). A proportion of α-synuclein localizes to mitochondria (Cole et al., 2008; Devi et al., 2008; Shavali et al., 2008) and recently, α-synuclein has been shown to increase ER-mitochondria contacts and to influence mitochondrial Ca^{2+} levels (Cali et al., 2012).

Finally, mutations in the *Mitofusin-2* gene cause some Charcot-Marie-Tooth disease type 2A (Barisic et al., 2008) and there is evidence that mitofusin-2 forms some of the molecular tethers that directly link ER and mitochondria (de Brito and Scorrano, 2008).

1.4.2 ER-mitochondria tethering proteins

Despite the importance of ER-mitochondria interactions to fundamental biological processes, the mechanisms that control these interactions and in particular, the

molecular identity of the tethers that physically connect ER and mitochondria are poorly understood. Electron tomography studies reveal that ER and mitochondria are linked by structures of different length (10 nm at smooth ER and 25 nm at rough ER) and this suggests that a number of proteins can physically connect these organelles (Csordas et al., 2006).

In yeast, proteins of the ER-mitochondria encounter structure (ERMES) act as a molecular tether between ER and mitochondria but ERMES orthologs in higher eukaryotes have not so far been identified (Kornmann et al., 2009). In a major study, mitofusin-2 was shown to link ER and mitochondria in mammalian cells (de Brito and Scorrano, 2008) but these findings have not been properly replicated. Indeed, strong evidence has just been presented that mitofusin-2 does not play any role in juxtaposing ER and mitochondria (Cosson et al., 2012).

Phosphofurin acidic cluster sorting protein-2 (PACS-2) is a sorting protein believed to be involved in mediating vesicle sorting and trafficking and which is associated with both ER and mitochondria (Simmen et al., 2005). Silencing of PACS-2 uncouples ER from mitochondria but since this involves mitochondrial fragmentation and altered morphology, it has been concluded that this effect on ER-mitochondria associations is probably indirect (Simmen et al., 2005).

IP3R in MAM and VDAC in mitochondria physically interact via the molecular chaperone BiP and this prompted the suggestion that these molecules represent ER-mitochondria tethers (Rapizzi et al., 2002; Szabadkai et al., 2006). However, IP3R

knockout cells have intact ER-mitochondria interactions ruling out a major role for these proteins as structural linkers (Csordas et al., 2006).

Recently, work from our research group identified the mitochondrial protein, PTPIP51 as a binding partner for the resident ER protein VAPB (De Vos et al., 2012). VAPB is anchored in the ER via a C-terminal membrane-spanning domain and its N-terminus projects into the cytoplasm (Kagiwada et al., 1998). PTPIP51 is anchored in the outer mitochondrial membrane via an N-terminal mitochondrial targeting sequence such that its C-terminus projects into the cytoplasm (De Vos et al., 2012). As such, VAPB and PTPIP51 represent candidate proteins for the structural tethers connecting ER with mitochondria that can be visualised by electron microscopy.

VAPB is described in detail above (see Section 1.2.4). PTPIP51 is a relatively poorly studied protein that is also known as family with sequence similarity 82 member A2 (FAM82A2), human cerebral protein-10 and regulator of microtubule dynamics protein-3 (RMD-3). PTPIP51 binds to protein tyrosine phosphatase-1B (PTP1B) and T-cell protein tyrosine phosphatase (Brobeil et al., 2010; Stenzinger et al., 2005) but the functional significance of these interactions is unclear. PTPIP51 also binds 14-3-3 proteins (Brobeil et al., 2012; Petri et al., 2011; Yu et al., 2008) but again, it is not clear how these interactions impact upon cellular function. RMD-3 is a putative homologue of PTPIP51 in *C. elegans* and another RMD family member, RMD-1 functions in chromosome segregation (Oishi et al., 2007). However, in mammalian cells PTPIP51 is an outer mitochondrial protein of unclear function that has been implicated in the regulation of cell morphology, motility and apoptosis and which contains an N-terminal transmembrane domain and a central coiled-coil domain (Brobeil et al., 2011; De Vos et

al., 2012; Lv et al., 2006; Yu et al., 2008). Both VAPB and PTPIP51 are ubiquitously expressed although their expression levels vary in different tissues (Lv et al., 2006; Skehel et al., 2000; Stenzinger et al., 2005).

1.5 Aims of the thesis

As detailed above, the finding that VAPB and PTPIP51 interact raised the possibility that these proteins represent at least some of the molecular tethers visualised in electron microscopy studies that physically link ER and mitochondria. Moreover, since mutant VAPB causes some forms of ALS, it is possible that defects in ER-mitochondria tethering and especially any involving VAPB and PTPIP51 might feature in ALS. The aims of this thesis were to investigate further these possibilities and specifically, to test two related hypotheses. The first is that the VAPB-PTPIP51 interaction mediates ER-mitochondria associations. The second is that ALS associated TDP-43 disrupts ER-mitochondria associations and that this disruption is linked to changes in the VAPB-PTPIP51 interaction. In addition, studies were commenced to investigate how mutant SOD1 and FUS influence the VAPB-PTPIP51 interaction and to test whether phosphorylation of either VAPB or PTPIP51 regulates their binding.

CHAPTER 2: MATERIALS AND METHODS

Unless stated otherwise, all chemicals were purchased from Sigma-Aldrich Co. (UK). All solutions and buffers were prepared using ultrapure water (resistivity ≥ 18.2 MΩ-cm) from an ELGA Purelab Ultra purification system (Veolia Water Systems Ltd., UK). When required, solutions were sterilised either by autoclaving or by filtration through a 0.2 μm pore size syringe filter (Nalgene).

In the text, some commonly used organic compounds are referred to using their non-systematic instead of systematic names, according to the guidelines of the International Union of Pure and Applied Chemistry: e.g., bromophenol blue was used instead of 4'-(1,1-dioxido-3H-2,1-benzoxathiole-3,3-diyl)bis(2,6-dibromophenol) (Panico, 1993). All units are written according to the guidelines of the Bureau International des Poids et Mesures (International Bureau of Weights and Measures) (BIPM, 2006).

2.1 Materials

2.1.1 Stock solutions

Acrylamide-bis-acrylamide (30%, 37:5:1 stabilised solution; Geneflow, UK)

Ammonium persulphate (APS; 10% (w/v); Geneflow, UK)

Ampicillin (amp; 100 mg/ml, filter sterilised)

β-mercaptoethanol (100%)

Bovine serum albumin (BSA; 5% (w/v))

Brilliant Blue G-Colloidal Coomassie

Citric acid (1 M)

4′, 6-diamidino-2-phenylindole (DAPI; 0.5 mg/ml in DMSO)

Dimethyl sulphoxide (DMSO; 100%)

Dithiothreitol (DTT; 1 M)

Ethanol (70% v/v)

Ethidium bromide (10 mg/ml)

Ethylenediaminetetraacetic acid (EDTA; 0.5 M)

Ethylene glycol-bis (β-aminoethylether) N,N,N’,N’-tetraacetic acid (EGTA; 0.5 M)

Fetal bovine serum (100%; Sera Laboratories)

Glacial acetic acid (100%)

Glycerol (10%, 50% and 100% v/v, autoclaved)

Glutaraldehyde (50%, distilled/EM grade; TAAB)

Hydrogen chloride (HCl; 1 M)

Hydrogen peroxide (30% w/w)

Kanamycin (100 mg/ml, filter sterilised)

K-HEPES ((4-(2-hydroxyethyl)piperazine-1-ethanesulfonic acid); 1 M; buffered with KOH to pH 7.4)

L-glutamine (200 mM; Invitrogen)

Magnesium chloride ($MgCl_2$; 1 M)

Methanol (100%)

Paraformaldehyde (PFA; 4% w/v in PBS)

Penicillin (10,000 IU/ml) and streptomycin (10 mg/ml; PAA Laboratories)

Pervanadate (100X)

Phenylmethysulphonyl fluoride (PMSF; 100 mM in isopropanol)

Phosphate-buffered saline (PBS; 10 mM phosphate buffer, 2.7 mM potassium chloride, 137 mM sodium chloride, pH 7.4 tablets)

Sodium azide (10% w/v)

Sodium dodecyl sulphate (SDS; 10% (w/v))

Sodium chloride (NaCl; 5 M)

Sodium hydroxide (NaOH; 10 M)

Sodium orthovanadate (Na_3VO_4; 200 mM, activated, pH 10.0)

N,N,N',N'-Tetramethylethylenediamine (TEMED; 100%)

Tris (hydroxymethyl) amino methane (Tris-HCl, buffered with HCl to pH 6.8-8.8)

Tris-buffered saline (TBS; 50 mM Tris, 150 mM NaCl, buffered with HCl to pH 7.6)

Trypsin-EDTA solution (1x; 0.05% trypsin, 0.02% EDTA in PBS; PAA Laboratories)

Tris-citrate (1 M Tris; buffered with citric acid to pH 7.4)

Triton X-100 (100%)

Tween-20 (100%)

2.1.2 General molecular biology reagents

2.1.2.1 Plasmids

See Tables 2.1 and 2.2 below

Table 2.1 Vectors

Vector	Vector Use	Manufacturer
pCI-neo	Mammalian expression vector	Promega
pEGFP-C1	Mammalian expression vector	Clontech
pECFP-N1	Mammalian expression vector	Clontech
pIRES2-AcGFP	Mammalian expression vector	Clontech

Table 2.2 Mammalian expression plasmids

Protein expressed	Vector backbone	Reference or source of plasmid
PTPIP51-HA+ phosphomutants	pCI-neo	(De Vos et al., 2012)
Myc-VAPB+ phosphomutants	pCI-neo	(De Vos et al., 2012)
EGFP	pEGFP-C1	Clontech
ECFP	pECFP-N1	Kurt De Vos (IoP)
ECFP-VAPB	pECFP-N1	Kurt De Vos (IoP)
pIRES2-GFP-PTPIP51-HA	pIRES2-AcGFP	Kurt De Vos (IoP)
EGFP-SOD1 EGFP-SOD1 G93A EGFP-SOD1 A4V	pEGFP-C1	(De Vos et al., 2007)
EGFP-TDP-43 EGFP-TDP-43 M337V EGFP-TDP-43 Q331K EGFP-TDP-43 A382T EGFP-TDP-43 G348C	pEGFP-C1	(Sreedharan et al., 2008)

EGFP-FUS EGFP-FUS R521C EGFP-FUS R521G EGFP-FUS R521H EGFP-FUS R518K	pEGFP-C1	Emma Gray (IoP)

2.1.2.2 Oligonucleotides

All the mutagenic oligonucleotides I used in these studies are listed in Table 2.3. PTPIP51$^{S44A/S46A/S50A}$, PTPIP51$^{S44D/S46D/S50D}$, PTPIP51$^{S212A/S221A/S225A}$, PTPIP51$^{S212A/S221A/S225D}$, PTPIP51$^{S44A/S46A/S50A/S212A/S221A/S225A}$ and PTPIP51$^{S44D/S46D/S50D/S212D/S221D/S225D}$ were obtained by mutating serine to alanine or aspartate respectively. In order to generate PTPIP51 constructs with all 6 phosphorylation sites mutated to alanine or aspartate, PTPIP51$^{S212A/S221A/S225A}$ and PTPIP51$^{S212D/S221D/S225D}$ were used as a template in a mutagenesis reaction with the primers for serine positions 44, 46 and 50. VAPB$^{T150A/S158A}$, VAPB$^{T150D/S158D}$, VAPB$^{S146A/T150A/S156A/S158A/S159A/S160A}$ and VAPB$^{S146D/T150D/S156D/S158D/S159D/S160D}$ were obtained by mutating serine or threonine to alanine and aspartate respectively.

Table 2.3 Mutagenic primers

Construct	Mutagenic primers
PTPIP51$^{S44A/S46A/S50A}$	5’-CAGCGTCATGGCCGCGCCCAGGCCCTGCCCAACGC CCTGGACTATACGCAG-3’ 5’-CTGCGTATAGTCCAGGGCGTTGGGCAGGGCCTGG GCGCGGCCATGACGCTG-3’
PTPIP51$^{S44D/S46D/S50D}$	5’-CAGCGTCATGGCCGCGACCAGGACCTGCCCAACG ACCTGGACTATACGCAG-3’ 5’-CTGCGTATAGTCCAGGTCGTTGGGCAGGTCCTGGT CGCGGCCATGACGCTG -3’

PTPIP51$^{S212A/S221A/S225A}$	5’-GGGAGAAAGGATGCTCTTGACTTGGAGGAAGAGG CAGCTGCAGGTGCCTCCGCTGCCCTGGAGGCTGG-3’ 5’-CCAGCCTCCAGGGCAGCGGAGGCACCTGCAGCTGC CTCTTCCTCCAAGTCAAGAGCATCCTTTCTCCC-3’
PTPIP51$^{S212D/S221D/S225D}$	5’-GGGAGAAAGGATGATCTTGACTTGGAGGAAGAGG CAGCTGACGGTGCCTCCGATGCCCTGGAGGCTGG-3’ 5’-CCAGCCTCCAGGGCATCGGAGGCACCGTCAGCTG CCTCTTCCTCCAAGTCAAGATCATCCTTTCTCCC-3’
VAPB$^{T150A/S158A}$	5’-CAAAGACAGAAGCACCAATAGTGTCTAAGTCTCTG GCTTCTTCTTTGG-3’ 5’-CCAAAGAAGAAGCCAGAGACTTAGACACTATTGG TGCTTCTGTCTTTG-3’
VAPB$^{T150D/S158D}$	5’-CAAAGACAGAAGATCCAATAGTGTCTAAGTCTCTGG ATTCTTCTTTGG-3’ 5’-CCAAAGAAGAATCCAGAGACTTAGACACTATTGGA TCTTCTGTCTTTG-3’
VAPB$^{S146A/T150A/S156A/S158A/S159A/S160A}$	5’-CCACAACTGCAGCAAAGACAGAAGCACCAATAGTG TCTAAGGCTCTGGCTGCTGCTTTGGATGACACCGAAG-3’ 5’-CTTCGGTGTCATCCAAAGCAGCAGCCAGAGCCTTA GACACTATTGGTGCTTCTGTCTTTGCTGCAGTTGTGG-3’
VAPB$^{S146D/T150D/S156D/S158D/S159D/S160D}$	5’-CCACAACTGCAGACAAGACAGAAGACCCAATAGTG TCTAAGGATCTGGATGATGATTTGGATGACACCGAAG-3’ 5’-CTTCGGTGTCATCCAAATCATCATCCAGATCCTTAG ACACTATTGGGTCTTCTGTCTTGTCTGCAGTTGTGG-3’

2.1.2.3 Growth of *E. coli* for DNA purification: media

Luria Bertani (LB) broth (powder; Invitrogen), 20 g/L sterilised by autoclaving

LB agar (powder; Invitrogen), 32 g/L sterilised by autoclaving

LB-amp broth (LB broth; ampicillin 100 µg/ml)

LB-kan broth (LB broth; kanamycin 80 µg/ml)

LB-amp/LB-kan agar (LB agar; ampicillin 100 µg/ml or kanamycin 80 µg/ml added when agar is less than 55°C)

Bacteria containing plasmids of interest were stored at -70°C in sterile 25% glycerol (v/v) solution in LB-amp or LB-kan broth.

2.1.2.4 Plasmid DNA preparation from *E. Coli*

Plasmids were isolated using a QIAprep® Spin Miniprep Kit (Qiagen Ltd, Hilden, Germany); the following reagents are provided with the kit:

Resuspension buffer P1 supplemented with RNase A

Lysis buffer P2

Neutralisation buffer N3

Wash buffer PB

Wash buffer PE supplemented with ethanol (70% (v/v) final ethanol concentration)

Elution buffer TE (10 mM Tris-HCl pH 8.0)

2.1.2.5 Agarose gel electrophoresis of nucleic acids

Solution for loading DNA samples in agarose gels (6X solution)

0.25% Bromophenol blue (w/v)

40% Sucrose (w/v)

Tris-Acetate-EDTA (TAE) running buffer (50X solution)

2 M Tris

5.7 % glacial acetic acid (v/v)

50 mM EDTA

pH to 8

Nucleic acid size markers

Phage λ DNA digested with Hind III (sizes in base pairs): 23,131; 9419; 6434; 4335; 2322; 2023; 564; 125.

1 kb DNA ladder (NEB; sizes in kilo bases): 10; 8; 6; 5; 4; 3; 2; 1.5; 1; 0.5.

2.1.2.6 Site-directed mutagenesis

Site-directed mutagenesis was performed using the QuikChange® XL mutagenesis kit (Stratagene). XL10-Gold® ultracompetent cells were provided with the kit. The following materials are supplied with the QuikChange® XL PCR-based site-directed mutagenesis kit:

Oligonucleotide control primer #1 (100 ng/μl):

5'-CCATGATTACGCCAAGCGCGCAATTAACCCTCAC-3'

Oligonucleotide control primer #2 (100 ng/μl):

5'-GTGAGGGTTAATTGCGCGCTTGGCGTAATCATGG-3'

pWhitescript™ 4.5 kb control template (5 μg/μl)

pUC18 transformation control plasmid (0.1 ng/μl in TE buffer)

QuickSolution

PfuTurbo® DNA polymerase

Dpn I restriction enzyme

XL10-Gold® ultracompetent cells

XL10-Gold® β-mercaptoethanol mix

Deoxyribonucleotide triphosphate (dNTP) mix (the composition of the mix is proprietary)

10X mutagenesis buffer

200 mM Tris-HCl (pH 8.8)

100 mM KCl

100 mM $(NH_4)_2SO_4$

20 mM $MgSO_4$

1% Triton X-100 (v/v)

1 mg/ml BSA

2.1.3 Protein analysis

2.1.3.1 Protein sample preparation

1X SDS sample buffer

50 mM Tris-HCl pH 6.8

2% SDS (w/v)

0.1% Bromophenol blue (w/v)

10% Glycerol (v/v)

100 mM DTT

5X SDS sample buffer

250 mM Tris-HCl pH 6.8

10% SDS (w/v)

0.5% Bromophenol blue (w/v)

50% Glycerol (v/v)

500 mM DTT

2.1.3.2 Sodium dodecyl sulphate-polyacrylamide gel electrophoresis (SDS-PAGE)

Resolving gel

375 mM Tris-HCl pH 8.8

8-12% Acrylamide (v/v)

0.1% SDS (w/v)

0.1% APS (w/v)

0.05% TEMED

Stacking gel

125 mM Tris-HCl pH 6.8

5 % Acrylamide (v/v)

0.1% SDS (w/v)

0.1% APS

0.1 % TEMED

Running Buffer

25 mM Tris

250 mM Glycine

0.1% SDS (w/v)

Electrophoresis markers

PageRuler™ Prestained Protein Ladder (Fermentas); 3-color ladder with 10 protein bands, sizes in kDa: 170; 130; 100; 70; 55; 40; 35; 25; 15; 10.

Precision Plus Protein Standards (Biorad); high molecular weight, sizes in kDa: 250; 150; 100; 75; 50; 37, 25; 20; 15; 10.

2.1.3.3 Immobilisation of proteins on nitrocellulose membranes

Blotting (transfer) buffer

25 mM Tris

192 mM Glycine

20% Methanol (v/v)

TBS-Tween (Tris-HCl buffered saline; Tween-20)

TBS pH 7.6

0.1% Tween-20 (v/v)

2.1.3.4 Antibody probing of membrane-bound proteins

Blocking buffer

0.1% (v/v) Tween-20

5% (w/v) dried skimmed milk in TBS

TBS-Tween

0.1% (v/v) Tween-20 in TBS

Enhanced chemiluminescence (ECL) development reagent kit (GE Healthcare)

The following reagents are provided with the kit:

Detection solution A (luminol solution)

Detection solution B (peroxide solution)

2.1.3.5 Protein staining

Colloidal Coomassie

16% Brilliant Blue G-Colloidal Coomassie (v/v)

20% Methanol (v/v)

Destain I

7% Glacial acetic acid (v/v)

25% Methanol (v/v)

Destain II

2% Glacial acetic acid (v/v)

25% Methanol (v/v)

Ponceau S red solution for staining of immunoblots

0.2% Ponceau S (w/v) in 7% glacial acetic acid (v/v)

2.1.4 Immunoprecipitation reagents

Immunoprecipitation lysis buffer

50 mM Tris-citrate pH 7.4

150 mM NaCl

1% (v/v) Triton X-100

5 mM EGTA

5 mM EDTA

EDTA-free Complete™ Protease Inhibitor Cocktail

PBS-Triton

0.1% (v/v) Triton X-100 in PBS

2.1.5 Antibodies

2.1.5.1 Primary antibodies

For a list of primary antibodies used in these studies see Table 2.4

Table 2.4 Primary antibodies

Antibody	Supplier	Monoclonal/Polyclonal, Species	Working dilution
GFP	Abcam	Polyclonal, rabbit	1:5000 (IB)
HA	Sigma	Polyclonal, rabbit	1:5000 (IB) 1:300 (IP)
9B11 (myc-tag)	Cell Signaling	Monoclonal, mouse	1:5000 (IB) 1:300 (IP)
Actin (AC-40)	Sigma	Monoclonal, mouse	1:5000 (IB)
α-tubulin (DM1A)	Sigma	Monoclonal, mouse	1:40,000 (IB)
PDI (RL77)	Affinity BioReagents	Monoclonal, mouse	1:2000 (IB) 1:200 (IF)
TOM20	Santa Cruz Biotechnology	Polyclonal, rabbit	1:200 (IF)
FAM82A2	Atlas Antibodies	Polyclonal, rabbit	1:1000 (IB)
PTPIP51 (#skr10)	In house; (De Vos et al., 2012)	Polyclonal, rabbit	1:200 (IF)
VAPB (#SK83)	In house; (Tudor et al., 2010)	Polyclonal, rat	1:2000 (IB)
VAPB (#3503)	In house; (Tudor et al., 2010)	Polyclonal, rabbit	1:200 (IF)
Mitofusin2	Sigma	Polyclonal, rabbit	1:5000 (IB)
Phospho-tyrosine (4G10)	Chemicon	Monoclonal, mouse	1:5000 (IB)

IB-immunoblot, IF-immunofluorescence, IP-immunoprecipitation

2.1.5.2 Secondary antibodies

For a list of secondary antibodies used in these studies see Table 2.5

Table 2.5 Secondary antibodies

Antibody	Supplier	Monoclonal/Polyclonal, Species	Working dilution
Anti-mouse Ig conjugated to horseradish peroxidase	Dako	Polyclonal, rabbit	1:5000 (IB)
Anti-rabbit Ig conjugated to horseradish peroxidase	Dako	Polyclonal, goat	1:5000 (IB)
Anti-rat Ig conjugated to horseradish peroxidase	Southern Biotech	Polyclonal, goat	1:5000 (IB)
Anti-mouse IgG coupled with Alexa Fluor 488	Invitrogen	Polyclonal, goat	1:500 (IF)
Anti-mouse IgG coupled with Alexa Fluor 568	Invitrogen	Polyclonal, goat	1:500 (IF)
Anti-rabbit IgG coupled with Alexa Fluor 647	Invitrogen	Polyclonal, goat	1:500 (IF)
Anti-mouse IgG coupled with Alexa Fluor 350	Invitrogen	Polyclonal, goat	1:500 (IF)

IB-immunoblot, IF-immunofluorescence

2.1.6 Fluorescence microscopy

Fixing solution

4% paraformaldehyde in PBS (v/v) 0.1% glutaraldehyde (v/v)

Quenching solution

0.05 M NH_4Cl in PBS

Permeabilising solution

0.25% Triton X-100 in PBS (v/v)

Blocking/antibody incubation solution

3% BSA in PBS (w/v)

Mowiol-DABCO mounting medium

10% (w/v) Mowiol® 4-88 (Calbiochem)

25% (w/v) glycerol

100 mM Tris-HCl pH 8.5

2.5% (w/v) DABCO (1,4-diazobicyclo[2.2.2]octane)

2.1.7 Duolink® *in situ* Proximity Ligation Assay (PLA)

The following reagents are provided with the Duolink® *in situ* PLA™ kit (Olink Bioscience, Uppsala, Sweden):

PLA probes MINUS and PLUS (secondary antibodies conjugated with a PLA nucleotide)

Antibody Diluent

Detection Reagent Orange (579 nm emission)

Ligation solution (5x) – Contains oligonucleotides that hybridize to the PLA probes and all components needed for ligation except the Ligase

Ligase (1 U/µl)

Amplification solution (5x) – Contains all components needed for Rolling Circle Amplification (RCA) except the Polymerase. Included are also oligonucleotide probes labeled with a fluorophore that hybridize to the RCA product

Polymerase (10 U/µl)

Wash Buffers A and B

2.1.8 Electron microscopy

Fixing solution

2.5% glutaraldehyde in 0.1M cacodylate buffer pH 7.2

Post-fixation solution

1% osmium tetroxide in 0.1M cacodylate buffer

Staining solutions

saturated uranyl acetate in 50% ethanol

0.1N lead citrate in NaOH

2.1.9 Mammalian cell culture

Chinese Hamster Ovary (CHO) cell medium

Nutrient Mixture Ham F-12 (HAM) with L-glutamine

10% fetal bovine serum (v/v)

100 U/ml Penicillin

100 µg/ml Streptomycin

CV-1, HEK293 and NSC34 cell medium

DMEM with 4.5 g/L glucose and L-glutamine

10% fetal bovine serum (v/v)

100 U/ml Penicillin

100 µg/ml Streptomycin

1X Trypsin-EDTA solution

0.25% Trypsin

1 mM EDTA

2.2 Methods

2.2.1 General microbiology methods

2.2.1.1 Storage and growth of *E. coli* for DNA purification

E. coli containing plasmids of interest were stored at -70 °C in sterile 25% (v/v) glycerol solution in LB broth containing the appropriate antibiotic for the plasmid vector.

To grow bacteria for DNA purification, *E. coli* containing the plasmid of interest were streaked out on LB agar plates (see section 2.1.2.3) containing the appropriate antibiotic for the plasmid vector and grown for 16 hours at 37°C. Single bacterial colonies were picked and grown in 5 ml LB-ampicillin broth or LB-kanamycin broth (see section 2.1.2.3) for approximately 16 hours at 37°C while shaking at 220 rpm. For larger culture volumes, 1 ml of confluent *E. coli* culture was added for each 100 ml of LB broth and cultured for a further 16 hours.

2.2.1.2 Preparation of plasmid DNA

The QIAfilter Plasmid Maxi and QIAgen Miniprep Kits (Qiagen Ltd.) were used according to manufacturer's instructions. These kits are based on the alkaline lysis method of DNA recovery (Sambrook et al., 1989). Typically 200 ml of culture was used for the Maxi Kit, resulting in approximately 500 μg of pure plasmid DNA and 5 ml of culture was used for the Miniprep Kit, resulting in approximately 25 μg of pure plasmid DNA.

2.2.1.3 Quantitation of nucleic acids

Spectrophotometric quantitation of plasmid DNA was performed using a NanoDrop 1000 (Thermo Scientific) spectrophotometer. The absorbance of samples at 260 nm and 280 nm was recorded. An optical density (OD) reading of 1 at a wavelength of 260 nm corresponds to a concentration of 50 µg/ml for double stranded DNA. Proteins are known to strongly absorb at a wavelength of 280 nm thus the ratio of OD readings at 260 and 280 nm ($OD_{260/280}$) gives an indication of purity of the sample. Pure DNA has an $OD_{260/280}$ value of 1.8 (Sambrook et al., 1989).

Plasmid DNA concentrations were also roughly quantified using ethidium bromide fluorescent quantitation. This method relies on the ability of ethidium bromide to bind to DNA. UV-induced fluorescence emitted by DNA-linked ethidium bromide is proportional to the total mass of DNA. The amount of DNA in a sample could then be quantified by visual comparison with the UV-induced fluorescence of a known quantity of a DNA standard or series of standards. This technique has a detection limit of as little as 5 ng of DNA.

2.2.1.4 Restriction enzyme digestion of plasmid DNA

Plasmid DNA was digested using the appropriate restriction enzyme and corresponding buffer according to the manufacturer's instructions (Invitrogen). 10 units of enzyme were used per µg of DNA (1 unit is usually the amount of enzyme required to cleave 1 µg of DNA in 1 hour at 37°C in the appropriate buffer). The volume of enzyme never exceeded 10% (v/v) of final reaction volume and the incubation time with the enzyme was 2 hours at 37°C. A typical diagnostic reaction contained 500 ng plasmid, 1 µl (10

units) restriction enzyme, 2 µl of 10x buffer in a final volume of 20 µl; all of the reaction was loaded and analysed by agarose gel electrophoresis.

2.2.1.5 Agarose gel electrophoresis of plasmid DNA

Agarose (ultra pure, electrophoresis grade, Invitrogen) was dissolved in boiling TAE buffer (see section 2.1.2.5) in a final concentration of 0.6-1.5% (w/v) and cast on a gel bed with a suitable comb using a horizontal gel apparatus (Hybaid). On setting, gels were placed in an electrophoresis tank containing TAE buffer to a level just above the gel surface. DNA samples containing DNA loading buffer (see Section 2.1.2.5) were loaded into the sample wells and were run at 100 V. Gels were stained with 10 µg/ml ethidium bromide to visualise DNA. Gels were then placed on a 3UV™ transilluminator emitting ultra violet light (λ=302 nm), visualised on a Sony video monitor and videographed using a Sony video graphic printer.

To determine the size of the separated DNA, nucleic acid size markers were used:
Phage λ DNA digested with Hind III, 1 kb DNA ladder.

2.2.1.6 PCR-based site-directed mutagenesis

PTPIP51-HA and myc-VAPB alanine/aspartate mutant constructs were generated using the mutagenic primers listed in Section 2.1.2.2 and a QuikChange® XL site-directed mutagenesis kit (Stratagene) according to the manufacturer's instructions (see Section 2.1.2.6).

The QuikChange® XL site-directed mutagenesis system is designed to produce mutations in double stranded plasmids using primers containing the entire mutation and

the high fidelity, thermostable PfuTurbo® DNA polymerase in PCR. Experimental reactions and control reactions, to test mutation efficiency using pWhitescript™ control plasmid, were set up as shown below and used for PCR as shown in Table 2.6. The pWhitescript™ mutagenesis control plasmid contains a stop codon instead of a glutamine codon in the gene of β-galactosidase thus β-galactosidase is inactive in cells containing this plasmid. Competent cells containing this plasmid appear white on LB-ampicillin agar plates pre-spread with X-gal (5-bromo-4-chloro-3-indoyl-β-D-galactopyranoside) and IPTG (isopropyl-1-thio-β-D-galactopyranoside) because the inactive β-galactosidase enzyme is unable to cleave X-gal to galactose and an insoluble blue product. During the mutagenesis the control primers mutate the stop codon back to glutamine in the β-galactosidase gene. The active β-galactosidase is able to cleave X-gal and the appearing blue products are obvious markers of the successful mutagenesis.

Reactions were performed in 0.2 ml PCR tubes (Thermo Fisher). Reactions were mixed gently by pipetting and then placed in a T3 Thermocycler (Biometra) for the PCR (cycling parameters are shown in Table 2.6). The lowest number of amplification cycles was used to minimise the possibility of errors by the DNA polymerase whilst at the same time generating enough amplified product for DNA purification. A sample of each PCR product was analysed for size, quality and quantity by restriction enzyme digestion and agarose gel electrophoresis alongside appropriate DNA markers (see Section 2.2.1.5).

Control reaction (reagents, except H_2O were supplied with the kit):

2 µl (10 ng) of pWhitescript™ control template DNA

5 µl of 10x mutagenesis buffer (see Section 2.1.2.6)

1 µl of dNTP mix

1.25 µl (125 ng) of oligonucleotide control primer #1

1.25 µl (125 ng) of oligonucleotide control primer #2

3 µl QuickSolution

36.5 µl H_2O to final volume of 50 µl

1 µl (2.5 U/µl) PfuTurbo® DNA polymerase

Experimental reaction (reagents, except DNA template, oligonucleotides and H_2O, were supplied with the kit):

5 µl of 10x mutagenesis buffer

10 ng DNA template

1 µl dNTP mix

125 ng of each oligonucletide

3 µl QuickSolution

H_2O to a final volume of 50 µl

1 µl (2.5 U/µl) PfuTurbo® DNA polymerase

Table 2.6 PCR-based site-directed mutagenesis cycling parameters

Step	Cycles	Temperature (°C)	Time
1	1	95	1 minute
2	18	95	50 seconds
		60	50 seconds
		68	1 minute/kb of plasmid length
3	1	68	7 minutes

2.2.1.7 Digesting the PCR product

Following PCR, the reactions were placed on ice, 1 µl (10 U/µl) of the Dpn I restriction enzyme (supplied with the kit) was added and the reaction was incubated at 37°C for 1 hour. The Dpn I endonuclease (target sequence 5'-Gm^{6}ATC-3') is specific for methylated and hemimethylated DNA and is used to digest parental DNA and to select for mutation-containing amplified DNA.

2.2.1.8 Transformation into XL10-Gold® ultracompetent cells

2 µl of XL10-Gold® β-mercaptoethanol mix (provided with the kit) was added to 45 µl thawed XL10-Gold® ultracompetent cells (provided with the kit) and the reaction incubated on ice for 10 minutes. 2 µl of the Dpn I-treated DNA was transferred to the competent cells and the reaction incubated on ice for 30 minutes. A second control was set up to verify transformation efficiency: 0.1 ng of pUC18 transformation control plasmid (provided with the kit) was added to 45 µl XL10-Gold® ultracompetent cells and incubated on ice for 30 minutes. The cells were then heat pulsed for 30 seconds at 42°C, and then placed on ice for 2 minutes. Following the heat pulse, 0.5 ml of super optimal broth with catabolite repression (S.O.C.) medium (Invitrogen) was added to the cells. Following incubation at 37°C for 1 hour with shaking at 220 rpm, the samples were spread on LB-kanamycin agar plates. The transformed control pWhitescript™ and pUC18 cells were plated on LB-ampicillin agar plates pre-spread with 40 µl of X-gal (20 mg/ml in DMSO) and 20 µl of 100 mM IPTG for colour selection. The plates were incubated at 37°C for 16 hours. The successfully mutagenised pWhitescript™ control colonies appeared as blue colonies. The number of pUC18 control colonies was greater than 100 colonies and most of them displayed the blue phenotype. The number of the

colonies for the experimental reaction was about 50 colonies. Plasmid DNAs were sequenced by Eurofins MWG Operon, UK to confirm the mutagenesis.

2.2.2 Protein analysis

2.2.2.1 Protein concentration determination (Bradford Assay)

Determination of protein concentration was carried out using a Bio-Rad protein assay kit according to the manufacturer's instructions (Bio-Rad, UK). The assay is using the colorimetric reaction described by Bradford (Bradford, 1976). The assay is based on the observation that the maximum absorbance for an acidic solution of Coomassie Brilliant Blue G-250 shifts from 465 nm to 595 nm when binding to protein occurs. In brief, eight dilutions were prepared from a freshly prepared BSA standard and four dilutions from each protein sample with the Bradford reagent. 50 µl of each dilution was transferred to a 96 well microtiter plate and absorbance readings were recorded at a wavelength of 595 nm using a VICTOR3 multilabel plate reader (Perkin Elmer). Sample protein concentrations were calculated using the recorded absorbance values and a standard curve drawn from the freshly prepared BSA standard.

2.2.2.2 SDS-PAGE of protein samples

For SDS-PAGE analyses of cell lysates, cells were washed in PBS, lysed on ice in appropriate amounts of 1x SDS sample buffer (final concentration 2 % SDS; see section 2.1.3.1) and then heated on a heat block for 5 minutes at 100 ºC. The protein samples were then separated by SDS-PAGE using the Mini-PROTEAN 3 gel electrophoresis system (Bio-Rad) with a discontinuous buffer system. Depending on the size of the proteins of interest, 8, 10 or 12% (v/v) acrylamide gels (see Section 2.1.3.2) were run at

a voltage of 100 V, until the dye front reached the bottom of the gel or proteins were separated as necessary.

To follow the progress of protein separation and to determine protein size, Precision Plus Protein Standards (Biorad) were used (see Section 2.1.3.2).

2.2.2.3 Immunoblotting (Western Blotting)

After SDS-PAGE, proteins were transferred from gels to a Protran nitrocellulose membrane (0.45 μm pore size; Whatman) using the wet method with the following filter sandwich:

Cathode – sponge / extra thick cellulose blot paper (Whatman) / SDS-PAGE gel / nitrocellulose membrane / extra thick cellulose blot paper / sponge – Anode.

This sandwich was assembled whilst totally immersed in transfer buffer (see Section 2.1.3.3), secured in cassettes and placed in a Mini Trans-Blot electrophoretic transfer cell (Biorad), and run at 100 V for 60 minutes or at 30 V for 16 h. Membranes containing transferred proteins were referred to as “blots”. Blots were incubated with Ponceau S solution (see Section 2.1.3.5) for 1 to 2 minutes to determine the efficiency of protein transfer. Blots were then rinsed for 1 to 2 minutes with ultrapure water to destain.

2.2.2.4 Antibody probing of membrane-bound proteins

Blots were incubated in blocking buffer (see Section 2.1.3.4) for 30 minutes at 20°C to reduce non-specific antibody binding. Blots were then incubated with an appropriate dilution of primary antibody in blocking buffer for 16 h at 4 °C (table 2.4 gives the

details of all primary antibodies used). Blots were then washed (3 x 10 minutes) in TBS-Tween (see Section 2.1.3.4) and an appropriate dilution of horseradish peroxidase-coupled secondary antibody in TBS-Tween was added for 1 hour at 20°C. Secondary antibodies were used depending on the species in which the primary antibody was raised (for details see Table 2.5). Following washing with TBS-Tween (3 x 10 minutes), immunoreactive species were visualised using enhanced chemiluminescence (ECL) development reagents (see Section 2.1.3.4) and Hyperfilm-ECL (GE Healthcare), according to the manufacturer's instructions. ECL protein signal visualisation is based on antibody bound horseradish peroxidase catalysed oxidation of luminol in the presence of hydrogen peroxide in alkaline conditions. Oxidised luminol is in an increased energy state and when luminol returns to ground state it emits the energy as light. In ECL detection the light output of luminol is enhanced by the presence of chemical enhancers (Whitehead et al., 1979). The light emission maximum of luminol is at 428 nm which is easily detectable by blue light sensitive autoradiography films. To visualise nitrocellulose membrane-bound proteins, detection solution A (luminol solution) and detection solution B (peroxide solution) were mixed in a 1:1 ratio in a final volume of 0.125 ml/cm^2 nitrocellulose membrane and incubated with the blot for 3 minutes at 20 ºC. Following incubation, blots were placed in an X-ray film cassette and Hyperfilm-ECL was placed on top of the membrane in a dark room, and exposed for a time varying between 5 seconds and 1 hour. The Hyperfilm-ECL was developed using a Konica Minolta SRX-101A developer.

Developed films were scanned using an Epson Perfection V700 Photo scanner (Seiko Epson Corp.). Signals on films were background-corrected and quantified using ImageJ developed by Wayne Rasband (NIH, Bethesda, USA; http://rsb.info.nih.gov/ij/) (Staal

et al., 2004). Each of the background-corrected OD signals was compared to an OD calibration curve obtained from a calibrated OD step tablet (Kodak) to ensure that signals were obtained within the linear range of the film. Only the signals within the linear OD range were used for statistical analysis.

In experiments investigating the effects of TDP-43, FUS and SOD1 on binding of PTPIP51 to VAPB (Chapter 4), signals from co-immunoprecipitating VAPB were normalized to immunoprecipitated PTPIP51-HA signals. The individual values were then compared to control EGFP signals; control signals were assigned a reference value of 1. In experiments investigating the effects of mutated phosphorylation sites in PTPIP51 (Chapter 5), signals from co-immunoprecipitating VAPB were normalized to immunoprecipitated PTPIP51-HA signals. The individual values from the mutants were then compared to wild-type PTPIP51 signals. Finally, in experiments investigating the effects of mutated phosphorylation sites in VAPB (Chapter 5), signals from co-immunoprecipitating PTPIP51 were normalized to immunoprecipitated myc-VAPB signals. The individual values from the mutants were then compared to wild-type VAPB signals. Statistical analyses were performed using GraphPad Prism 5 software (GraphPad Software Inc., San Diego, CA). The statistical tests performed are detailed in the figure legends.

2.2.2.5 Immunoprecipitation

All steps of immunoprecipitation (IP) experiments were performed at 4°C or on ice. Cells were harvested by trypsinisation and washed once in PBS. 1/20 of the sample was removed ("Input") and lysed in 5X SDS sample buffer (see Section 2.1.3.1). The rest of the sample was incubated in immunoprecipitation lysis buffer (see Section 2.1.4) for 1

hour after which the lysates were centrifuged at 100,000xg for 40 minutes to pellet insoluble particles. Supernatants were transferred to fresh tubes and were precleared by incubation with 25 µl of Protein G-sepharose beads (50% (v/v) in PBS-Triton) (see Section 2.1.4) for 30 minutes. Following centrifugation at 2,000xg for 30s to settle the beads, supernatants were transferred to fresh tubes and total protein concentrations were quantified by Bradford assay (see Section 2.2.2.1). The protein concentration was adjusted to 1 µg/µl if needed and equal amounts of protein (500 µg) for each sample were then used for immunoprecipitation. The appropriate primary antibody was added (see Table 2.4) and the samples were incubated with mild mixing on a rotary shaker for 16 hours at 4°C. After the addition of 30 µl Protein G-sepharose beads (50% (v/v) in PBS-Triton), the samples were incubated for a further 2 hours on a rotary shaker before centrifuging at 2,000xg for 30 s to pellet the beads. The pelleted beads were retained and washed four times with 1 ml PBS-Triton. The bound proteins were then eluted from the beads by incubation in 50 µl of 1X SDS sample buffer, heated at 100°C for 5 minutes and used for SDS-PAGE.

2.2.2.6 Mass spectrometry studies

Mass spectrometry studies were performed in collaboration with the Proteomics Facility at the Institute of Psychiatry. Identification of phosphorylation sites from transfected cells was performed essentially as described previously for other proteins (Standen et al., 2003). Briefly, VAPB and PTPIP51 were immunoprecipitated from transfected CHO cells using the myc- or the HA-tags. The two proteins were resolved by SDS-PAGE, the gels stained with Colloidal Coomassie (see section 2.1.3.5) and the band corresponding to VAPB or PTPIP51 excised, reduced with 10 mM dithiothreitol (30 minutes at 56°C) and derivatised with 55 mM iodoacetamide (20 minutes in the dark at

20°C). The proteins were then digested with trypsin (Roche Molecular Biochemical) for 4 hours at 37°C. Digested peptides were extracted from the gel pieces with two wash cycles of 50 mM NH_4HCO_3 and acetonitrile, lyophilised and resuspended in 20 μl of 50 mM NH_4HCO_3.

Peptide digests were analysed by liquid chromatography tandem mass spectrometry (LC/MS/MS). Chromatographic separations were performed using an Ultimate LC system (Dionex, UK). Peptides were resolved by reversed-phase chromatography on a 75 μm, C18 PepMap column. A gradient of acetonitrile in 0.05% formic acid was delivered over 60 minutes to elute the peptides at a flow rate of 200 nl/min. Peptides were ionised by electrospray ionisation using a Z-spray source fitted to a QTof-micro (Waters Corp.). The instrument was set to run in automated switching mode, selecting precursor ions based on their intensity and charge state, for sequencing by collision-induced fragmentation. The MS/MS analyses were conducted using collision energy profiles that were chosen based on the mass-to-charge ratio (m/z) and the charge state of the peptides.

The mass spectral data was processed into peak lists containing the m/z value of each precursor ion and the corresponding fragment ion m/z values and intensities. Data were searched against a custom-built database using the Mascot searching algorithm (Matrix Science, UK). Peptides and phospho-peptides of VAPB and PTPIP51 were identified by matching the MS/MS data against mass values generated from the theoretical fragmentation of peptides based on the search criteria set. Specifically, tryptic cleavage with up to 3 missed cleavages, carbamidomethyl modification of cysteine residues, oxidised methionine, N-acetylation of the protein and phosphorylation of

serine/threonine and tyrosine residues. All the amino acid modifications were selected as variable modifications in the software. The exact location of phosphorylation within each peptide was determined by the pattern of fragment ions produced.

2.2.3 Microscopy

2.2.3.1 Immunofluorescence

All steps of the procedure were performed at 20 ºC. CV1 cells grown on glass coverslips were washed once with PBS (see Section 2.1.1) to remove culture medium and incubated in fixing solution (see Section 2.1.6) for 10 minutes. Cells were then washed twice with PBS to remove the fixing solution and quenching solution (see Section 2.1.6) was added for 15 minutes to remove excess paraformaldehyde and reduce autofluorescence. Following quenching, the cells were washed once with PBS, permeabilised for 3 minutes and blocked with blocking solution (see Section 2.1.6) for 30 minutes to reduce non-specific binding for 30 minutes. Incubation with primary antibodies in blocking solution was then carried out for 1 hour. All primary antibodies that were used during the experiments are listed in Table 2.4. The cells were then washed five times with PBS for 5 minutes before being incubated with the secondary antibody in blocking solution for 45 minutes. Fluorescent labelled secondary antibodies were chosen depending on the species in which the primary antibody was raised and the fluorophore (for details see Table 2.5).

Following incubation with the secondary antibody the cells were washed three times with PBS. Nucleic acids were stained with 50 µg 4′,6-Diamidino-2-phenylindole (DAPI; see Section 2.1.1) for 5 minutes, followed by a further 5-6 washes in PBS. Finally, coverslips were mounted onto slides using Mowiol-DABCO mounting medium

(see Section 2.1.6). Conventional images were captured using Leica LAS AF software on a Leica DM5000 B microscope equipped with a Leica DFC360 FX camera and 10x/0.30NA, 40x/0.75NA or 63x/1.25NA HCX-PL-FLUOTAR objectives (all from Leica Microsystems CMS GmbH, Mannheim, Germany). Confocal images were captured using a Zeiss LSM 510 META confocal microscope at the appropriate excitation wavelengths with a 63x/1.4NA Zeiss Plan-APOCHROMAT objective (Carl Zeiss AG, Oberkochen, Germany).

Co-localization of PDI (an ER marker) with TOM20 (a mitochondrial marker) was identified and quantified using ImageJ with the Intensity Correlation Analysis plug-in on whole cells. Intensity correlation analysis represents a robust method for quantitatively determining the relative co-localization of dye signals obtained from advanced microscopy. Conventional dye overlay methods that are often used in double immunofluorescence microscopy are limited in that they can report incorrect co-localization of two proteins. By contrast, intensity correlation analysis determines whether the pixel intensities from two signals vary in synchrony, making it a powerful method for judging whether two proteins co-localize. The values obtained from the analyses are reported as an intensity correlation quotient (ICQ), which is a statistically testable, single value assessment of the relationship between two stained protein pairs (Li et al., 2004). For dependent staining (co-localization) $0<ICQ\leq+0.5$, for random staining ICQ=0, and for segregated staining $0>ICQ\geq-0.5$ (no co-localization). Comparison of means was carried out using a one-way ANOVA combined with the Tukey post-hoc analysis to adjust for multiple comparisons.

2.2.3.2 *In situ* Proximity Ligation Assay™ (PLA™)

Interactions between PTPIP51 and VAPB were visualized and quantified using a proximity ligation assay (Soderberg et al., 2006). For these experiments, a commercial kit (Olink Bioscience, Uppsala, Sweden) was used according to the manufacturer's instructions. In this assay, fixed cells are probed with primary antibodies and then secondary antibodies coupled with complementary oligonucleotides are applied. If the distance between the two antibody-coupled oligonucleotides is less than 40 nm, they can interact through subsequent addition of two further oligonucleotides and join to form a closed circle. This can then be amplified by rolling-circle amplification with DNA polymerase to produce a concatemeric DNA strand onto which the detection probes hybridise.

CV1 cells grown on glass coverslips were fixed, probed with VAPB and PTPIP51 primary antibodies followed by Duolink secondary antibodies. All following incubations were performed using the reagents provided in the Duolink kit (Section 2.1.7). Complementary PLA probes raised in the appropriate species were mixed with the Duolink Antibody Diluent and incubated with the samples in a pre-heated humidity chamber for 1 h at 37°C. The coverslips were then washed twice for 5 minutes with Wash Buffer A and incubated with the Ligation solution in a pre-heated humidity chamber for 30 minutes at 37°C. The reagents used in the amplification step are light sensitive and all the subsequent procedures were performed avoiding direct exposure to light. After two 2 minutes washes with Wash Buffer A, the coverslips were incubated with the Amplification-Polymerase solution in a pre-heated humidity chamber for 100 minutes at 37°C. After two 10 minute washes in Wash Buffer B, the coverslips were air-dried, mounted, and viewed using a Leica DM5000 fluorescence microscope (Leica

Microsystems GmbH, Wetzlar, Germany). Images were captured using a 63x/1.25NA HCX-PL-FLUOTAR oil immersion lens and PLA signals were analyzed using the Particle analysis function of ImageJ (National Institute of Mental Health, Bethesda, Maryland, USA).

2.2.3.3 Transmission electron microscopy

NSC34 cells grown on 60 mm Petri dishes were washed once with 0.1 M cacodylate buffer and then fixed with 2.5% glutaraldehyde in cacodylate buffer (see Section 2.1.8) for 3 hours at 20°C. The cells were then gently removed from the surface of the dish with a plastic scraper and centrifuged at 800xg for 10 minutes to form a pellet. The cell pellet was washed in 0.1 M cacodylate buffer pH 7.2 and then post-fixed for 1 hour in 1% osmium tetroxide in 0.1M cacodylate buffer. Following a wash in 0.1 M cocodylate buffer, the samples were block stained for 1 hour with 1% uranyl acetate in water before dehydration through a graded series of alcohols and embedding in Taab resin. 70 nm sections were cut on a Leica Ultracut E microtome and stained with lead citrate (0.1N).

Samples were viewed on a Tecnai 12 electron microscope (FEI) fitted with an AMT camera and digital images were captured at a magnification of 2900x, 4800x and 6800x. The mitochondrial perimeter, the length of ER apposed to mitochondria and the lengths of tethers connecting mitochondrial outer membranes to ER membranes were determined in a blind manner using the ImageJ software (NIH, Bethesda, USA; http://rsb.info.nih.gov/ij/).

2.2.4 Mammalian cell culture and transfection methods

2.2.4.1 NSC34, CV-1, CHO and HEK293 cell culture

The cells were maintained in monolayer culture in DMEM/HAM media containing 10% FBS and supplements (see Section 2.1.9) at 37°C under an atmosphere of 5% CO_2. Cells were passaged when they formed an approximately 80% confluent layer in the culture vessel. Medium was removed and cells were washed once with sterile PBS (see Section 2.1.1). To dislodge cells from the surface of the vessel, enough trypsin-EDTA solution (see Section 2.1.9) was added to cover the monolayer (e.g. 1 ml trypsin-EDTA solution for a 25 cm^2 flask) and the cells were incubated at 37°C for 2-3 minutes. Full media (e.g. 4 ml for a 25 cm^2 flask) was then added to inactivate the trypsin, and cells were pipetted up and down to triturate them. Finally, the cell suspension was distributed into vessels for further culturing.

2.2.4.2 Transient transfection

Transient transfection of CV-1 cell cultures

CV-1 cells were transfected using ExGen 500 (Thermo Scientific), a polyethylenimine based transfection reagent. Polyethylenimine is a cationic polymer with high proton buffer capacity ("proton sponge effect"). The mechanism of polyethylenimine based transfection has been described (Boussif et al., 1995; Sonawane et al., 2003). The positively charged polyethylenimine polymer interacts with negatively charged DNA and forms small particles (polyplexes). Polyplexes settle on and bind to anionic cell surface residues and are taken up by the cells via endocytosis (Boussif et al., 1995). The "proton sponge effect" of polyethylenimine neutralises the acidic pH of the endosome/lysosome and this results in a charge driven chloride influx into the endosome. The chloride influx causes osmotic swelling and disruption of the endosome

and allows the escape of the polyplexes from the endosome (Sonawane et al., 2003). The DNA then dissociates from the polyplex and translocates to the nucleus.

Transfections were conducted according to the manufacturer's instructions. Cells were plated on 13 mm diameter coverslips in 24 well plates (Greiner Bio-One) the day before transfection so that they reached approximately 50% confluence on the day of transfection. For each transfection, the amounts of reagents were vortexed as indicated in Table 2.7 for 10 s. The transfection solution was then incubated for 10 minutes at 20°C and added drop-wise to the cells. The cells were analysed 24-48 hours post-transfection.

Table 2.7 Amounts of reagents for ExGen 500 based transient transfection

Plate Format	DNA/well (µg)	ExGen 500/well (µl)	150 mM NaCl/well (µl)
24 well plate	0.5	2.1	25
12 well plate	1	4.3	50

Lipid based transfection of CHO cell cultures

CHO cells were transfected with Lipofectamine (Invitrogen) according to the manufacturer's instructions, using 10 µg plasmid DNA and 40 µl Lipofectamine™ per 10 cm diameter Petri dish. The cells were plated out the day before the transfection experiment so that they reached 50-80% confluency on the day of transfection, and were harvested for analysis 24 hours post-transfection.

Lipid based transfection of HEK293 cell cultures

HEK293 cells were transfected with FuGENE-6 (Promega) at a 3:1 ratio (FuGENE-6:DNA) according to manufacturer's instructions, using 1 μg of plasmid DNA and 3 μl FuGENE-6 for a well in a 6 well plate. The cells were plated 24 hours prior to transfection so that they reached 50% confluency on the day of transfection, and were harvested for immunoprecipitation experiments 24-48 hours post-transfection.

Lipid based transfection of NSC34 cell cultures

NSC34 cells were transfected with Lipofectamine 2000 (Invitrogen) according to the manufacturer's instructions, using 20 μg plasmid DNA and 80 μl Lipofectamine 2000 per 175 cm^3 flask. The cells were plated out 24 hours before the transfection experiment so that they reached 25-30% confluency on the day of transfection, and were harvested for analysis 24 hours post-transfection.

2.2.4.3 Delivery of siRNA to cell cultures

Small interfering RNA (siRNA) duplexes (VAPB, PTPIP51 and non-targeting control) were purchased from Dharmacon and Origene and were described previously (De Vos et al., 2012). Duplexes were diluted in 1x resuspension buffer purchased from Dharmacon (60 mM KCl, 6 mM HEPES pH 7.5, and 200 mM $MgCl_2$) and stored as 100 μM aliquots at -20ºC.

Human VAPB siRNA sequence (Dharmacon):

UGUUACAGCCUUUCGAUUAUU

Human PTPIP51 siRNA sequence (Dharmacon):

CCUUAGACCUUGCUGAGAUUU

Mouse VAPB siRNA sequence (Dharmacon):

UGUUACAGCCUUUCGAUUAUU

Mouse PTPIP51 siRNA sequence (Origene):

GGAUGACAACGCUGGCAAAGGGUCT

Delivery of siRNAs to CV1 cells

VAPB and PTPIP51 were knocked down in CV1 cells using Lipofectamine™ 2000 (Invitrogen) according to manufacturer's instructions, and using the amount of reagents indicated in Table 2.8. Cells were plated out the day before so they reached 30% confluency on the day of transfection. Transfection reagent and culture medium were removed 24 hours post-transfection and replaced with fresh culture medium. Cells were used for analysis 96 hours post-transfection.

Table 2.8 Delivery of human VAPB and PTPIP51 siRNA to CV1 cells

Plate Format	siRNA concentration (nM)	Lipofectamine 2000/well (µl)
12 well	100	2
24 well	100	1

Delivery of siRNAs to NSC34 cells

Mouse VAPB and PTPIP51 respectively were knocked down in NSC34 cells using Lipofectamine™ 2000 (Invitrogen) according to manufacturer's instructions, and using the amount of reagents indicated in Table 2.9. Cells were plated 24 hours before so they reached 30% confluency on the day of transfection. Transfection reagent and culture

medium were removed 24 hours post-transfection and replaced with fresh culture medium. Cells were harvested 96 hours post-transfection.

Table 2.9 Delivery of mouse VAPB and PTPIP51 siRNA to NSC34 cells

Plate Format	siRNA concentration (nM)	Lipofectamine 2000/well (μl)
60 mm	50	20
12 well	50	4

2.2.5 Treatment of HEK293 cells with the tyrosine phosphatase inhibitor pervanadate

Pervanadate was prepared as a 100X stock by mixing 50 μl 200 mM sodium orthovanadate with 1.6 μl of 30% (w/w) hydrogen peroxide in 948 μl of water. The reaction was left for 5 minutes at 20°C, producing 10 mM sodium orthovanadate and 16.3 mM hydrogen peroxide (Derkinderen et al., 2005; Huyer et al., 1997). The excess hydrogen peroxide was removed by adding 200 μg/ml catalase (Sigma) and incubating for an additional 5 minutes at 20°C. The reaction mix was diluted 1:100 with fresh cell culture medium and the cells were treated for 20 minutes.

2.2.6 Fluorescence-activated cell sorting (FACS) of NSC34 cells

NSC34 cells were grown in 175 cm^3 flasks, transfected with plasmid DNA using Lipofectamine 2000 and incubated for 24 hours. Following trypsinisation, the cells were counted, filtered through a 40 μm BD Falcon™ cell strainer and resuspended in PBS at a concentration of 8-10 million/ml in 5 ml BD Falcon™ round-bottom tubes. All the following steps of the sorting procedure were performed at 4°C.

The cells expressing ECFP, ECFP-tagged or AcGFP constructs (positive fraction) and the untransfected cells (the negative fraction) were analyzed and sorted based on their fluorescence, using a BD FACSAria™ cell sorter employing a 100 μm nozzle and applying $13.7x10^4$ Pa (20 psi) sheath pressure. For detecting EGFP fluorescence, cells were excited using a blue laser (488 nm), a 505 Long pass filter and a 525/550 band pass filter. Sterile PBS was used as sheath fluid. The sample was maintained at 4°C and was sorted at a rate of less than 5000 events/second and at a flow rate of less than 6. The positive cells were collected in PBS with 5% FCS and underwent a post-sorting purity testing that involved re-analysing a proportion of the cells. Only the samples achieving a purity of over 98% were processed further. A proportion were also plated on coverslips and analysed by fluorescence microscopy to further confirm the purity of transfected cells in the final sorted population. Cells were then harvested and processed for electron microscopy as described (see Section 2.2.3.3).

CHAPTER 3: VAPB AND PTPIP51 MEDIATE ER-MITOCHONDRIA ASSOCIATIONS

3.1 Introduction

As detailed in Section 1.4, up to approximately 20% of the mitochondrial surface is closely apposed to ER membranes. These regions facilitate a variety of signalling processes between the two organelles including Ca^{2+} and phospholipid exchange (Csordas et al., 2006; Hayashi et al., 2009; Lebiedzinska et al., 2009; Rizzuto et al., 2009; Rizzuto et al., 1998; Rusinol et al., 1994).

Tethers that link ER to mitochondria have been visualized in electron microscopy studies. These range from approximately 10 nm to 25 nm in length, suggesting that a number of different molecules are responsible for physically connecting ER and mitochondria (Csordas et al., 2006). However, the nature of these tethers is still not clear. Several molecules such as Drp1 (Pitts et al., 1999) and PACS2 (Simmen et al., 2005) have been shown to indirectly regulate ER-mitochondria contacts. Interaction between IP3 receptors on the ER and voltage dependent anion channel-1 (VDAC1) on mitochondria via the molecular chaperone Binding immunoglobulin Protein (BiP) has been proposed to link ER to mitochondria (Szabadkai et al., 2006), but IP3 receptor deficient cells show normal ER-mitochondria interactions suggesting other molecules are responsible for the physical linkage (Csordas et al., 2006). In yeast, proteins of the ER-mitochondria encounter structure (ERMES) act as a molecular tether between ER and mitochondria but orthologs of these proteins in higher eukaryotes have not been identified so far (Kornmann et al., 2009). In mammalian cells, mitofusin-2 dimers have been shown to link ER and mitochondria (de Brito and Scorrano, 2008). However, other groups could not replicate this finding, which involved mainly light microscopy studies. Moreover, a recent study involving electron microscopy of mitofusin-2 knockout cells has revealed that loss of mitofusin-2 actually increases ER-mitochondria contacts

(Cosson et al., 2012). Thus, the identity of the molecular tethers that physically connect ER and mitochondria in mammalian cells is not properly known.

Previous work from our research group demonstrated that outer mitochondrial membrane protein PTPIP51 interacts with integral ER protein VAPB (De Vos et al., 2012). PTPIP51 is anchored in the outer mitochondrial membrane via an N-terminal transmembrane domain with the remaining C-terminus projecting into the cytoplasm (De Vos et al., 2012). VAPB is anchored in the ER via its C-terminal membrane spanning domain with its N-terminus projecting into the cytosol (Kagiwada et al., 1998). As such, VAPB and PTPIP51 are plausible candidates that might represent at least some of the linkers visualized by electron microscopy which act as ER-mitochondria tethers.

In this chapter, the role of VAPB and PTPIP51 in mediating ER-mitochondria interactions was tested. If PTPIP51 and VAPB form some of the physical links between ER and mitochondria, then modulating the expression of these proteins is predicted to alter ER-mitochondria associations. The expression levels of VAPB and PTPIP51 were thus modulated and ER-mitochondria associations then monitored by electron and light microscopy. VAPB and PTPIP51 expression were reduced via siRNAs and elevated via transfection.

For the electron microscopy studies, the NSC34 motor neuron cell line was used. This cell line was chosen as some of the later studies (see Chapter 4) involved analysing the effects of proteins associated with familial ALS on ER-mitochondria associations and the VAPB-PTPIP51 interaction. NSC34 cells were developed by fusing mouse

embryonic motor neurons with mouse neuroblastoma cells (Cashman et al., 1992) and exhibit morphological and physiological features of spinal motor neurons (Matusica et al., 2008). Thus, they represent a suitable model for studying how insults associated with ALS might affect ER-mitochondria associations.

For the confocal light microscopy studies, CV1 cells were utilised. This is an established cell line initially extracted from *Cercopithecus aethiops* kidney fibroblasts (Jensen et al., 1964). CV1 cells have a highly spread morphology and are suitable for analysing the distribution of intracellular organelles (e.g. see (De Vos et al., 2012)).

3.2 Results

3.2.1 VAPB and PTPIP51 mediate ER-mitochondria associations in electron microscopy studies using NSC34 cells

To investigate the role of VAPB and PTPIP51 in mediating ER-mitochondria interactions, expression of VAPB and PTPIP51 were first modulated and ER-mitochondria associations then quantified by electron microscopy in NSC34 cells. This involved capturing images of mitochondria in appropriately manipulated cells and then calculating the % of the mitochondrial surface closely apposed (less than 25 nm) to ER. The quantification was performed using the ImageJ software (http://rsb.info.nih.gov/ij/) (see Section 2.2.3.3).

First, VAPB and PTPIP51 expression was reduced using siRNAs. Consistent with a previous study (De Vos et al., 2012), siRNA knockdown of VAPB did not influence the expression of PTPIP51 and knockdown of PTPIP51 did not influence the expression of VAPB (Figure 3.1). Moreover, the expression levels of mitofusin-2 (another protein suggested to mediate ER-mitochondria interaction (de Brito and Scorrano, 2008)) were not affected by the siRNA knockdown of either VAPB or PTPIP51. In control siRNA treated cells, approximately 12% of the mitochondrial surface was closely associated with ER (Figure 3.2). However, siRNA knockdown of either VAPB or PTPIP51 significantly reduced these values to 8% (VAPB siRNA) and 6% (PTPIP51 siRNA). Loss of PTPIP51 was the more potent in disrupting ER-mitochondria interactions (Figure 3.2).

Next, the expression of VAPB and PTPIP51 was elevated via transfection. Cells were transfected with either ECFP control vector, ECFP-VAPB (Morotz et al., 2012) or

PTPIP51 that was expressed using a bicistronic internal ribosome entry site (IRES) vector with AcGFP. To monitor the effect of VAPB and PTPIP51 co-expression, the cells were transfected with ECFP-VAPB and HA tagged PTPIP51. Since these transient transfections achieved a transfection efficiency of only 30-50%, the ECFP/AcGFP tags were further utilized to isolate transfected cells using a BD® FACS Aria cell sorter. The cell sorting achieved over 98% positive cells (Figure 3.3). This was further confirmed by monitoring ECFP, ECFP-VAPB and PTPIP51 expression in the sorted cells by fluorescence and immunofluorescence microscopy. This staining confirmed the efficiency of the sorting procedure (see for example staining for ECFP-VAPB and PTPIP51 in ECFP-VAPB/PTPIP51-HA co-transfected cells in Figure 3.4).

As expected, the proportion of the mitochondrial surface closely associated with ER in control cells expressing ECFP alone was not significantly different to that in cells treated with control siRNA (Figure 3.5A). However, expression of either VAPB or PTPIP51 markedly increased the percentage of mitochondrial surface in touch with ER to approximately 18% or 26% respectively (Figure 3.5A). Interestingly, overexpression of PTPIP51 was more potent than VAPB at promoting ER-mitochondria interactions and this is consistent with the siRNA studies where loss of PTPIP51 was more effective at disrupting ER-mitochondria interactions (Figure 3.2 and 3.5A).

The effect of overexpressing both VAPB and PTPIP51 was also investigated and here a dramatic increase in ER-mitochondria interactions was observed. In these co-transfected cells, approximately 60% of the mitochondrial surface was closely associated with ER (Figure 3.5A and 3.5B).

3.2.2 VAPB and PTPIP51 mediate ER-mitochondria co-localization in confocal light microscopy studies using CV1 cells

For these investigations, CV1 cells were utilized due to their flattened and spread morphology which facilitates such morphological analyses. Other groups have utilized confocal microscopy to study ER-mitochondria interactions (e.g. (Area-Gomez et al., 2012; de Brito and Scorrano, 2009; Rizzuto et al., 1998)). In this set of experiments, ER was detected by immunostaining for the integral ER protein, protein disulfide isomerase (PDI) and mitochondria were detected by immunostaining for translocase of outer mitochondrial membrane 20 (TOM20). The co-localization of PDI and TOM20 was quantified using intensity correlation analysis (ICA) and data presented as relative intensity correlation quotients (ICQ) (Li et al., 2004). ICA is one of the most rigorous methods for studying co-localization of proteins by confocal microscopy since it compares the scatter plots of two stains against the product of the pixel intensity difference for each of the two stains from their respective means. Thus, unlike other methods which simply compare co-localization of pixels, ICA determines whether the pixel intensities from two signals vary in synchrony.

First, the cells were transfected with control siRNA, PTPIP51 siRNA or VAPB siRNA and ER and mitochondria co-localization monitored by immunostaining. The co-localization of PDI and TOM20 was significantly decreased after either VAPB or PTPIP51 depletion (Figure 3.6) and this was consistent with the electron microscopy results (Figure 3.2). However, unlike the electron microscopy studies, there was no significant difference between loss of VAPB and loss of PTPIP51. This may be explained by the reduced resolution of the light microscope compared to the electron microscope which results in a corresponding decrease in sensitivity.

Secondly, VAPB and/or PTPIP51 were overexpressed in the CV1 cells. Cells were transfected with ECFP control, ECFP-VAPB, hemagglutinin-tagged PTPIP51 (PTPIP51-HA) or ECFP-VAPB+PTPIP51-HA. Transfection of VAPB or PTPIP51 both increased co-localization of ER and mitochondria and in agreement with the electron microscopy studies, this phenotype was particularly striking in VAPB+PTPIP51 co-transfected cells (Figure 3.7). In these co-transfected cells, a dramatic reorganization of the ER was observed so that it co-aligned with mitochondria (Figure 3.7).

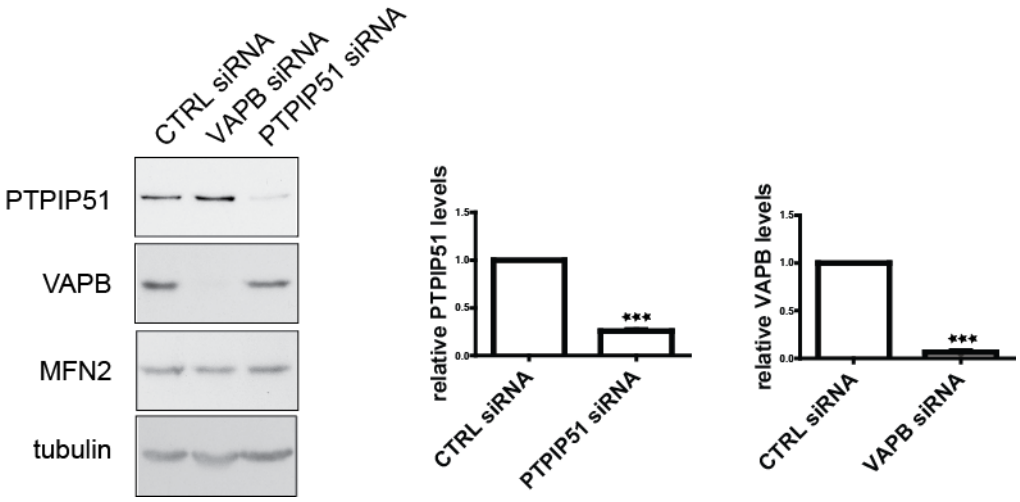

Figure 3.1 siRNA knockdown of VAPB or PTPIP51

Immunoblots showing siRNA knockdown of VAPB or PTPIP51 in NSC34 cells. siRNA knockdown of VAPB does not affect expression of PTPIP51, siRNA knockdown of PTPIP51 does not affect expression of VAPB and siRNA knockdown of either VAPB or PTPIP51 do not affect expression of mitofusin 2 (MFN2). Also shown is an immunoblot of tubulin as a loading control. Bar charts show PTPIP51 or VAPB expression levels following quantification of signals from immunoblots normalized to tubulin. Statistical significance was determined by a paired t-test. n=4; error bars are SEM; ***$p<0.001$.

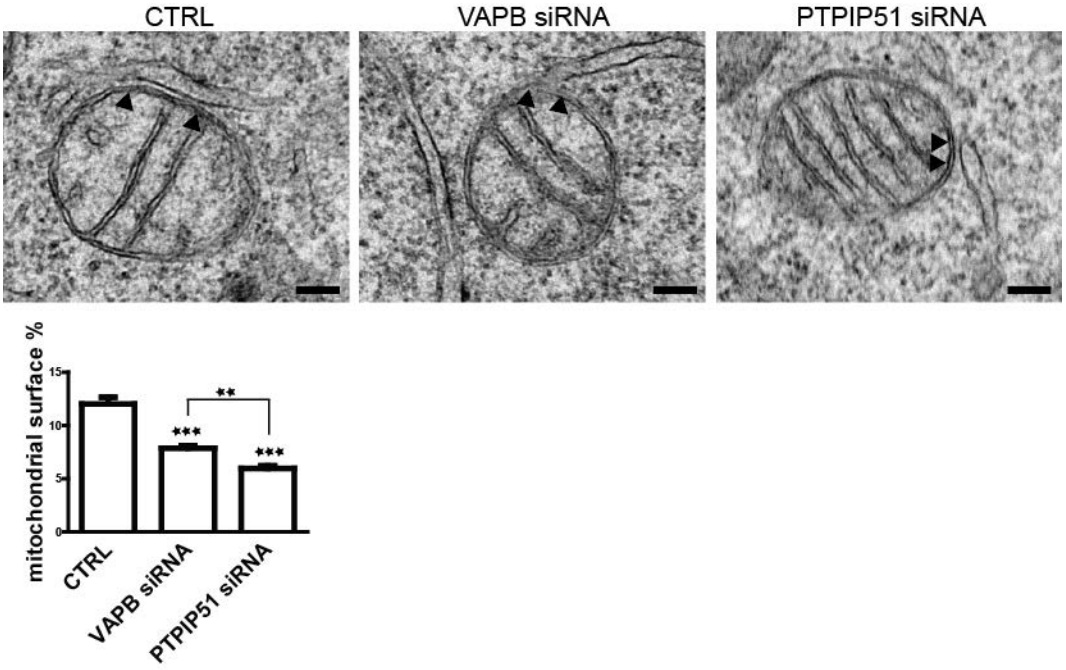

Figure 3.2 siRNA knockdown of VAPB or PTPIP51 reduces ER-mitochondria associations

Representative electron micrographs of ER-mitochondria contacts in control siRNA (CTRL), VAPB or PTPIP51 siRNA treated cells. Arrowheads show ER-mitochondria contact sites. Scale bar=100 nm. Bar chart shows percentage of mitochondrial surface closely apposed to ER in the different samples. Statistical significance was determined by one-way ANOVA followed by Tukey's multiple comparison test. n=34-40 cells and 341-623 mitochondria; error bars are SEM; **p<0.01, ***p<0.001.

A

a

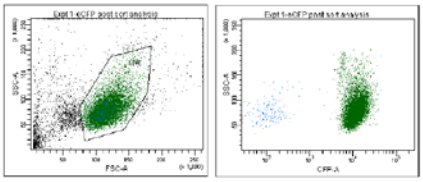

b

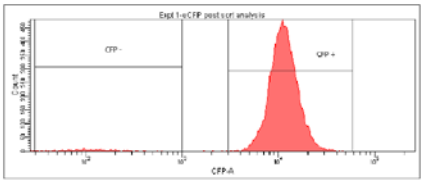

c

TUBE: ECFP post-sort analysis

POPULATION	#EVENTS	%PARENT	%TOTAL
ALL EVENTS	12,383	###	100.0
LIVE	10,027	81.0	81.0
CFP+	9,962	99.4	80.4
CFP-	64	0.6	0.5

B

a

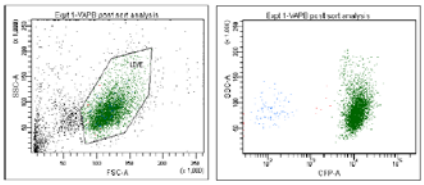

b

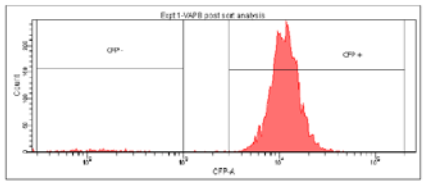

c

TUBE: VAPB post-sort analysis

POPULATION	#EVENTS	%PARENT	%TOTAL
ALL EVENTS	6,604	###	100.0
LIVE	5,123	77.6	77.6
CFP+	5,023	98.0	76.1
CFP-	88	1.7	1.3

C

a

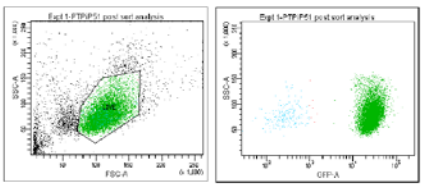

b

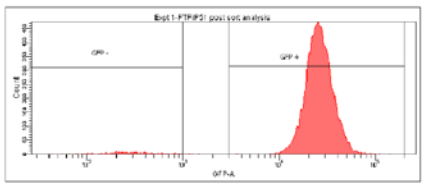

c

TUBE: PTPIP51 post-sort analysis

POPULATION	#EVENTS	%PARENT	%TOTAL
ALL EVENTS	12,102	###	100.0
LIVE	9,851	81.4	81.4
GFP+	9,749	99	80.6
GFP-	88	0.9	0.7

D

a

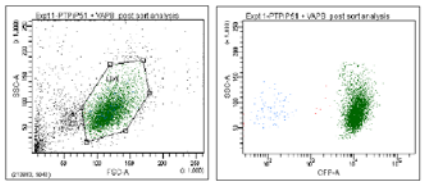

b

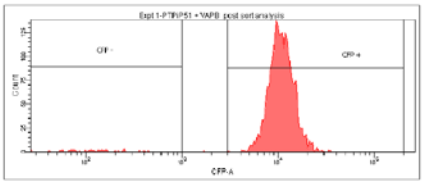

c

TUBE: PTPIP51 + VAPB post-sort analysis

POPULATION	#EVENTS	%PARENT	%TOTAL
ALL EVENTS	6.604	###	100.0
LIVE	2,537	38.4	38.4
CFP+	2,491	98.2	37.7
CFP-	45	1.8	0.7

Figure 3.3 FACS post-sorting analyses demonstrating high purity of ECFP/AcGFP positive samples

NSC34 cells transfected with ECFP control vector (A), ECFP-VAPB (B), PTPIP51 in IRES vector with AcGFP (C) or ECFP-VAPB + PTPIP51-HA (D) were sorted using ECFP or AcGFP. The scatter plots (A-a, B-a, C-a, D-a) illustrate high cell viability and low amounts of cell debris in the sorted population. The area charts (A-b, B-b, C-b, D-b) display an ECFP/AcGFP positive cell population (CFP/GFP+) distinct from the very few negative cells (CFP/GFP-). The tables (A-c, B-c, C-c, D-c) show the percentage of viable cells in the sorted population and the percentage of ECFP/AcGFP positive cells within the live population.

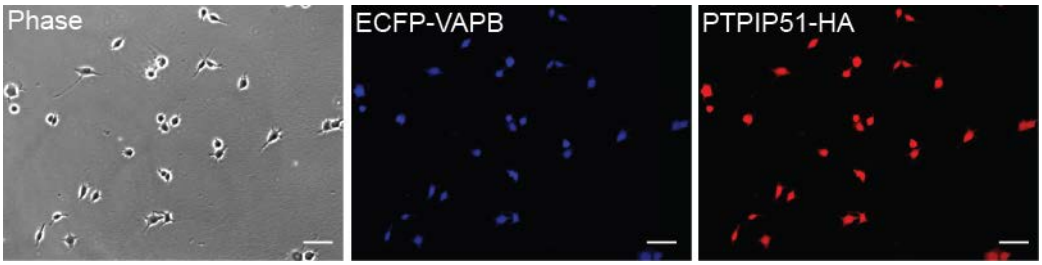

Figure 3.4 Confirmation of cell sorting purification of ECFP-VAPB and PTPIP51-HA expressing cells.

NSC34 cells co-transfected with ECFP-VAPB and PTPIP51-HA were sorted, plated onto coverslips and immunostrained for PTPIP51 using the HA epitope tag. VAPB was visualized via the ECFP tag. Low magnification images show phase contrast (to visualize cells), ECFP-VAPB and PTPIP51-HA signals. Scale bar=100 μm. Immunoblots revealed that VAPB and PTPIP51 were overexpressed by approximately 3-5 fold in the transfected cells (data not shown but see (Morotz et al., 2012)).

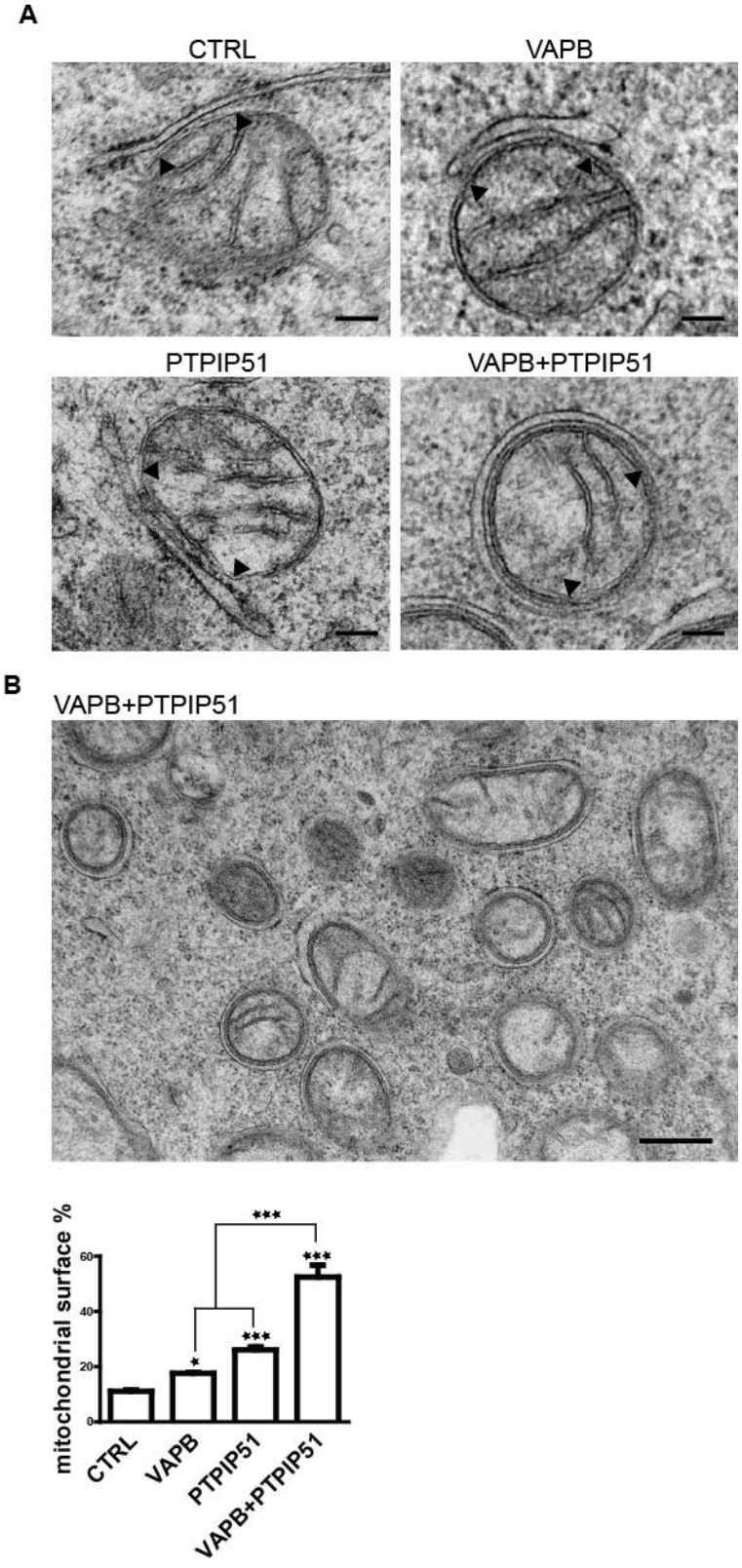

Figure 3.5 Overexpression of VAPB and/or PTPIP51 increases ER-mitochondria associations

(A) Representative electron micrographs of ER-mitochondria contacts in NSC34 cells transfected with control ECFP vector (CTRL), ECFP-VAPB (VAPB), PTPIP51 or ECFP-VAPB + PTPIP51 (VAPB+PTPIP51). Arrowheads show ER-mitochondria contact sites. Scale bar=100 nm. Bar chart shows percentage of mitochondrial surface closely apposed to ER in the different samples. Statistical significance was determined by one-way ANOVA followed by Tukey's multiple comparison test. n=30-35 cells and 358-623 mitochondria; error bars are SEM; *$p<0.05$, ***$p<0.001$. (B) Lower magnification electron micrograph of cell transfected with VAPB and PTPIP51 to show numerous mitochondria with closely apposed ER. Scale bar=500 nm.

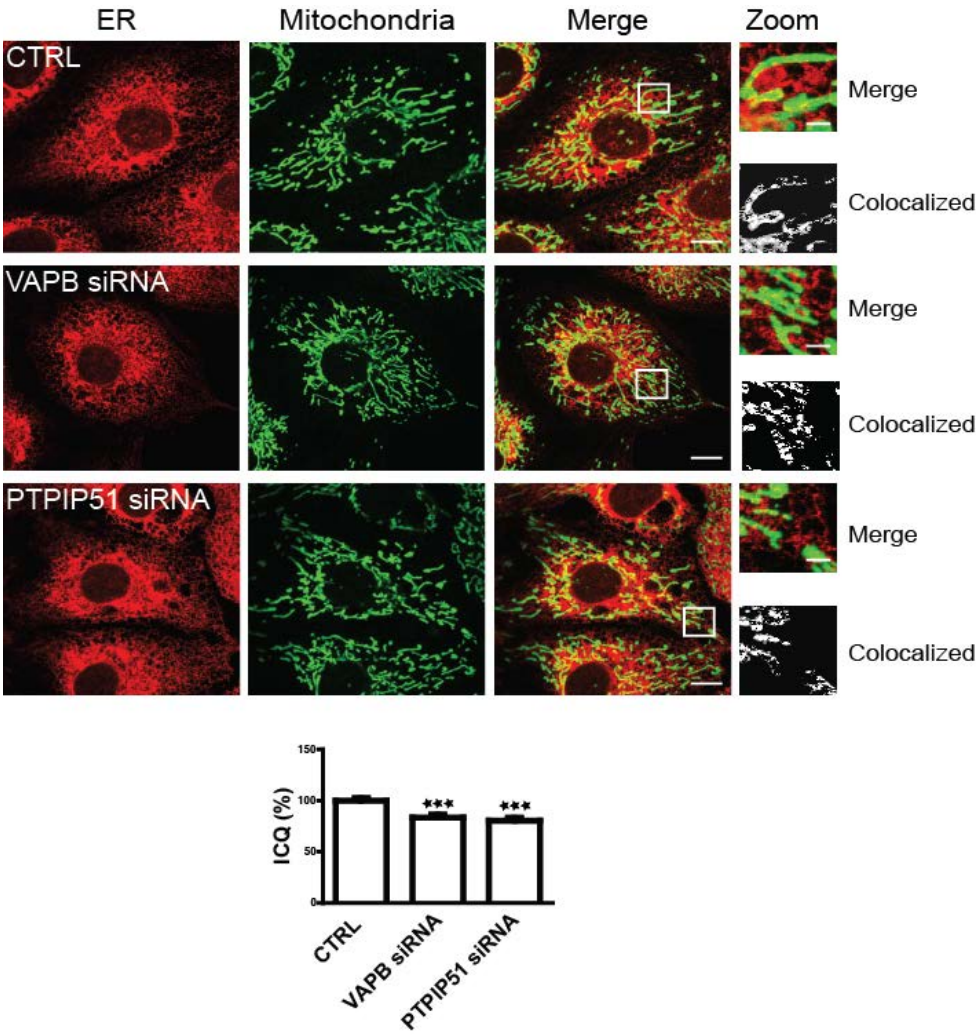

Figure 3.6 siRNA knockdown of VAPB or PTPIP51 reduces co-localization of ER and mitochondria

Confocal immunostaining of CV-1 cells transfected with control siRNA (CTRL), VAPB siRNA or PTPIP51 siRNA and immunostained for ER (using mouse PDI antibody) and mitochondria (using rabbit TOM-20 antibody) as indicated. Zoom shows high magnification of boxed area with co-localized pixels. Scale bars are 20 μm and 4 μm (zoom). Bar chart shows ICQ values (with control siRNA represented as 100%) in the different transfections. Statistical significance was determined by one-way ANOVA with Tukey's post-hoc test. n=24-52 cells; error bars are SEM; ***$p<0.001$.

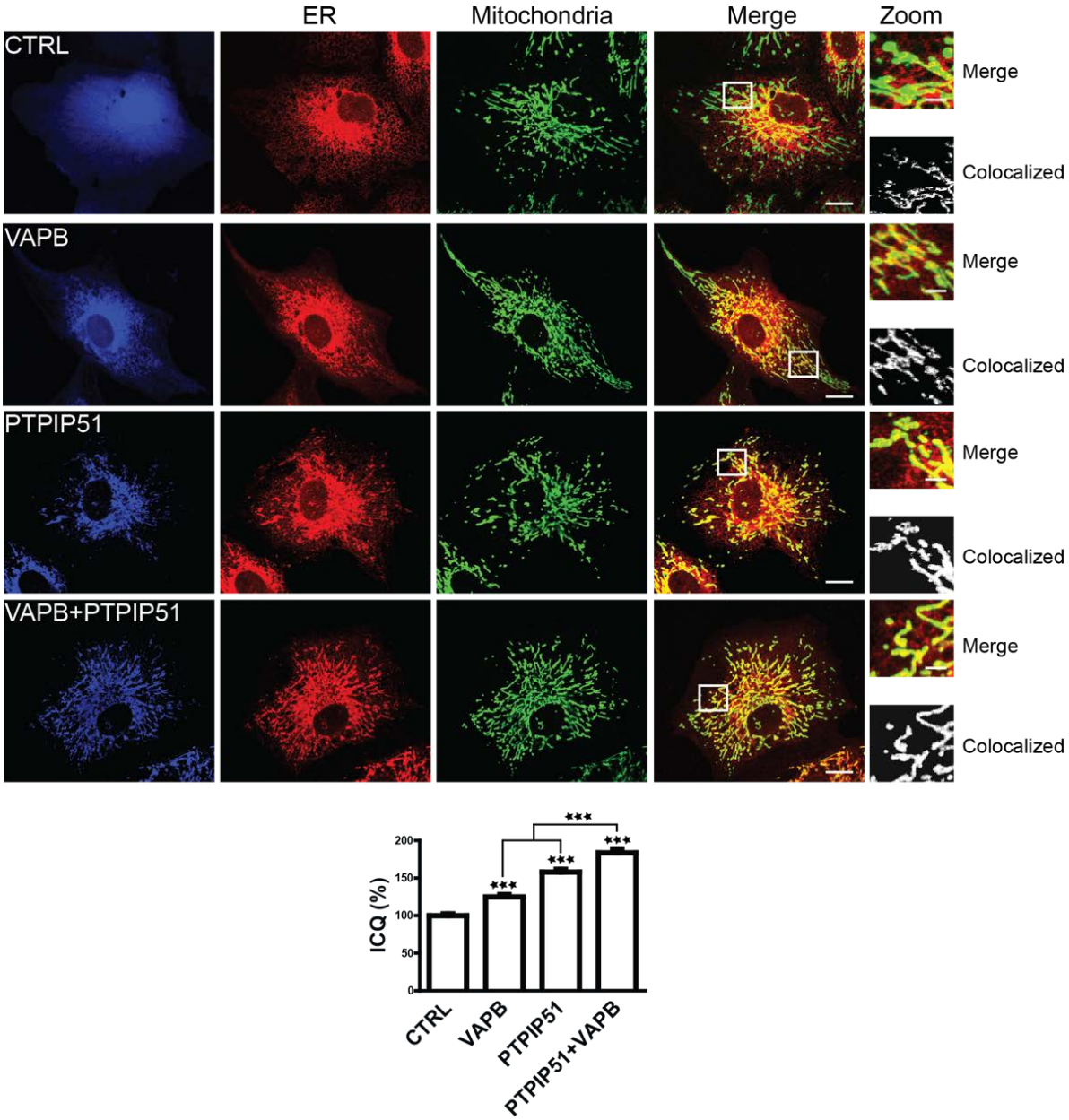

Figure 3.7 Overexpression of VAPB, PTPIP51 and VAPB with PTPIP51 all increase co-localization of ER and mitochondria

Confocal immunostaining of CV-1 cells transfected with control ECFP vector (CTRL), ECFP-VAPB (VAPB), PTPIP51-HA (PTPIP51) or ECFP-VAPB+PTPIP51-HA (VAPB+PTPIP51) and immunostained for ER (using mouse PDI antibody) and mitochondria (using rabbit TOM-20 antibody) as indicated. In ECFP-VAPB+PTPIP51-HA co-transfected cells, only ECFP-VAPB labeling is shown but duplicate coverslips were immunostained for PTPIP51-HA and this demonstrated that approximately 95% of

cells expressed both transfected proteins (data not shown). This data is consistent with many previous reports which show that most co-transfected cells express both plasmids (e.g. (Ackerley et al., 2000). Zoom shows high magnification of boxed area with co-localized pixels. Scale bars are 20 μm and 4 μm (zoom). Bar chart shows ICQ values (with ECFP control represented as 100%) in the different transfections. Statistical significance was determined by 1-way ANOVA with Tukey's post-hoc test. n=34-52 cells; error bars are SEM; ***$p<0.001$.

3.3 Discussion

Despite their fundamental importance to a variety of physiological processes, the mechanisms that mediate and regulate ER-mitochondria interactions are still not properly understood. In particular, the identity of the molecular tethers that physically connect ER and mitochondria are not fully characterised. Mitofusin-2 has been shown to tether ER to mitochondria (de Brito and Scorrano, 2008) but more recent work involving electron microscopy studies of ER-mitochondria associations in mitofusin-2 knockout cells have challenged this finding (Cosson et al., 2012).

Recent work in our research group identified an interaction between the resident ER protein VAPB and the mitochondrial protein PTPIP51. VAPB is anchored in the ER via a C-terminal membrane-spanning domain such that its N-terminus projects into the cytoplasm (Kagiwada et al., 1998) and PTPIP51 is an outer mitochondrial membrane protein whose C-terminus projects into the cytoplasm (De Vos et al., 2012). Therefore, VAPB and PTPIP51 represent plausible candidate tethers at the ER-mitochondria interface.

In this chapter, modulating VAPB and PTPIP51 expression was shown to significantly affect ER-mitochondria associations in both electron and confocal microscopy analyses. Both approaches have been previously utilised to visualise ER-mitochondria interactions (Csordas et al., 2010; Rizzuto et al., 1998). However, electron and confocal microscopy can produce conflicting results (Cosson et al., 2012; de Brito and Scorrano, 2008) and it has been suggested that electron microscopy is more suitable for investigating ER-mitochondria juxtaposition because of its higher resolution (Cosson et al., 2012; Rowland and Voeltz, 2012).

Interestingly, electron and confocal studies have produced complementary results in this chapter. siRNA knockdown of VAPB or PTPIP51 reduced ER-mitochondria associations, whereas overexpression of VAPB and/or PTPIP51 markedly increased ER-mitochondria associations using both microscopy methods. Indeed, VAPB and PTPIP51 co-expression produced a remarkable phenotype detectable by both electron and confocal microscopy in which the ER and mitochondria redistribute to form close associations. Alterations to ER-mitochondria interactions are known to affect Ca^{2+} exchange between these organelles and it has previously been demonstrated that modulating VAPB and PTPIP51 expression induces such changes in Ca^{2+} transmission (De Vos et al., 2012). Together, these findings support the conclusion that VAPB and PTPIP51 form at least one of the molecular scaffolds that mediate ER-mitochondria associations.

The ER-mitochondria interface is also involved in regulating cell survival and increased interactions between the two organelles may promote mitochondrial Ca^{2+} overload and apoptosis (Csordas et al., 2006; Rowland and Voeltz, 2012). Interestingly, one of the initial studies investigating PTPIP51 function reports cytochrome c release and caspase activation in PTPIP51 overexpressing cells (Lv et al., 2006). Thus, the markedly increased ER-mitochondria association induced by PTPIP51 overexpression in this study might provide a mechanism for the proapoptotic effect of overexpressing PTPIP51.

The findings that VAPB and PTPIP51 regulate ER-mitochondria associations have implications for a number of physiological processes. Key functions such as

phospholipid synthesis and trafficking, Ca^{2+} transmission, mitochondrial transport and biogenesis have been proposed to be regulated by ER-mitochondria associations (Rowland and Voeltz, 2012).

Thus, phospholipid synthesis is regulated by the ER-mitochondria encounter structure (ERMES) in yeast (Kornmann et al., 2009), although a tethering complex controlling lipid metabolism in higher eukaryotes has not been identified. Nonetheless, the mitochondrial protein Miro1 is the animal homologue of the ERMES subunit Gem1 (Kornmann et al., 2011) and controls mitochondrial morphology and movement along microtubules through a Ca^{2+} sensor (Fransson et al., 2006; Macaskill et al., 2009; Wang and Schwarz, 2009). Interestingly, Miro1 also interacts with the proposed ER-mitochondria tethering protein mitofusin-2, providing another link between the ER-mitochondria interface and mitochondrial dynamics (Misko et al., 2010). Furthermore, dynamin-related protein 1, a protein controlling mitochondrial division, is also localized at ER-mitochondria contact sites (Friedman et al., 2011) and can fragment the mitochondrial network, block interorganellar Ca^{2+} currents and protect against apoptosis (Szabadkai et al., 2004).

Ca^{2+} transmission between ER and mitochondria is mediated by IP3 receptors (ER membrane) and VDAC1 (mitochondrial membrane) ion channels, which can modulate apoptotic responses (Rizzuto et al., 1998; Szabadkai et al., 2006). Both pro- and anti-apoptotic Bcl-2 family members can regulate the ER Ca^{2+} levels by altering IP3 receptor phosphorylation or by directly interacting with the IP3 receptors (Oakes et al., 2005; White et al., 2005). Promielocytic leukemia protein has also been recently shown to regulate IP3 receptor activity and the mobilization of Ca^{2+} to the mitochondria

(Giorgi et al., 2010). Thus, lipid synthesis, mitochondrial homeostasis, Ca^{2+} transmission and apoptosis are all intimately connected at the ER-mitochondria interface. This implies the molecular scaffolds tethering ER to mitochondria are essential for maintaining these functions. The results described in this chapter which support a role for VAPB and PTPIP51 in regulating ER-mitochondria association thus have major relevance to a number of physiological processes.

Finally, it will be important to assess the significance of altered ER-mitochondria contacts for human disease. Indeed, damage to ER-mitochondria associations and consequent alterations to lipid metabolism and Ca^{2+} transmission are now linked to neurodegenerative disorders such as Alzheimers's disease and Parkinson's disease (Area-Gomez et al., 2012; Cali et al., 2012; Zampese et al., 2011). This aspect is explored in more detail in the next chapter, where ER-mitochondria associations are investigated in the presence of ALS associated insults.

CHAPTER 4: BOTH WILD-TYPE AND ALS MUTANT TDP-43 REDUCE ER-MITOCHONDRIA ASSOCIATIONS

4.1 Introduction

As discussed in Chapter 1 (Section 1.4), changes to ER-mitochondria associations are predicted to have important effects on the neuronal homeostasis. The prolonged and excessive tightening of ER-mitochondria contacts will likely lead to increased Ca^{2+} signalling between the two organelles, mitochondria Ca^{2+} overload and induction of apoptosis (Csordas et al., 2006; Rowland and Voeltz, 2012). Conversely, the loosening of contacts may affect Ca^{2+}-dependent regulation of ATP synthesis by mitochondria. This is likely to have a profound effect at synapses since mitochondria are enriched in this compartment and perform essential functions in maintaining ionic potential (Csordas et al., 2006; Rowland and Voeltz, 2012).

This raises the intriguing possibility that human pathogenic processes target proteins at the MAM interface and ER-mitochondria associations. Indeed, a number of studies have focused attention on defective ER-mitochondria contacts and communication in neurodegenerative diseases (see for reviews (Rowland and Voeltz, 2012; Schon and Area-Gomez, 2010)).

Alzheimer's disease-associated presenilins have been shown to increase ER-mitochondria contacts and induce alterations to both Ca^{2+} and lipid metabolism (Area-Gomez et al., 2012; Zampese et al., 2011). Likewise, Parkinson's disease associated α-synuclein has been shown to enhance ER-mitochondria interactions and increase mitochondrial Ca^{2+} levels (Cali et al., 2012). Moreover, pathogenic proteins associated with Huntington's disease aberrantly interact with the IP3 receptors (Tang et al., 2003) and loss of IP3 receptor function is associated with some forms of spinocerebellar ataxia (van de Leemput et al., 2007). Finally, mutations in the gene encoding the ER-

mitochondria tethering protein mitofusin-2 cause some forms of Charcot-Marie-Tooth disease (Barisic et al., 2008).

Similar to other neurodegenerative diseases, a number of ALS associated proteins are located at the ER-mitochondria interface and can affect ER-mitochondria communication. Notably, VAPB is located in MAM and mutant VAPB causes familial ALS, disrupts ER structure and ER to mitochondria Ca^{2+} exchange (De Vos et al., 2012; Fasana et al., 2010; Kim et al., 2010a; Langou et al., 2010; Nishimura et al., 2004; Teuling et al., 2007; Tudor et al., 2010). A consequence of altered Ca^{2+} transmission at the MAM is impaired mitochondrial transport described in ALS mutant VAPB expressing neurons (Morotz et al., 2012). Mutant SOD1 and FUS also perturb ER structure and can induce ER stress and UPR (Farg et al., 2012; Saxena et al., 2009). In addition, ALS associated mutant SOD1 interacts with and damages VDAC1 (Israelson et al., 2010), an outer mitochondrial membrane Ca^{2+} channel closely associated to IP3 receptors in the ER membrane (Rapizzi et al., 2002; Szabadkai et al., 2006). However, although ALS associated insults can disrupt ER-mitochondria communication, changes in physical associations between the two organelles have not yet been explored.

In this chapter, the effect of wild-type and ALS mutant TDP-43 on ER-mitochondria associations was investigated. Accumulations of TDP-43 are a common pathological feature in a variety of neurodegenerative diseases including ALS (Arai et al., 2006; Neumann et al., 2006) and *TARDBP* mutationsare causative for familial forms of ALS (Sreedharan et al., 2008). Although normally located mostly in the nucleus, pathogenic TDP-43 translocates to the cytoplasm where it may induce local damage. Interestingly, the ER stress response coordinated at ER-mitochondria contact sites was recently found

to be disrupted in TDP-43 transgenic rats (Tong et al., 2012).

To further explore the role of TDP-43 at the ER-mitochondria interface, ER-mitochondria associations were monitored by electron and light microscopy in NSC34 motor neuron cells transfected with either wild-type or an ALS mutant TDP-43 (TDP-43 M337V). In addition, the effect of expressing either wild-type or ALS mutant TDP-43 on the VAPB-PTPIP51 interaction was quantified using both proximity ligation assays and immunoprecipitation assays. Finally, preliminary results are presented to determine the effects of expressing wild-type and ALS mutants of FUS and SOD1 on the VAPB-PTPIP51 interaction in immunoprecipitation experiments.

As described in Chapter 3, NSC34 motor neuron cells were used for the electron microscopy studies and CV1 cells were used for the confocal light microscopy studies. For the immunoprecipitation studies, NSC34 cells were utilised.

4.2 Results

4.2.1 Expression of wild-type and ALS mutant TDP-43 disrupt ER-mitochondria associations in electron microscopy studies using NSC34 cells

To investigate the effect of TDP-43 on ER-mitochondria interactions, wild-type and familial ALS mutant TDP-43 were first transfected into NSC34 cells and ER-mitochondria associations then quantified by electron microscopy. This involved capturing images of mitochondria in appropriately manipulated cells and then calculating the percentage of the mitochondrial surface closely apposed (less than 25 nm) to ER. The quantification was performed using the ImageJ software (http://rsb.info.nih.gov/ij/) (see Section 2.2.3.3).

First, cells were transfected with EGFP control vector, EGFP-TDP-43 or ALS mutant EGFP-TDP-43 M337V. Since these transient transfections achieved transfection efficiencies of only 30% to 50%, the EGFP tags were further utilized to isolate transfected cells using a BD® FACS Aria cell sorter. The cell sorting achieved over 98% EGFP positive cells, which were further processed for the electron microscopy analyses (Figure 4.1). In control cells expressing EGFP alone, approximately 12% of the mitochondrial surface was closely associated with ER (Figure 4.2) and this was similar to that in cells expressing ECFP or treated with control siRNA (see Figures 3.1 and 3.5). However, the expression of both wild-type and TDP-43 M337V led to significant, approximate 50% reductions in ER-mitochondria associations (Figure 4.2).

4.2.2 TDP-43 disrupts ER-mitochondria co-localization in confocal microscopy studies using CV1 cells

For these investigations, CV1 cells were utilized due to their highly spread and flattened phenotype which facilitates immunofluorescent morphological analyses. As described in Chapter 3, ER was detected by immunostaining for the integral ER protein PDI and mitochondria were detected by immunostaining for TOM20. The co-localization of PDI and TOM20 was quantified using ICA and data presented as relative intensity correlation quotients (ICQ) (Li et al., 2004). ICA is a rigorous method for studying co-localization of proteins by confocal microscopy which compares the scatter plots of two stains against the product of the pixel intensity difference for each of the two stains from their respective means.

The cells were transfected with EGFP control vector, EGFP-TDP-43 or EGFP-TDP-43 M337V and ER and mitochondria co-localization monitored by immunostaining. The transfection of EGFP-TDP-43 or EGFP-TDP-43 M337V both decreased co-localization of PDI and TOM20 (Figure 4.3) and this was consistent with the EM results (Figure 4.2).

4.2.3 TDP-43 does not affect expression of VAPB, PTPIP51 or mitofusin-2

The finding that wild-type TDP-43 and TDP-43 M337V both disrupt ER-mitochondria interactions is consistent with the phenotypes seen in transgenic mice where expression of both wild-type and mutant TDP-43 all induce disease (Shan et al., 2010; Stallings et al., 2010; Wils et al., 2010; Xu et al., 2010). TDP-43 has been linked to mRNA metabolism and gene expression (Buratti and Baralle, 2012; Polymenidou et al., 2011; Tollervey et al., 2011). Therefore, it was enquired whether transfection of wild-type or

TDP-43 M337V influenced the expression of VAPB, PTPIP51 or mitofusin-2, a further protein that has been linked to ER-mitochondria associations. To do so, NSC34 cells transfected with control EGFP, EGFP-TDP-43 or EGFP-TDP-43 M337V were purified using a cell sorter via the EGFP fluorescent tag as described above. These purified cell populations were then analysed by immunoblotting for VAPB, PTPIP51 and mitofusin-2. However, no differences in the expression of any of these proteins were detected in the different samples (Figure 4.4). Thus, the reduction in ER-mitochondria interactions seen in cells expressing wild-type TDP-43 or TDP-43 M337V is not due to changes in expression of VAPB, PTPIP51 or mitofusin-2.

4.2.4 TDP-43 induced disruption of ER-mitochondria associations is accompanied by changes in VAPB-PTPIP51 interaction

Since VAPB and PTPIP51 mediate ER-mitochondria associations and these associations are disrupted by TDP-43 expression, the influence of TDP-43 on the VAPB-PTPIP51 interaction was investigated. To do so, VAPB-PTPIP51 binding was first monitored using a proximity ligation assay (Soderberg et al., 2006) (see Section 2.2.3.2). CV1 cells were transfected with EGFP control vector, wild-type EGFP-TDP43, ALS mutant EGFP-TDP-43 M337V or EGFP-TDP-43 A382T and then probed with VAPB and PTPIP51 primary antibodies. The proximity of VAPB to PTPIP51 in these cells was then detected following labeling with secondary antibodies coupled to complementary oligonucleotides (one for each of the two primary antibodies). If the distance between the two antibody-coupled oligonucleotides is less than 40 nm, they hybridize and generate fluorescent signals.

To first test the specificity of the assay, one or both primary antibodies were omitted from the reaction in control untransfected cells and this resulted in no or very few proximity ligation signals (Figure 4.5). In agreement with previous studies using this assay to monitor the VAPB-PTPIP51 interaction (De Vos et al., 2012), robust positive signals were obtained when both the primary antibodies were used (Figure 4.5). Transfection of EGFP control vector did not significantly influence the numbers of proximity ligation signals compared to non-transfected cells (Figure 4.6). However, the numbers of proximity ligation signals were significantly reduced in cells transfected with either wild-type or two different ALS mutants of TDP-43 (Figure 4.6).

The effect of TDP-43 on the VAPB-PTPIP51 interaction was also monitored using immunoprecipitation assays in cells transfected with EGFP control vector, wild-type EGFP-TDP-43 or four different ALS mutants of EGFP-TDP-43 (TDP-43 M337V, TDP-43 Q331K, TDP-43 A382T and TDP-43 G348C). PTPIP51 was immunoprecipitated from PTPIP51-HA co-transfected cells using the anti-HA antibody and the amounts of bound endogenous VAPB detected by immunoblotting. Expression of wild-type TDP-43 and four different ALS associated mutants of TDP-43 all reduced the amount of VAPB that was associated with PTPIP51 in these assays (Figure 4.7). Thus, expression of ALS associated TDP-43 disrupts ER-mitochondria interactions and this is associated with a decrease in the binding of VAPB to PTPIP51 as detected in two different assays (proximity ligation and immunoprecipitation assays).

4.2.5 ALS associated FUS but not SOD1 disrupts VAPB binding to PTPIP51 in immunoprecipitation assays

The above studies demonstrated that ALS-associated TDP-43 disrupts ER-mitochondria interactions and that this is associated with a decrease in binding of VAPB to PTPIP51. To begin to investigate whether other insults associated with familial ALS might also disrupt binding of VAPB to PTPIP51, the effects of expressing wild-type and ALS mutants of FUS and SOD1 on the VAPB-PTPIP51 interaction was investigated in immunoprecipitation experiments. Cells were co-transfected with PTPIP51-HA and either EGFP control, wild-type EGFP-FUS, ALS mutants of EGFP-FUS, wild-type EGFP-SOD1 or ALS mutants of EGFP-SOD1. ALS mutants of FUS were FUS R521C, FUS R521G, FUS R521H, FUS R518K. ALS mutants of SOD1 were SOD1 G93A and SOD1 A4V. PTPIP51 was then immunoprecipitated using the HA tag and the amounts of co-immunoprecipitating endogenous VAPB detected by immunoblotting.

Expression of wild-type and all four ALS mutants of FUS all reduced the amounts of VAPB associated with PTPIP51 in these assays (Figure 4.8). However, neither wild-type nor ALS mutant SOD1 affected the amounts of VAPB that co-immunoprecipitated with PTPIP51 (Figure 4.9). Thus, ALS FUS, but not SOD1 disrupts the VAPB-PTPIP51 interaction in a manner similar to that of TDP-43.

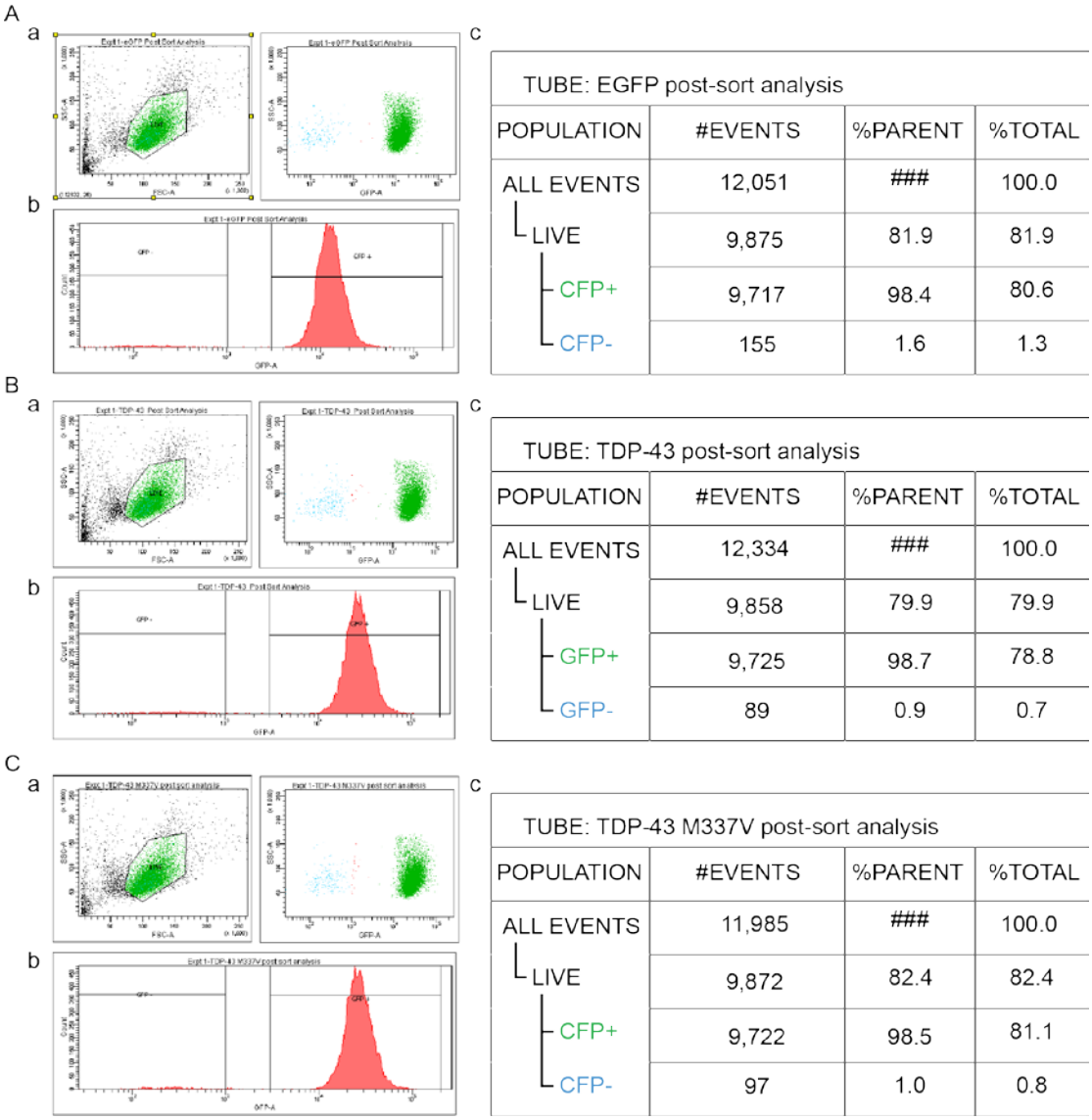

Figure 4.1 FACS post-sorting analyses demonstrating purification of EGFP positive samples

NSC34 cells transfected with EGFP control vector (A), EGFP-TDP-43 (B) or EGFP-TDP-43 M337V (C) were sorted based on their EGFP tags. The scatter plots (A-a, B-a, C-a) illustrate high cell viability and low amounts of cell debris in the sorted population. The area charts (A-b, B-b, C-b) display an EGFP positive cell population (GFP+) distinct from the very few negative cells (GFP-). The tables (A-c, B-c, C-c) show the percentage of viable cells in the sorted population and the percentage of EGFP positive cells within the live population.

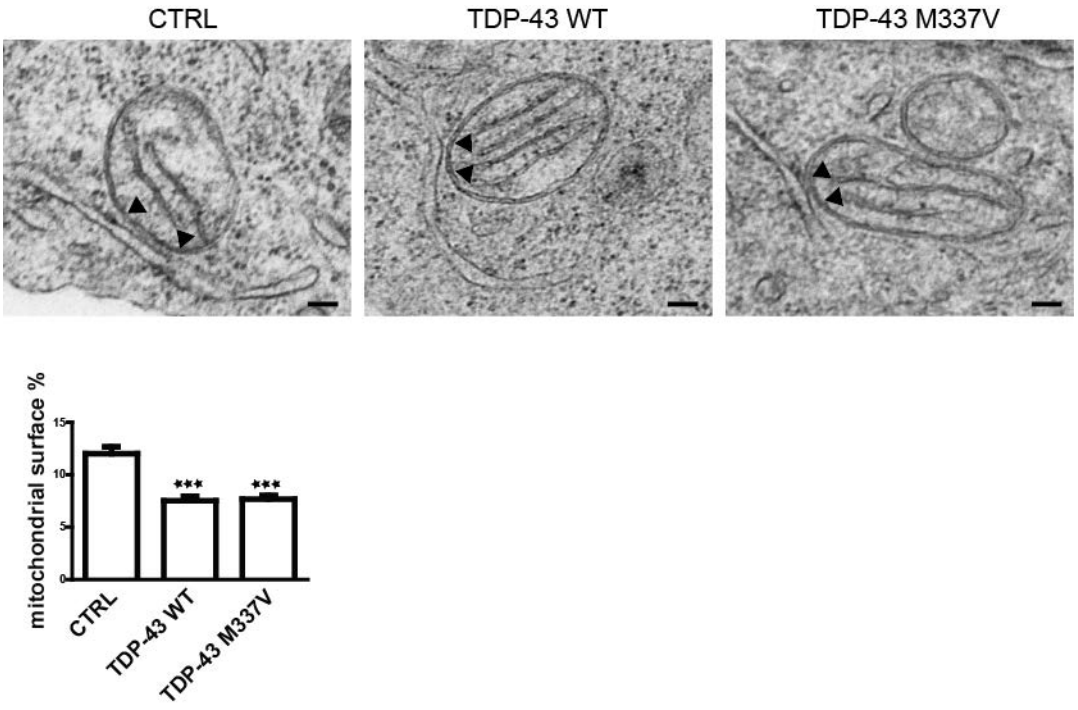

Figure 4.2 Expression of wild type and ALS mutant TDP-43 reduce ER-mitochondria associations

Representative electron micrographs of ER-mitochondria contacts in NSC34 cells transfected with control EGFP vector (CTRL), EGFP-TDP-43 or EGFP-TDP-43M337V as indicated. Scale bar is 100 nm. Arrowheads show ER-mitochondria contact sites. Bar chart shows % of mitochondrial surface closely apposed to ER in the different samples. Data were analysed by one-way ANOVA followed by Tukey's multiple comparison test. n=34-40 cells and 483-747 mitochondria; error bars are SEM; ***$p<0.001$.

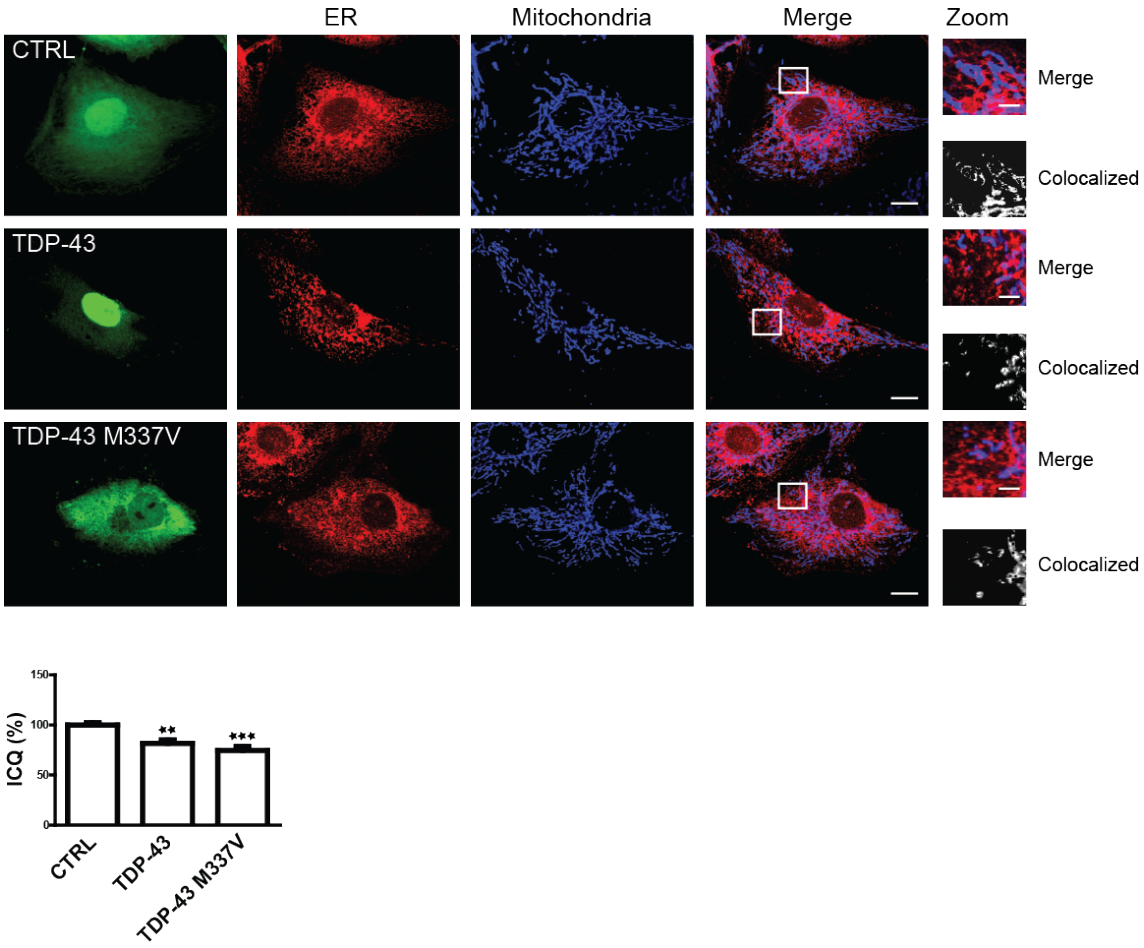

Figure 4.3 Expression of wild type or ALS mutant TDP-43 reduce ER-mitochondria co-localization

Confocal immunostaining of CV-1 cells transfected with control EGFP vector (CTRL), EGFP-TDP-43 or EGFP-TDP-43-M337V and immunostained for ER (using mouse PDI antibody) and mitochondria (using rabbit TOM-20 antibody) as indicated. Zoom shows high magnification of boxed area with co-localized pixels. Scale bars=20 μm, 4 μm (zoom). Bar chart shows ICQ values (with EGFP control represented as 100%) in the different transfections. Data were analysed by one-way ANOVA with Tukey's post-hoc test. n=36-49 cells; error bars are SEM; **p<0.01, ***p<0.001.

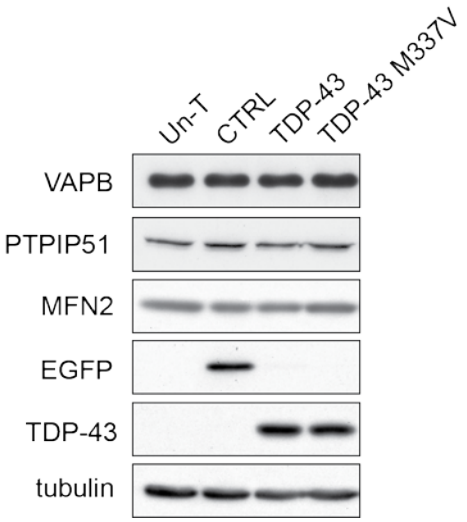

Figure 4.4 Overexpression of wild-type or ALS associated mutant TDP-43 do not alter expression of VAPB, PTPIP51 or mitofusin-2 (MFN2)

Immunoblots of NSC34 cells either untransfected (Un-T) or transfected with EGFP as a control (CTRL), EGFP-TDP-43 or EGFP-TDP-43 M337V. Transfected cells were purified via the EGFP tag using a cell sorter and the samples probed on immunoblots as indicated. Tubulin is shown as a loading control.

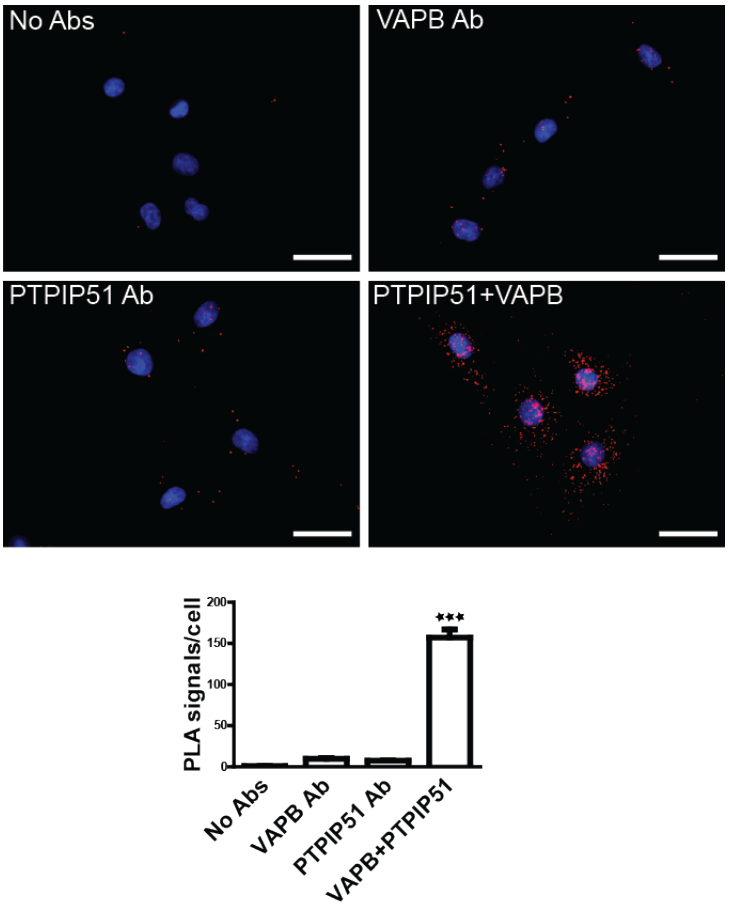

Figure 4.5 Specificity of the Duolink proximity ligation assay for VAPB and PTPIP51

Non-transfected CV1 cells were labeled with no primary antibodies (No Abs), with VAPB antibody alone (VAPB Ab), with PTPIP51 antibody alone (PTPIP51 Ab) or with both VAPB and PTPIP51 antibodies (PTPIP51+VAPB). In agreement with previous studies (De Vos et al., 2012), omission of one or both of the primary antibodies produced no or very few proximity ligation signals. However, probing with both VAPB and PTPIP51 antibodies produced strong positive ligation signals. Scale bar is 40 μm. Bar charts show numbers of proximity signals/cell in the different transfections. Data were analysed by one-way ANOVA and Tukey's post hoc test. n=30 cells; error bars are SEM, ***$p<0.001$.

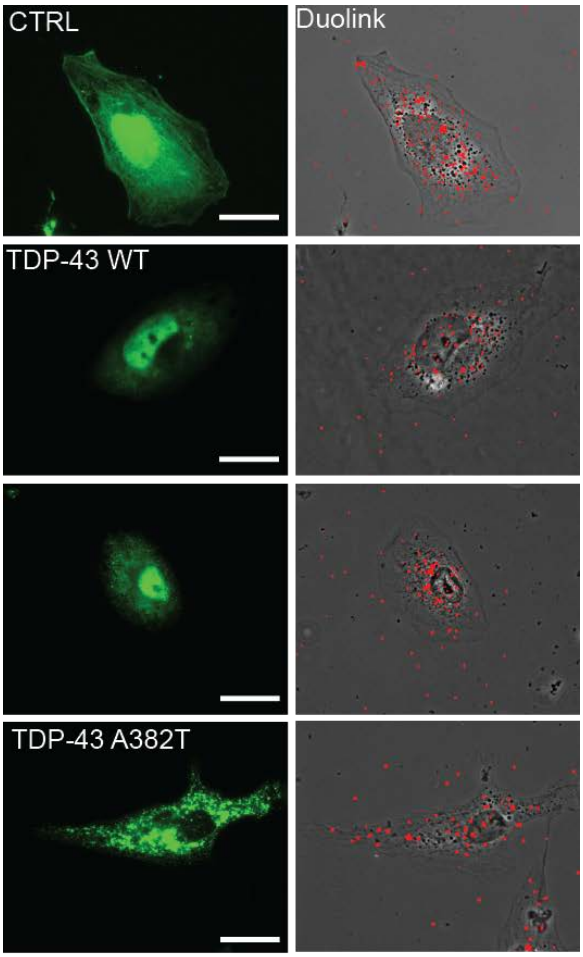

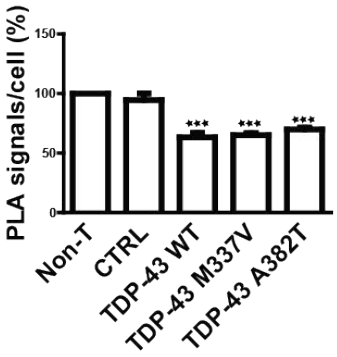

Figure 4.6 Expression of wild-type or ALS associated mutants of TDP-43 all reduce the interaction of VAPB with PTPIP51 in proximity ligation assays

CV1 cells were transfected with either EGFP control vector (CTRL), EGFP-TDP-43, EGFP-TDP-43 M337V or EGFP-TDP-43 A382T and proximity ligation assays performed using rat anti-VAPB and rabbit anti-PTPIP51 primary antibodies. Representative cells transfected with EGFP, EGFP-TDP-43, EGFP-TDP43 M337V and

EGFP-TDP43 A382T are shown. Scale bar is 40 μm. Bar charts show relative % of proximity signals/cell in the different transfections. Data were analysed by one-way ANOVA and Tukey's post hoc test. n=30 cells; error bars are SEM, ***$p<0.001$.

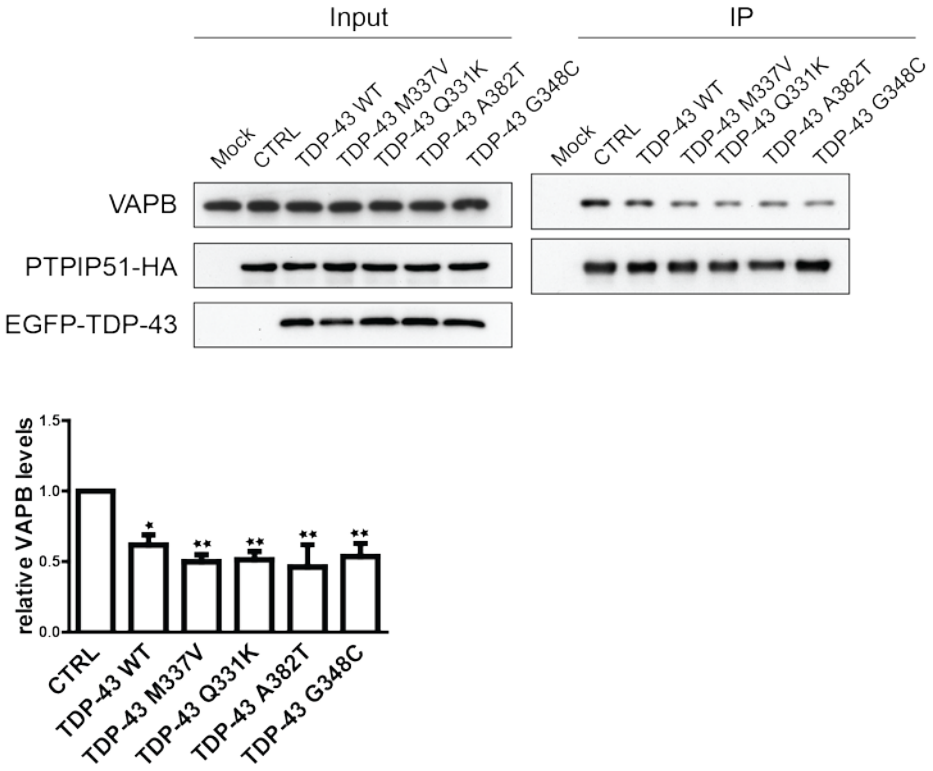

Figure 4.7 Expression of wild-type or ALS associated mutants of TDP-43 (TDP-43 Q331K, TDP-43 M337V, TDP-43 G348C and TDP-43 A382T) reduce the binding of VAPB to PTPIP51 in immunoprecipitation assays

Cells were either mock transfected (Mock) or co-transfected with PTPIP51-HA and either EGFP control vector (CTRL) or wild type or ALS mutants of TDP-43. PTPIP51 was immunoprecipitated using the HA-tag and the amounts of endogenous bound VAPB detected by immunoblotting. No signals were obtained for either VAPB or PTPIP51 in immunoprecipitations from mock transfected cells which demonstrates the specificity of the immunoprecipitations. Both inputs and immunoprecipitations (IP) are shown. Bar charts show relative levels of VAPB bound to PTPIP51 in the immunoprecipitations following quantification of signals from immunoblots. VAPB signals were normalized to immunoprecipitated PTPIP51-HA signals. Data were analysed by one-way ANOVA and Tukey's post hoc test. n=5; error bars are SEM, *$p<0.05$, **$p<0.01$.

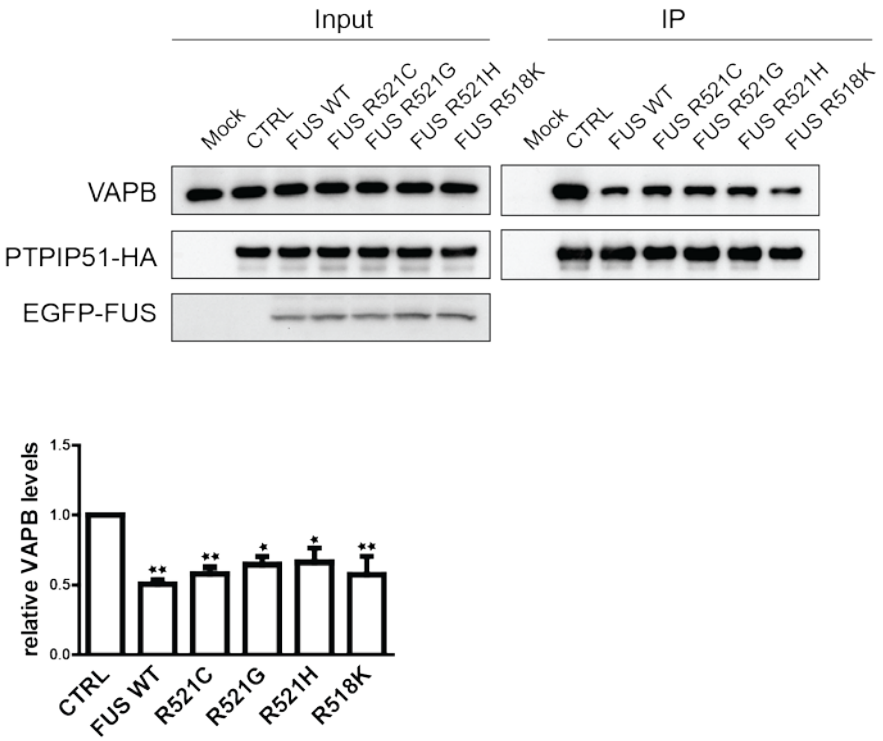

Figure 4.8 Expression of wild-type or ALS associated mutants of FUS (FUS R521C, FUS R521G, FUS R521H and FUS R518K) reduce the binding of VAPB to PTPIP51 in immunoprecipitation assays

Cells were either mock transfected (Mock) or co-transfected with PTPIP51-HA and either EGFP control vector (CTRL) or wild type or ALS mutants of FUS. PTPIP51 was immunoprecipitated using the HA-tag and the amounts of endogenous bound VAPB detected by immunoblotting. No signals were obtained for either VAPB or PTPIP51 in immunoprecipitations from mock transfected cells which demonstrates the specificity of the immunoprecipitations. Both inputs and immunoprecipitations (IP) are shown. Bar charts show relative levels of VAPB bound to PTPIP51 in the immunoprecipitations following quantification of signals from immunoblots. VAPB signals were normalized to immunoprecipitated PTPIP51-HA signals. Data were analysed by one-way ANOVA and Tukey's post hoc test. n=5; error bars are SEM, *$p<0.05$, **$p<0.01$.

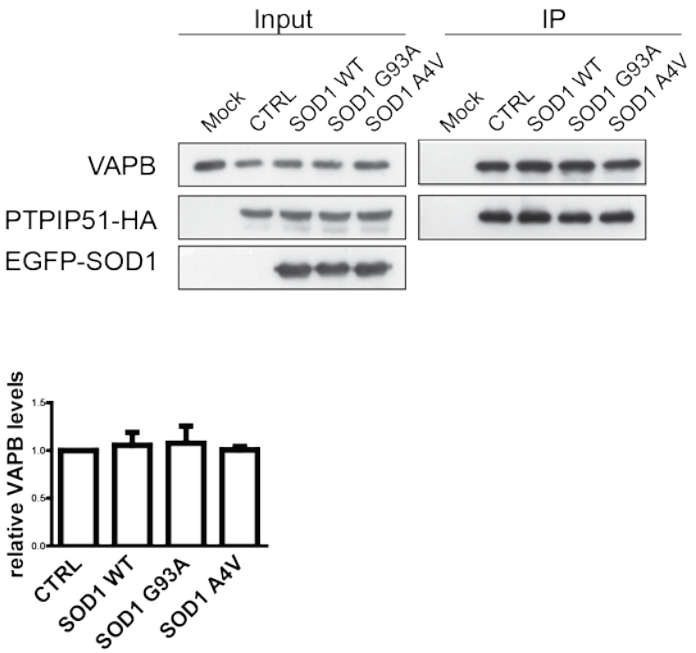

Figure 4.9 Expression of wild-type or ALS associated mutants of SOD1 (SOD1 G93A, SOD1 A4V) do not influence the binding of VAPB to PTPIP51 in immunoprecipitation assays

Cells were either mock transfected (Mock) or co-transfected with PTPIP51-HA and either EGFP control vector (CTRL) or wild type or ALS mutants of SOD1. PTPIP51 was immunoprecipitated using the HA-tag and the amounts of endogenous bound VAPB detected by immunoblotting. No signals were obtained for either VAPB or PTPIP51 in immunoprecipitations from mock transfected cells which demonstrates the specificity of the immunoprecipitations. Both inputs and immunoprecipitations (IP) are shown. Bar charts show relative levels of VAPB bound to PTPIP51 in the immunoprecipitations following quantification of signals from immunoblots. VAPB signals were normalized to immunoprecipitated PTPIP51-HA signals. Data were analysed by one-way ANOVA. n=3; error bars are SEM.

4.3 Discussion

Abnormal accumulations of TDP-43 are a hallmark pathology in a number of neurodegenerative diseases including ALS and FTD (Arai et al., 2006; Neumann et al., 2006). However, the molecular mechanisms by which defective TDP-43 metabolism might induce disease are not clear. Overexpression of both wild-type and familial ALS associated mutants of TDP-43 all induce disease in transgenic rodents (Shan et al., 2010; Stallings et al., 2010; Swarup et al., 2011; Wils et al., 2010; Xu et al., 2010; Xu et al., 2011b; Zhou et al., 2010). Moreover, elevated TDP-43 expression has been observed in sporadic ALS patients (Kasai et al., 2009; Suzuki et al., 2010). Together, these findings suggest that overexpression of wild-type TDP-43 is pathogenic in ALS.

The cellular targets of pathogenic TDP-43 are not fully understood but disruption to both mitochondria (Braun et al., 2011; Shan et al., 2010; Xu et al., 2010; Xu et al., 2011b) and ER stress signaling pathways (Suzuki et al., 2011; Suzuki and Matsuoka, 2012; Tong et al., 2012) have been described. These findings focus attention on the ER-mitochondria axis. Moreover, several recent studies have implicated defective ER-mitochondria contacts in some related neurodegenerative diseases including Alzheimer's and Parkinson's diseases (Area-Gomez et al., 2012; Cali et al., 2012; Zampese et al., 2011).

In this chapter, both wild-type and ALS associated mutant TDP-43 were shown to reduce ER-mitochondria associations in both electron and confocal microscopy analyses. Moreover, the TDP-43-induced change in ER-mitochondria contacts was accompanied by decreases in VAPB-PTPIP51 interactions demonstrated in two

different assays. It thus seems likely that the effect of TDP-43 on ER-mitochondria associations involves a TDP-43-induced decrease in binding of VAPB to PTPIP51.

In order to begin to determine whether other ALS-associated insults also influence ER-mitochondria associations and the VAPB-PTPIP51 interaction, the effects of wild-type and ALS mutant FUS and SOD1 on VAPB-PTPIP51 binding was studied. This involved immunoprecipitation experiments similar to those performed for TDP-43. These experiments revealed that overexpression of both wild-type and ALS associated FUS decreased the VAPB-PTPIP51 interaction. Interestingly, expression of wild-type FUS (like wild-type TDP-43) is pathogenic in transgenic mice (Mitchell et al., 2012). By contrast, overexpression of wild-type or ALS mutant SOD1 did not influence the VAPB-PTPIP51 interaction. It appears that the effect of mutant SOD1 on the ER-mitochondria axis and especially on the VAPB-PTPIP51 connection may be different to that of TDP-43 and FUS. However, SOD1 has been shown to damage VDAC1, a protein believed to contribute to ER-mitochondria associations (Israelson et al., 2010; Szabadkai et al., 2006). Therefore, it is possible that all these ALS insults perturb ER-mitochondria associations, but the precise target for mutant SOD1 damage within MAM axis is different to TDP-43 and FUS. Clearly, future studies to quantify ER-mitochondria associations in the presence of wild-type and ALS mutant FUS and SOD1 using electron microscopy methods similar to those described in this thesis will help resolve these issues.

The regulation of ER-mitochondria associations is fundamental to a number of physiological processes and both abnormal tightening or loosening of ER-mitochondria contacts are predicted to have detrimental effects to cells. In particular, excessive

tightening of contacts may sensitize mitochondria to Ca^{2+} overload leading to opening of the mitochondrial permeability transition pore and apoptosis (Hajnoczky et al., 2006; Szabadkai et al., 2006).

By contrast, loosening of ER-mitochondria contacts will affect Ca^{2+}-dependent regulation of the tricarboxylic acid cycle and ATP synthesis by mitochondria (Csordas et al., 2006; Rowland and Voeltz, 2012). Synaptic dysfunction is a key and early feature of ALS and the energy requirements of synapses are especially high; ATP is required to drive the pumps that maintain ionic potential at the synapse (Laughlin et al., 1998). Disruption to mitochondrial ATP synthesis is thus predicted to have particularly detrimental effects at the synapse.

Another piece of evidence suggests that controlling the distance between ER and mitochondria can determine the rate of Ca^{2+} refilling in neighboring ER regions (Arnaudeau et al., 2001). Therefore, this raises the possibility that reduced ER-mitochondria contacts might decrease intraluminal ER Ca^{2+}, which in turn could affect proper protein folding, inducing ER stress and triggering the UPR (Lodish and Kong, 1990; Zhang and Kaufman, 2008). In addition, close interorganellar contacts are essential in the early phases of ER stress and uncoupling mitochondria from ER renders cells more vulnerable to stress (Bravo et al., 2011). Indeed, chronic ER stress and UPR are common findings in ALS patients and represent some of the earliest pathogenic changes detected in this disease ((Kanekura et al., 2009) and see Section 1.3.7). Chronic unresolved UPR can trigger cell death programmes through the activation of C/EBP homologous protein or c-Jun N-terminal kinase and both these pathways have recently been found to be activated by TDP-43 (Suzuki and Matsuoka, 2012, 2013).

Finally, detaching mitochondria from the ER membranes can prevent local Ca^{2+} uptake in regions with high Ca^{2+} concentrations, thus diminishing mitochondrial Ca^{2+} buffering and elevating intracellular Ca^{2+} levels. Indeed, delayed mitochondrial Ca^{2+} uptake and higher intracellular peaks have been described following ablation of proposed ER-mitochondria tethering proteins VAPB, PTPIP51 or mitofusin-2 (de Brito and Scorrano, 2008; De Vos et al., 2012). Elevated cytosolic Ca^{2+} could prove particularly disruptive in motor neurons, which have weak Ca^{2+} buffering systems in physiological conditions and rely heavier on their mitochondrial Ca^{2+} buffering capacity (see for review (von Lewinski and Keller, 2005)). Thus, diminished mitochondrial Ca^{2+} uptake combined with the increased glutamate activity previously described in ALS may further accelerate motor neuron demise.

In summary, the results in this chapter reveal a novel pathogenic role for TDP-43 in decreasing ER-mitochondria associations via the VAPB-PTPIP51 interaction. This may perturb Ca^{2+} homeostasis and ATP production, therefore contributing to motor neuron degeneration. However, the mechanisms by which TDP-43 disrupts the VAPB-PTPIP51 interaction are unclear; TDP-43 did not alter the expression of either VAPB or PTPIP51. A further possible route by which TDP-43 could influence the VAPB-PTPIP51 binding might be via post-translational changes such as phosphorylation of either VAPB or PTPIP51. This topic was investigated further in the next chapter of this thesis.

CHAPTER 5: VAPB AND PTPIP51 PHOSPHORYLATION AS A REGULATORY MECHANISM FOR CONTROLLING THEIR INTERACTION

5.1 Introduction

The results in Chapter 3 support a role for VAPB and PTPIP51 in mediating ER-mitochondria associations. It is likely that ER-mitochondria interactions are dynamic and alter in response to physiological changes. The tightening of ER-mitochondria associations will increase Ca^{2+} and possibly phospholipid exchange between the two organelles. This may be required in situations of high energy demand since Ca^{2+} regulates the tricarboxylic acid cycle and ATP synthesis by mitochondria (Csordas et al., 2006; Rowland and Voeltz, 2012). However, prolonged and excessively close ER-mitochondria associations are likely to promote mitochondrial Ca^{2+} overload, leading to opening of the permeability transition pore and apoptosis (Csordas et al., 2006; Rowland and Voeltz, 2012). As such, it is possible that cellular mechanisms controlling the levels of ER-mitochondria association involve modulation of the VAPB-PTPIP51 interaction.

Reversible phosphorylation is the most common posttranslational modification to proteins and is a potent mechanism for influencing protein function and also protein-protein interactions. Indeed, a recent study investigating the interaction profile of PTPIP51 suggests that phosphorylation on tyrosine residues can influence its interaction with several binding partners such as 14-3-3β, Raf-1 and protein tyrosine phosphatase-1B (PTP1B) (Brobeil et al., 2012).

In order to properly examine the possibility that phosphorylation regulates the VAPB-PTPIP51 interaction, potential phosphorylation sites in both of these proteins first need to be identified. This will then facilitate the identification of kinases and

phosphatases that regulate VAPB and PTPIP51 phosphorylation and the experimental manipulation of VAPB/PTPIP51 phosphorylation state.

In this chapter, the phosphoryalytion of PTPIP51 and VAPB was investigated. Firstly, mass spectrometric sequencing of PTPIP51 and VAPB was undertaken and several serine and threonine phosphorylation sites were identified in both proteins. Secondly, mutagenic approaches were used in which identified sites were altered to preclude phosphorylation or to mimic permanent phosphorylation. The effects of these mutations on VAPB-PTPIP51 binding was then studied in immunoprecipitation assays.

5.2 Results

5.2.1 Purification of PTPIP51 by immunoprecipitation and separation on SDS-PAGE

To identify phosphorylation sites within PTPIP51, the first approach taken was to sequence the protein via mass spectrometry. Mass spectrometry is a powerful method to detect posttranslational modifications; the sensitivity and accuracy of this method allows analyses of amounts as little as 10 nanograms for individual proteins (Larsen et al., 2006). However, phosphorylation is usually present at sub-stoichiometric levels and the likelihood of finding such modification increases with a larger amount of starting material. Thus, HA-tagged PTPIP51 was exogenously expressed in cultured CHO cells by transfection in order to increase the amounts of protein available for the mass spectrometry analysis. High transfection efficiencies are usually achieved in CHO cells, which are often used to obtain high yields of transfected proteins including large scale production of pharmaceutical proteins (Omasa et al., 2010). The HA tag on the transfected PTPIP51 also enabled the purification of PTPIP51 by immunoprecipitation methods using an antibody directed against the HA epitope.

Thus, HA-tagged PTPIP51 was transfected into CHO cells and purified by immunoprecipitation with anti-HA and separation on SDS-PAGE. As a control to demonstrate the specificity of the immunoprecipitation, control vector transfected CHO cells were subjected to immunoprecipitation with the same anti-HA antibody and immunoprecipitations from both samples were performed with no HA antibody. As shown in Figure 5.1A, a protein species corresponding to the correct size of PTPIP51 was specifically detected in the PTPIP51 transfected CHO cell samples. Probing

immunoblots of the same samples confirmed that this species was PTPIP51 (Figure 5.1 B) and mass spectrometry further confirmed this result (Figure 5.2).

5.2.2 Identification of phosphorylation sites in PTPIP51 by mass spectrometry

Following extraction of the PTPIP51-HA protein band from the SDS PAGE gels and trypsin digestion, the peptides mixture was subjected to LC/MS/MS as described in section 2.2.2.6. Tandem mass spectrometry analyses identified the band as PTPIP51 with a sequence coverage of 58% (Figure 5.2A). Four phosphopeptides were identified (Figure 5.2B) and after amino acid sequencing of each phosphopeptide by MS/MS, phosphorylation was assigned to serine 44 (S44) (Figure 5.3), serine 46 (S46) (Figure 5.4), serine 50 (S50) (Figure 5.5) and serine 212 (S212) (Figure 5.6).

S44, S46 and S50 are located between the transmembrane domain and the coiled coil domain of PTPIP51. S212 is found between the coiled coil domain and the C-terminus of PTPIP51 (Figure 5.7). In the same region of the protein, two other phosphorylation sites (S221, S225) have been previously identified in a phosphoproteomics screen (Chen et al., 2009). Due to their close proximity to S212, all 6 phosphoserine residues were mutated.

5.2.3 PTPIP51 is phosphorylated on tyrosine residue(s)

Although the above mass spectrometry studies identified phosphorylation of PTPIP51 on serine residues, no phosphorylation on tyrosines was detected. To assess whether PTPIP51 is also phosphorylated on tyrosine, a different strategy was chosen. This involved using the tyrosine phosphatase inhibitor pervanadate (Huyer et al., 1997) and an antibody that specifically detects proteins phosphorylated on tyrosine residues

(antibody 4G10). Pervanadate was used to inhibit tyrosine phosphatases as to induce tyrosine phosphorylation of proteins in CHO cells transfected with PTPIP51-HA. Phosphorylation on tyrosines was then detected with the 4G10 antibody. Thus, cells expressing transfected HA-tagged PTPIP51 were treated with pervanadate (as described in Section 2.2.4.1), lysed and PTPIP51 was immunoprecipitated with the anti-HA antibody. The immunoprecipitated material was analysed by immunoblotting with antibody 4G10 and anti-HA antibody. As shown in Figure 5.8, no signals from either antibody were detected in the absence of immunoprecipitating HA antibody demonstrating the specificity of the immunoprecipitations. Immunoprecipitated PTPIP51-HA from untreated cells did not react or reacted only weakly with antibody 4G10 (seen following extended exposures of the immunoblots; Figure 5.8). However, in cells treated with pervanadate, a robust 4G10 signal was detected demonstrating that inhibition of tyrosine phosphatases drives increased phosphorylation of PTPIP51.

The weak 4G10 reactivity under basal conditions (Figure 5.8) might explain the failure of the previous mass spectrometry experiments to identify phosphorylation of tyrosines in PTPIP51. Therefore the mass spectrometry analysis was repeated after treating the cells with pervanadate. Thus, PTPIP51-HA was exogenously expressed in cultured CHO cells, the cells treated with pervanadate and PTPIP51-HA protein immunoprecipitated using the anti-HA antibody. Following separation of proteins on SDS-PAGE (as in Figure 5.1), the samples were subjected to LC/MS/MS analyses. These identified the protein as PTPIP51 with a sequence coverage of 57% but no tyrosine phosphopeptides were detected.

5.2.4 Purification of VAPB by immunoprecipitation and separation on SDS-PAGE

The same approach as for PTPTIP51 was used to identify phosphorylation sites in myc tagged VAPB. VAPB was transfected into CHO cells, purified by immunoprecipitation and SDS-PAGE and then sequenced by LC/MS/MS.

As a control to demonstrate the specificity of the immunoprecipitation, control vector transfected CHO cells were subjected to immunoprecipitation with the same anti-myc antibody and immunoprecipitations from both samples were performed with no antibody. As shown in Figure 5.9A, a protein species corresponding to the correct size of VAPB was specifically detected in the transfected CHO cell samples. Immunoblotting of the same samples revealed this species was VAPB (Figure 5.9B) and mass spectrometry further confirmed this result (Figure 5.10).

5.2.5 Identification of phosphorylation sites in VAPB by mass spectrometry

Following extraction of the myc-VAPB protein band from the SDS PAGE gels and trypsin digestion, the peptide mixture was subjected to LC/MS/MS as described in section 2.2.2.5. Tandem mass spectrometry analyses identified the band as VAPB with sequence coverage of 54% (Figure 5.10A). Two phosphopeptides were identified (Figure 5.10B) and after amino acid sequencing of each phosphopeptide by MS/MS, phosphorylation was assigned to threonine 150 (T150) (Figure 5.11) and serine 158 (S158) (Figure 5.12).

T150 and S158 are located between the MSP domain and the coiled coil domain of VAPB (Figure 5.13). Although the mass spectrometry analyses identified phosphorylation of VAPB on serine and threonine residues, no phosphorylation on

tyrosines was detected. In the same region, previous mass spectrometry studies have identified other phosphorylation sites on serine residues (S146, S156, S159 and S160) (Christensen et al., 2010; Olsen et al., 2010; Weber et al., 2012; Wu et al., 2010). Thus all six identified sites were mutated for the immunoprecipitation analyses.

5.2.6 Mutation of the PTPIP51 and VAPB phosphorylation sites does not affect the PTPIP51-VAPB interaction

To investigate the role of PTPIP51 phosphorylation, mutants were generated and their ability to interact with VAPB was monitored in immunoprecipitation assays from transfected HEK293 cells. The previously identified phosphorylated residues in PTPIP51 were mutated to alanine to preclude phosphorylation or to aspartate to mimic permanent phosphorylation. There are many examples where replacing serines with a negatively charged residue such as an aspartate accurately mimics the effect of phosphorylation of the site (e.g. (Ackerley et al., 2003; Eidenmuller et al., 2000; Raingeaud et al., 1996)).

The effect of phosphorylation mutants of PTPIP51 on binding to VAPB was monitored first. To achieve this, two sets of triple mutants were created: PTPIP51$^{S44A/S46A/S50A}$, PTPIP51 $^{S44D/S46D/S50D}$, PTPIP51$^{S212A/S221A/S225A}$ and PTPIP51 $^{S212D/S221D/S225D}$. In addition, all six serine residues were mutated to alanine or aspartate respectively. PTPIP51 wild-type (PTPIP51), PTPIP51$^{S44A/S46A/S50A}$, PTPIP51$^{S44D/S46D/S50D}$, PTPIP51$^{S212A/S221A/S225A}$, PTPIP51$^{S212D/S221D/S225D}$, PTPIP51$^{S44A/S46A/S50A/S212A/S221A/S225A}$ and PTPIP51 $^{S44D/S46D/S50D/S212D/S221D/S225D}$ were separately transfected into HEK293 cells and specifically immunoprecipitated using the HA tag. PTPIP51wt, PTPIP51$^{S44A/S46A/S50A}$, PTPIP51$^{S44D/S46D/S50D}$, PTPIP51$^{S212A/S221A/S225A}$, PTPIP51$^{S212D/S221D/S225D}$,

PTPIP51$^{S44A/S46A/S50A/S212A/S221A/S225A}$ and PTPIP51 $^{S44D/S46D/S50D/S212D/S221D/S225D}$ all interacted equally well with endogenous VAPB in these assays and no signals for either PTPIP51 or VAPB were obtained from control transfected cells demonstrating the specificity of the immunoprecipitations (Figure 5.14). Thus, the interaction between transfected PTPIP51-HA and endogenous VAPB is not influenced by altering the identified phosphorylation sites in PTPIP51 to either preclude or mimic permanent phosphorylation.

In order to investigate the role of VAPB phosphorylation, mutants were generated and their ability to interact with endogenous PTPIP51 was monitored in immunoprecipitation assays from transfected HEK293 cells. In the same way as for PTPIP51, the previously identified phosphorylated residues in VAPB were mutated to alanine to preclude phosphorylation or to aspartate to mimic permanent phosphorylation. Two sets of mutants were created that include the identified phosphorylated residues and the additional serine residues identified in VAPB by others: VAPB$^{T150A/S158A}$, VAPB$^{T150D/S158D}$, VAPB$^{S146A/T150A/S156A/S158A/S159A/S160A}$ and VAPB$^{S146D/T150D/S156D/S158D/S159D/S160D}$. VAPB wild-type (VAPB), VAPB$^{T150A/S158A}$, VAPB$^{T150D/S158D}$, VAPB$^{S146A/T150A/S156A/S158A/S159A/S160A}$ and VAPB$^{S146D/T150D/S156D/S158D/S159D/S160D}$ were separately transfected into HEK293 cells and specifically immunoprecipitated using the myc tag. VAPBwt, VAPB$^{T150A/S158A}$, VAPB$^{T150D/S158D}$, VAPB$^{S146A/T150A/S156A/S158A/S159A/S160A}$ and VAPB$^{S146D/T150D/S156D/S158D/S159D/S160D}$ all interacted equally well with endogenous PTPIP51 in these assays and no signals for either PTPIP51 or VAPB were obtained from control transfected cells demonstrating the specificity of the immunoprecipitations (Figure 5.15). Thus, the interaction between transfected myc-VAPB and endogenous

PTPIP51 is not influenced by altering the identified phosphorylation sites in VAPB to either preclude or mimic permanent phosphorylation. Interestingly however, mutating all 6 identified phosphorylation sites to aspartate markedly slowed the migration of VAPB on SDS-PAGE (Figure 5.15).

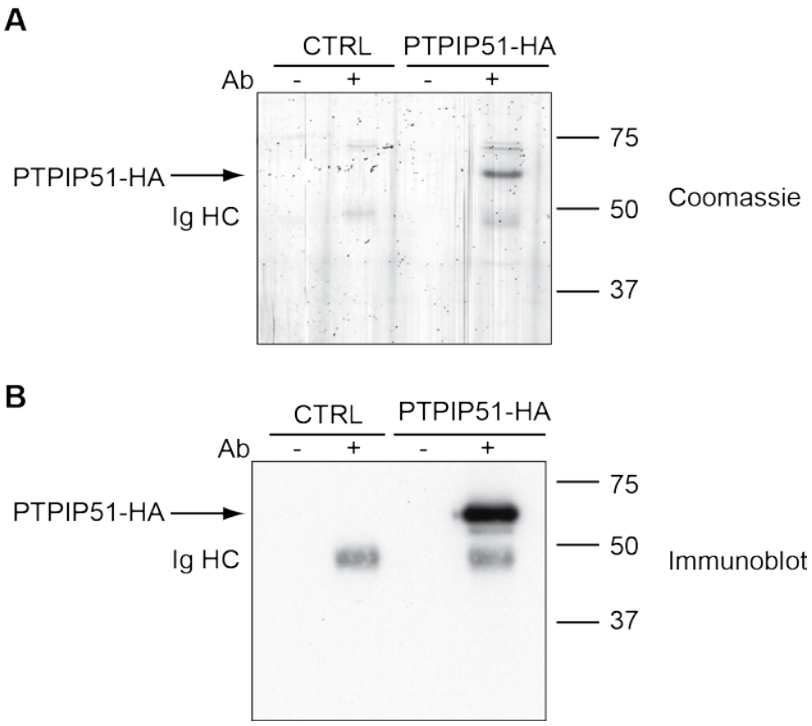

Figure 5.1 Purification of PTPIP51-HA by immunoprecipitation

CHO cells were transfected with either control vector (CTRL) or PTPIP51-HA and transfected PTPIP51-HA was immunoprecipitated using anti-HA antibody. (A) shows Coomassie Blue stained gel. (B) shows immunoblot probed with anti-HA antibody to detect PTPIP51-HA. -Ab and +Ab refer to absence or presence of the anti-HA antibody in the immunoprecipitations. The positions of PTPIP51-HA and immunoglobulin heavy chain (Ig HC) of the anti-HA antibody are shown. Molecular mass markers are shown on the right.

A

MSRLGALGGARAGLGLLLGTAAGLGFLCLLYSQRWKRTQRHGRSQSLPNSLD
YTQTSDPGRHVMLLRAVPGGAGDASVLPSLPREGQEKVLDRLDFVLTSLVALR
REVEELRSSLRGLAGEIVGEVRCHMEENQRVARRRRFPFVRERSDSTGSSSVYF
TASSGATFTDAESEGGYTTANAESDNERDSDKESEDGEDEVSCETVKMGRKDS
LDLEEEAASGASSALEAGGSSGLEDVLPLLQQADELHRGDEQGKREGFQLLLN
NKLVYGSRQDFLWRLARAYSDMCELTEEVSEKKSYALDGKEEAEAALEKGDE
SADCHLWYAVLCGQLAEHESIQRRIQSGFSFKEHVDKAIALQPENPMAHFLLGR
WCYQVSHLSWLEKKTATALLESPLSATVEDALQSFLKAEELQPGFSKAGRVYIS
KCYRELGKNSEARWWMKLALELPDVTKEDLAIQKDLEELEVILRD

B

Peptide sequence	Residue	m/z
HGR**S**QSLPNSLDYTQTSDPGR	41-61	799.41
KD**S**LDLEEEAASGASSALEAGGSSGLEDVLPLLQQADELH	210-250	1430.1
SQSLPN**S**LDYTQTSDPGR	44-61	1023.5
SQ**S**LPNSLDYTQTSDPGR	44-61	1023.5

Figure 5.2 Phosphorylation sites identified in PTPIP51

(A) Sequence of human PTPIP51 with the MS/MS sequence coverage obtained after trypsin digestion shown as underlined. Four phosphorylation sites were identified (S44, S46, S50 and S212) which are highlighted. (B) PTPIP51 phosphopeptides obtained by MS/MS sequencing with their mass/charge (m/z) ratios. Phosphorylated residues are shown in bold and highlighted.

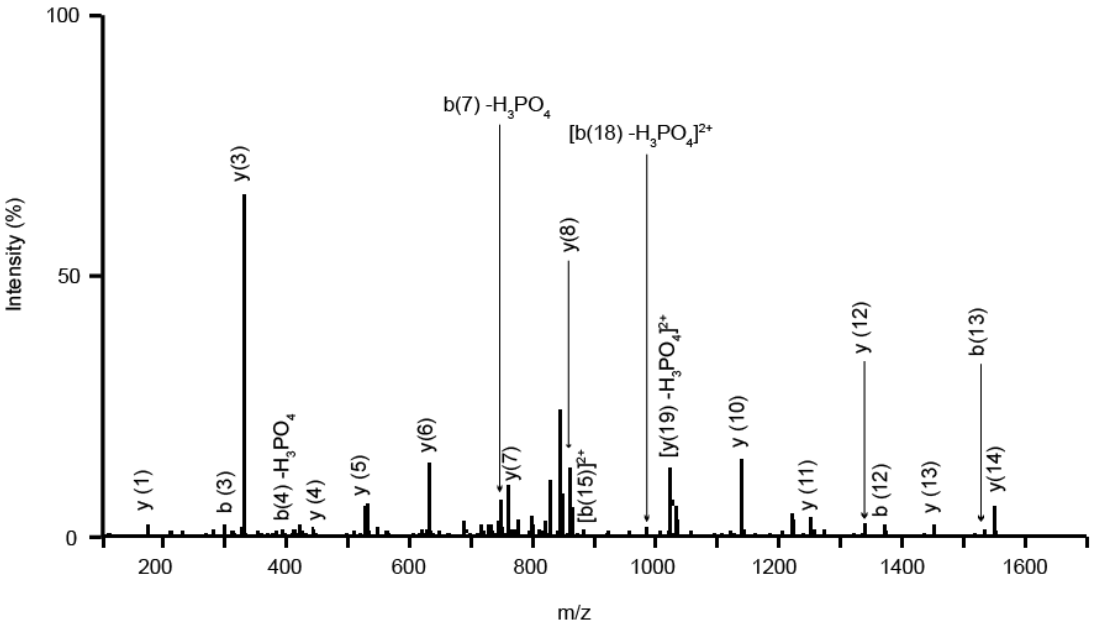

Figure 5.3 Identification of PTPIP51 S44 as a phosphorylation site by LC/MS/MS

Tandem MS/MS spectrum of the PTPIP51 phosphopeptide HGR**S**QSLPNSLDYTQTSDPGR (residues 41-61) fragment ion series after collision induced dissociation. The m/z of the fragment ions is plotted against intensity and the detected ions of the b- and y-ion collision series are indicated. The pattern of fragment ions produced localizes the phosphorylation site to S44 (highlighted in the peptide sequence) with b-ions identified from b(4). The mass difference between b(3) and b(4) and the release of phosphoric acid from b(4) (b(4)-H_3PO_4) are consistent with a phosphorylation on S44.

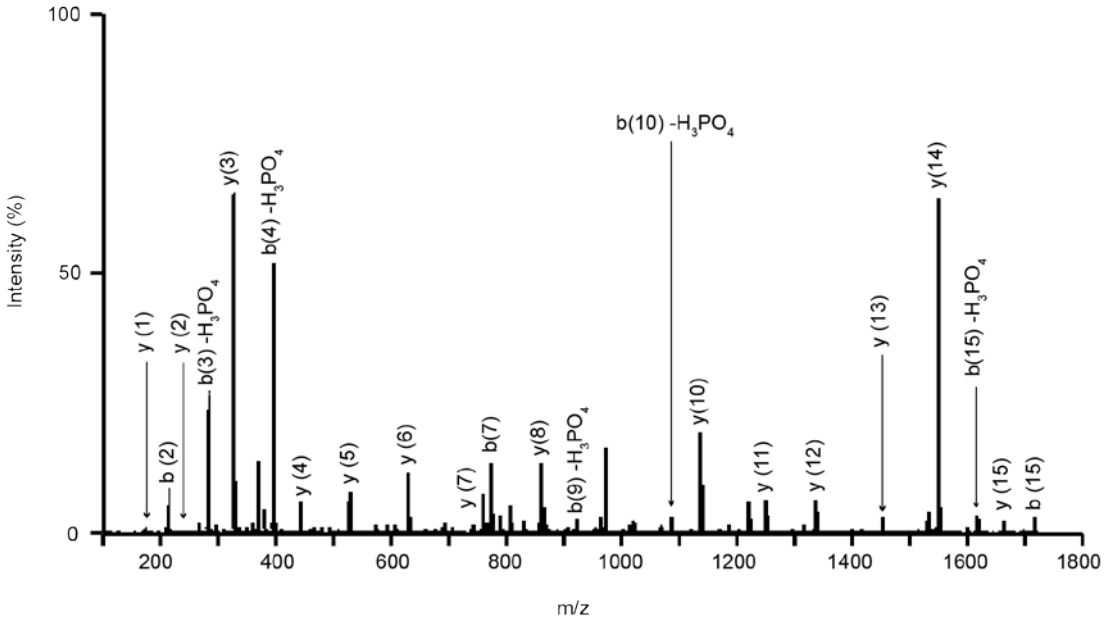

Figure 5.4 Identification of PTPIP51 S46 as a phosphorylation site by LC/MS/MS

Tandem MS/MS spectrum of the PTPIP51 phosphopeptide SQ**S**LPNSLDYTQTSDPGR (residues 44-61) fragment ion series after collision induced dissociation. The m/z of the fragment ions is plotted against intensity and the detected ions of the b- and y-ion collision series are indicated. Diagnostic neutral loss of phosphoric acid ($-H_3PO_4$) from the parent ion is present at m/z 974.55^{2+}. The sequence tag from y(1-8) and y(11-15) provides strong evidence for the peptide sequence assignment and neutral loss from b(3), b(4), b(10) and b(15), but not b(2), localizes the phosphorylation site to S46 (highlighted in the peptide sequence). Consecutively matched y- and b-ions without neutral loss indicate no phosphorylation of other potential sites (S44, S50, T54, T56 or S57).

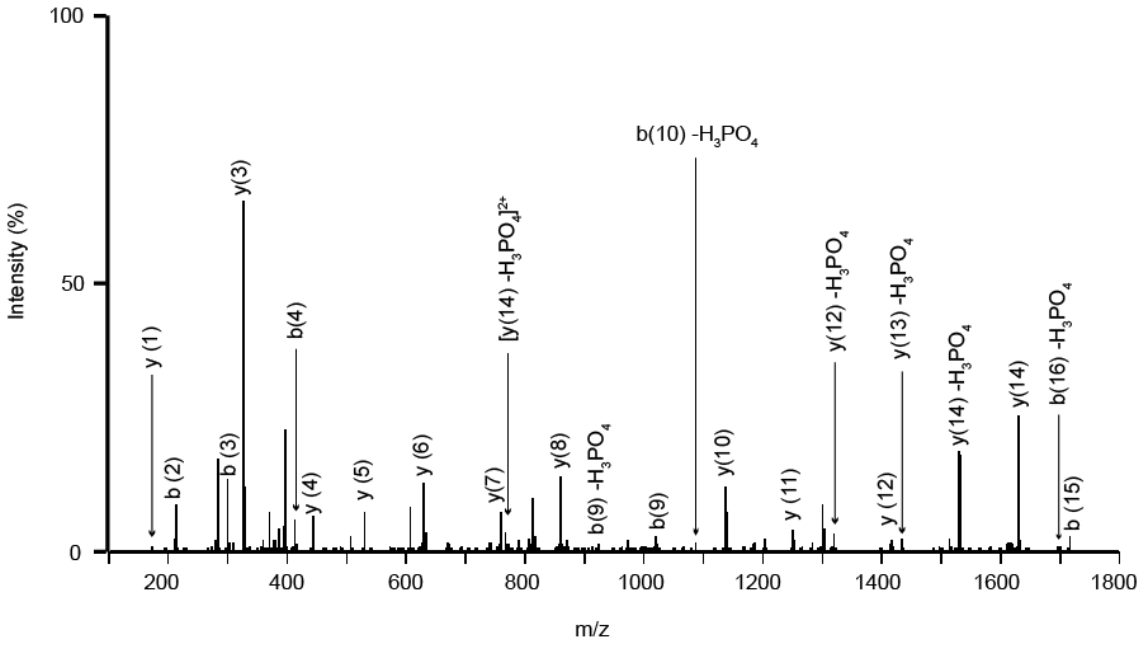

Figure 5.5 Identification of PTPIP51 S50 as a phosphorylation site by LC/MS/MS

Tandem MS/MS spectrum of the PTPIP51 phosphopeptide SQSLPN**S**LDYTQTSDPGR (residues 44-61) fragment ion series after collision induced dissociation. The m/z of the fragment ions is plotted against intensity and the detected ions of the b- and y-ion collision series are indicated. Neutral loss from b(9), but not b(3) (S46) for the b-ion series and from y(12) but not y(5) (S57), y(6) (T56) or y(8) (T54) for the y-ion series localize the phosphorylation to S50 (highlighted in the peptide sequence).

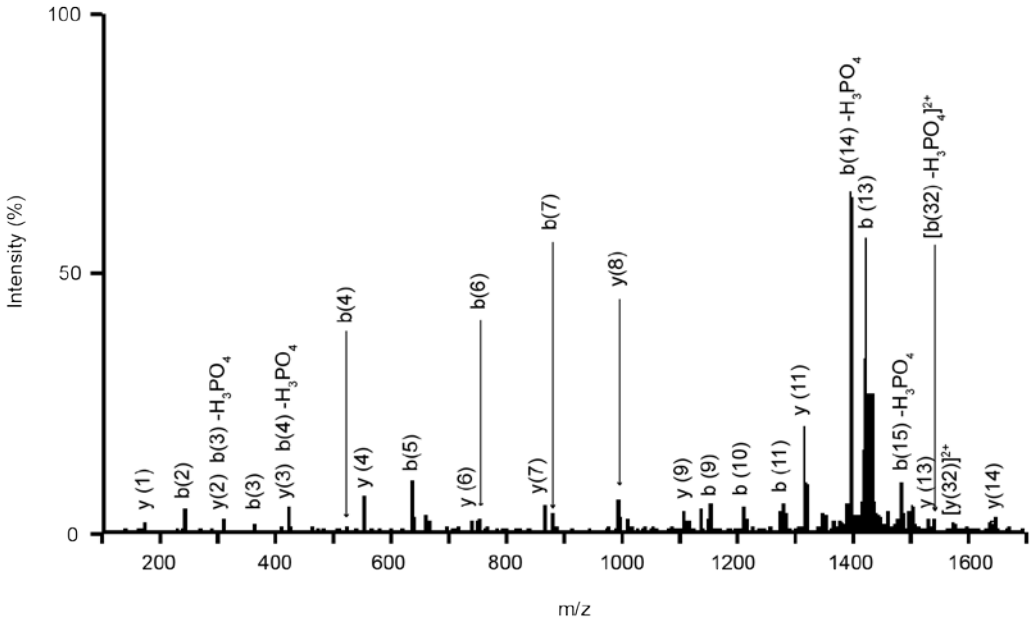

Figure 5.6 Identification of PTPIP51 S212 as a phosphorylation site by LC/MS/MS

Tandem MS/MS spectrum of the PTPIP51 phosphopeptide KDSLDLEEEAASGASSALEAGGSSGLEDVLPLLQQADELHR (residues 210-250) fragment ion series after collision induced dissociation. The m/z of the fragment ions is plotted against intensity and the detected ions of the b- and y-ion collision series are indicated. The ion at m/z 1398.25^{3+} corresponding to a neutral loss from the parent suggests phosphorylation of serine or threonine. Assignment of b(3-5) and b(9-11) and the loss of phosphate from b(3), but not b(2) localize the modification to S212 (highlighted in the peptide sequence).

Figure 5.7 Schematic representation of PTPIP51 structure showing positions of phosphorylation sites identified by mass spectrometry

PTPIP51 encompasses an N-terminal transmembrane domain and a coiled coil domain.

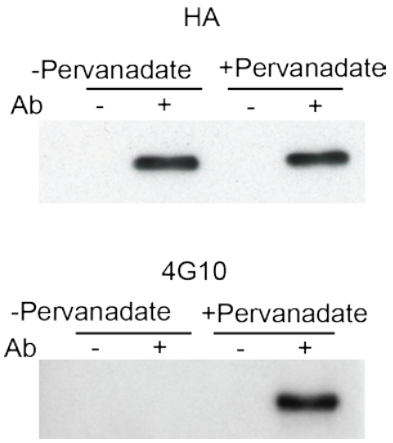

Figure 5.8 PTPIP51 is phosphorylated on tyrosine residue(s)

PTPIP51 is phosphorylated on tyrosine(s) in pervanadate-treated CHO cells. CHO cells were transfected with PTPIP51-HA and treated with either vehicle or the tyrosine phosphatase inhibitor pervanadate as indicated (- pervanadate; + pervanadate). PTPIP51-HA was immunoprecipitated using the anti-HA antibody and the samples were probed on immunoblots with anti-HA or phosphotyrosine antibody 4G10 as indicated. -Ab and +Ab refer to absence or presence of the anti-HA antibody in the immunoprecipitations. Signals for the PTPIP51-HA are only seen in the presence of immunoprecipitating HA antibody and treatment with pervanadate induced a strong PTPIP51 signal with antibody 4G10.

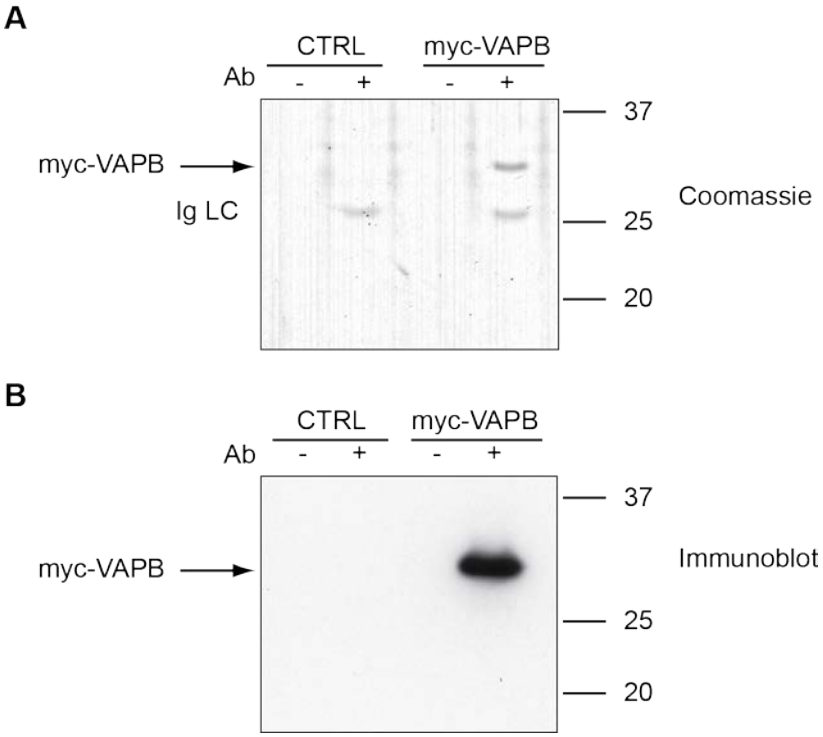

Figure 5.9 Purification of myc-VAPB by immunoprecipitation

CHO cells were transfected with either control vector (CTRL) or myc-VAPB and transfected myc-VAPB was immunoprecipitated using anti-myc antibody. (A) shows Coomassie Blue stained gel. (B) shows immunoblot probed with anti-myc antibody 9B11 to detect myc-VAPB. -Ab and +Ab refer to absence or presence of the anti-myc antibody in the immunoprecipitations. The positions of myc-VAPB and immunoglobulin light chain (Ig LC) of the anti-myc antibody are shown. Molecular mass markers are shown on the right.

A

MAKVEQVLSLEPQHELKFRGPFTDVVTTNLKLGNPTDRNVCFKVKTTAPRRYC
VRPNSGIIDAGASINVSVMLQPFDYDPNEKSKHKFMVQSMFAPTDTSDMEAVW
KEAKPEDLMDSKLRCVFELPAENDKPHDVEINKIISTTASKTETPIVSKSLSSSLD
DTEVKKVMEECKRLQGEVQRLREENKQFKEEDGLRMRKTVQSNSPISALAPTG
KEEGLSTRLLALVVLFFIVGVIIGKIAL

B

Peptide sequence	Residues	m/z
SL**S**SSLDDTEVK	156-167	680.79
IISTTASKTE**T**PIVSK	140-155	878.45

Figure 5.10 Phosphorylation sites identified in VAPB

(A) Sequence of VAPB with the MS/MS sequence coverage obtained after trypsin digestion shown as underlined. Two phosphorylation sites were identified (T150, S158) which are highlighted. (B) VAPB phosphopeptides obtained by MS/MS sequencing with their mass/charge (m/z) ratios. Phosphorylated residues are shown in bold and highlighted.

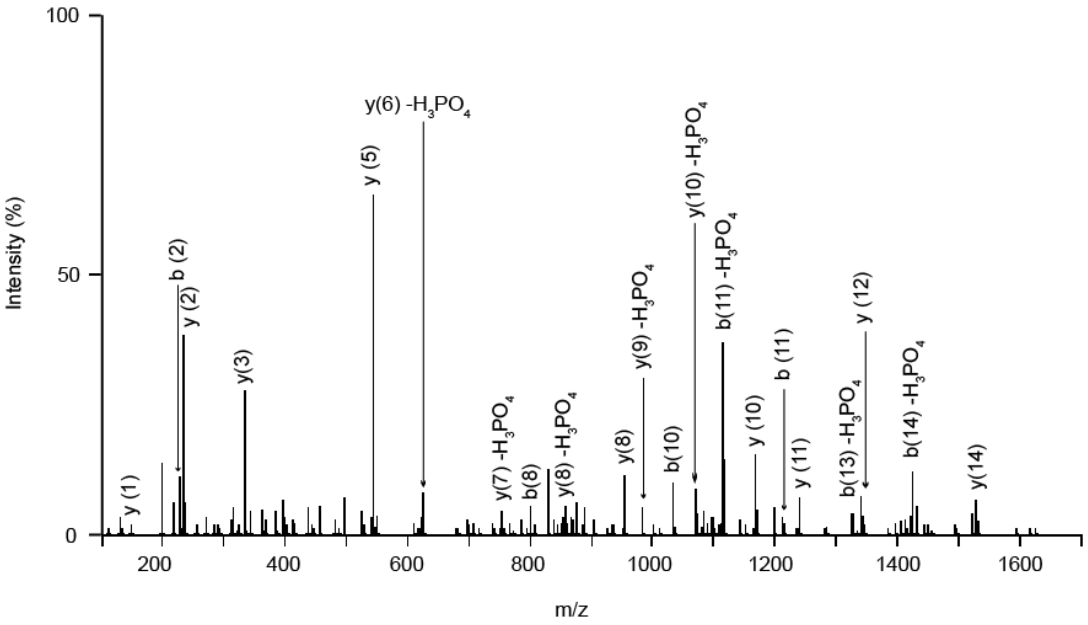

Figure 5.11 Identification of VAPB T150 as a phosphorylation site by LC/MS/MS

Tandem MS/MS spectrum of the VAPB phosphopeptide IISTTASKTE**T**PIVSK (residues 140-155) fragment ion series after collision induced dissociation. The m/z of the fragment ions is plotted against intensity and the detected ions of the b- and y-ion collision series are indicated. The sequence tag of y-ions from y(6) to y(10) are identified with a neutral loss of phosphoric acid but not at y(5), therefore localizing the phosphorylation to T150 (highlighted in the peptide sequence). Further evidence for this localization is determined by neutral loss from the b(11) ion ($-H_3PO_4$) and not at other serine or threonine residues in the sequence.

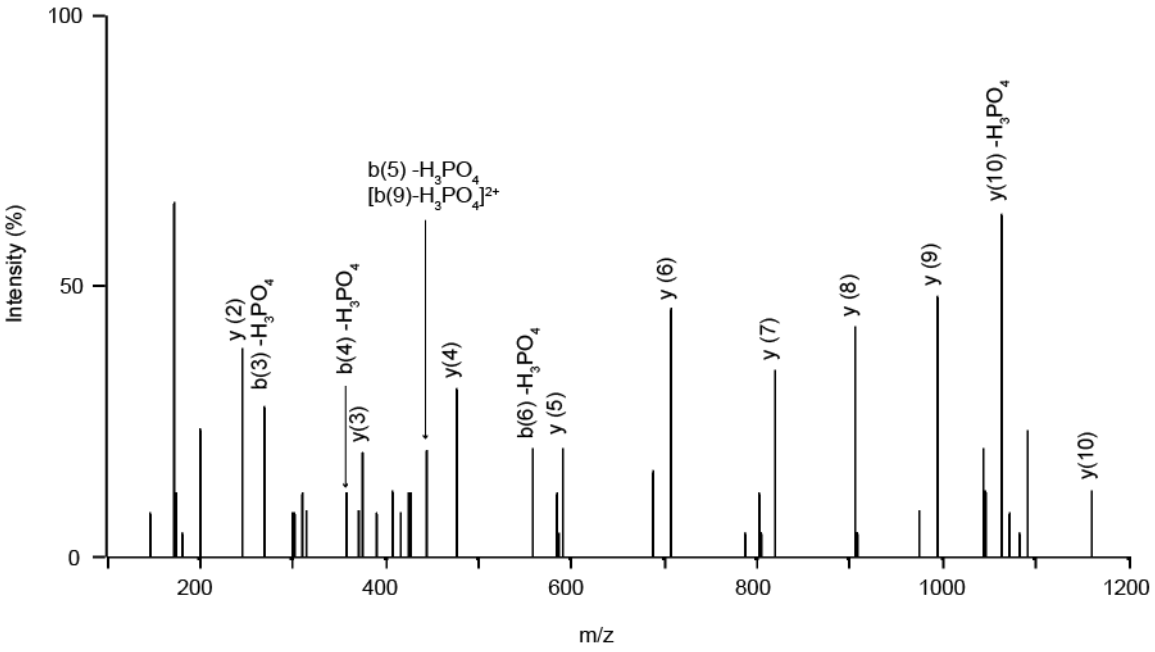

Figure 5.12 Identification of VAPB S158 as a phosphorylation site by LC/MS/MS

Tandem MS/MS spectrum of the VAPB phosphopeptide SL**S**SSLDDTEVK (residues 156-167) fragment ion series after collision induced dissociation. The m/z of the fragment ions is plotted against intensity and the detected ions of the b- and y-ion collision series are indicated. A constant neutral loss from the parent ion is not identified but ions at b(4-6) show a neutral loss of phosphoric acid ($-H_3PO_4$). The y(10) ion with neutral loss also confirms localization of the phosphorylation to the serine residue S158 (highlighted in the peptide sequence).

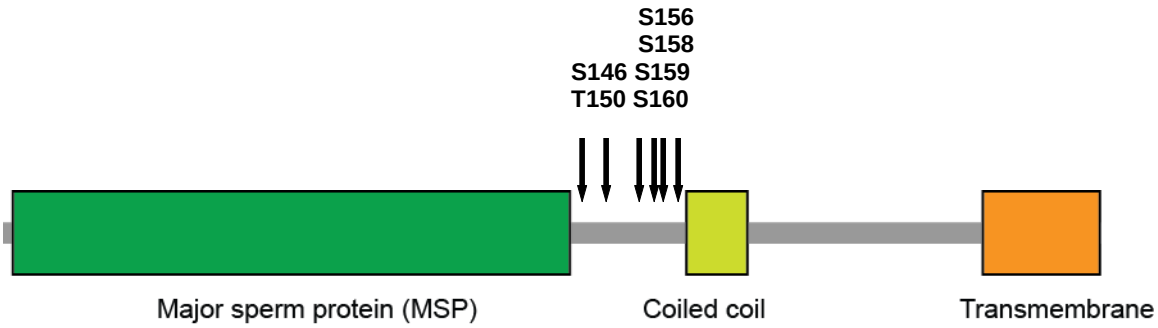

Figure 5.13 Schematic representation of VAPB structure showing positions of phosphorylation sites identified by mass spectrometry

VAPB encompasses three main domains: a major sperm protein (MSP) domain, a coiled coil domain and a transmembrane domain required for ER membrane localization. The MSP domain is positioned towards the N-terminus and the transmembrane domain is positioned towards the C-terminus of the protein. Threonine 150 (T150) and serine 158 (S158) are located between the MSP domain and the coiled coil domain. In previous studies, other phosphorylation sites have also been identified in this region of the protein, including S146, S156, S159 and S160.

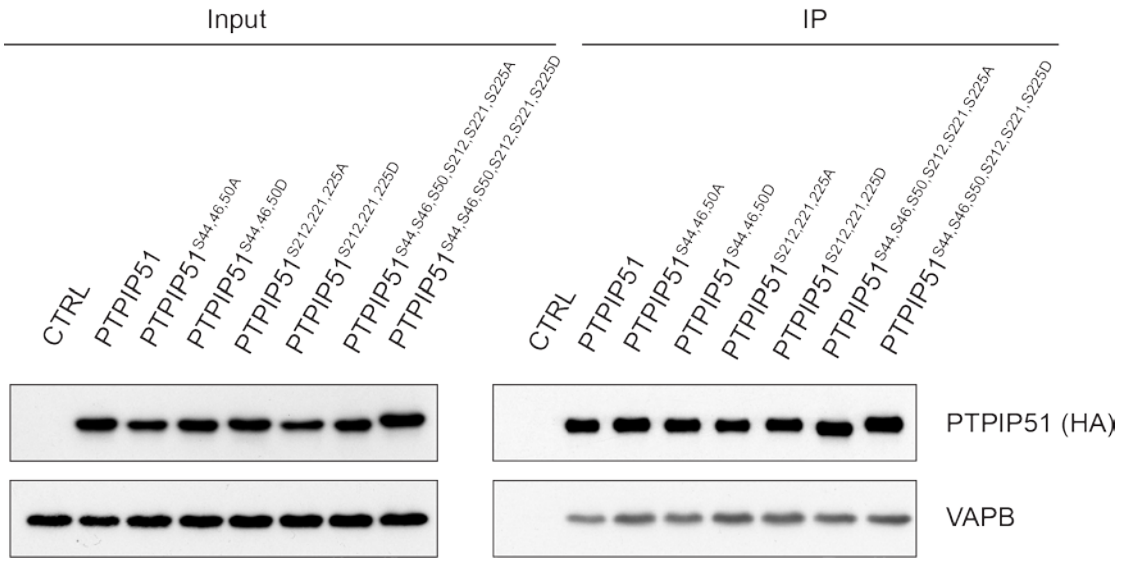

Figure 5.14 Mutation of PTPIP51 residues to alanine to preclude phosphorylation and aspartate to mimic permanent phosphorylation do not affect PTPIP51 binding to VAPB

HEK293 cells were transfected with either control vector (CTRL), PTPIP51-HA wild-type (PTPIP51), PTPIP51$^{S44A/S46A/S50A}$, PTPIP51$^{S44D/S46D/S50D}$, PTPIP51$^{S212A/S221A/S225A}$, PTPIP51$^{S212D/S221D/S225D}$, PTPIP51$^{S44A/S46A/S50A/S212A/S221A/S225A}$ or PTPIP51 $^{S44D/S46D/S50D/S212D/S221D/S225D}$ and PTPIP51 immunoprecipitated using anti-HA to the HA epitope tag. Samples were probed on immunoblots for PTPIP51 using anti-HA and endogenous VAPB using antibody sk83. Samples of the input lysates and immunoprecipitates (IP) are shown. No VAPB signal was obtained from control vector transfected cells, which demonstrates the specificity of the immunoprecipitations. VAPB signals were normalized to immunoprecipitated PTPIP51-HA signals. Data were analysed by one-way ANOVA (n=3) and this revealed no differences between binding of wild-type or the phosphorylation mutants of PTPIP51 to VAPB.

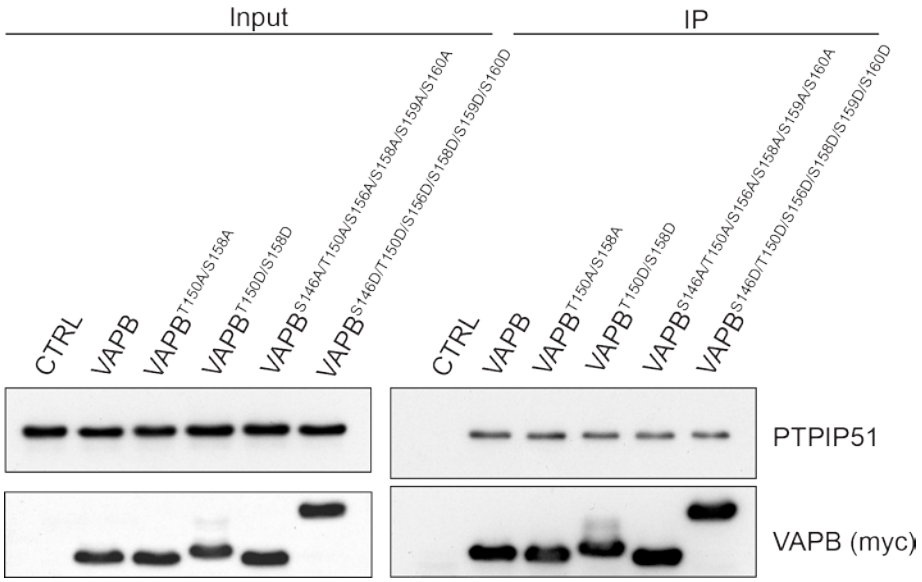

Figure 5.15 Mutation of VAPB residues to alanine to preclude phosphorylation and aspartate to mimic permanent phosphorylation does not affect VAPB binding to PTPIP51

HEK293 cells were transfected with either control vector (CTRL), VAPB wild-type (VAPB), $VAPB^{T150A/S158A}$, $VAPB^{T150D/S158D}$, $VAPB^{S146A/T150A/S156A/S158A/S159A/S160A}$ or $VAPB^{S146D/T150D/S156D/S158D/S159D/S160D}$ and VAPB immunoprecipitated using anti-myc to the myc epitope tag. Samples were probed on immunoblots for VAPB using anti-myc and endogenous PTPIP51 using antibody FAM82A2. Samples of the input lysates and immunoprecipitates (IP) are shown. No PTPIP51 signal was obtained from control vector transfected cells, which demonstrates the specificity of the immunoprecipitations. PTPIP51 signals were normalized to immunoprecipitated myc-VAPB signals. Data were analysed by one-way ANOVA (n=3) and this revealed no differences between the binding of wild-type or the phosphorylation mutants of VAPB to PTPIP51.

5.3 Discussion

In this chapter, the role of phosphorylation in modulating the VAPB-PTPIP51 interaction was investigated. For this purpose, VAPB and PTPIP51 were transfected into CHO cells and purified by immunoprecipitation and SDS-PAGE using the myc- or HA-tags. The proteins were then analyzed by mass spectrometry and this approach identified phosphorylated serine and threonine residues in both VAPB and PTPIP51. In addition, treating the cells with the tyrosine phosphatase inhibitor pervanadate revealed that tyrosine phosphorylation occurs in PTPIP51. However, the phosphorylated tyrosine residues were not identified via mass spectrometry. One reason for this may be that phosphorylation on tyrosines is a less common event than phosphorylation on serine or threonine residues. Indeed, phosphorylation of tyrosines accounts for only 1.8% of the total phosphoproteome (Olsen et al., 2006). Also, the low sequence coverage (57%) obtained in this experiment might have hampered the detection of phosphopeptides.

To investigate how phosphorylation might influence the VAPB-PTPIP51 interaction, the identified serine and threonine residues in VAPB and PTPIP51 were mutated to either alanine to preclude phosphorylation, or to aspartate to mimic permanent phosphorylation. However, mutation of these sites did not affect binding of VAPB to PTPIP51 in immunoprecipitation assays. Interestingly, mutation of all 6 phosphorylation sites in VAPB produced a marked shift in migration on SDS-PAGE. This might suggest that phosphorylation of some or all of these sites induces conformational changes to VAPB.

The above results suggest that, at least on the sites manipulated here, phosphorylation of PTPIP51 or VAPB does not affect the VAPB-PTPIP51 interaction. However, recent

studies have identified other phosphorylation sites which were not investigated in this thesis (see www.phosphosite.org). These sites include residues T54, S149, S151, T152, S154, S155, S156, Y176 in PTPIP51 and residues S204, S206, S209, T214, S221 and T222 in VAPB. Therefore, the regulation of the VAPB-PTPIP51 interaction via phosphorylation cannot be excluded based solely on the data presented here. Interestingly, a recent study investigating the effects of PTPIP51 tyrosine phosphorylation on its interaction profile has found that phosphorylation of tyrosine 176 increases the binding of PTPIP51 to PTP1B, 14-3-3β and Raf-1 (Brobeil et al., 2012). These results suggest that PTPIP51 phosphorylation on tyrosine residues might be an important target for modulating the interaction with binding partners. Further studies are needed to investigate the existence of additional tyrosine phosphorylation sites and whether they can regulate the interaction with VAPB.

A further mechanism which might influence VAPB-PTPIP51 interactions involves the proteolytic cleavage of VAPB. Indeed, the MSP domain situated at the N-terminus of VAPB can be cleaved and secreted to modulate axon guidance and mitochondrial morphology (Gkogkas et al., 2011; Han et al., 2012; Tsuda et al., 2008). Since the N-terminal domain of VAPB protrudes into the cytosol and is responsible for the interaction with PTPIP51, VAPB cleavage may also sever this connection and detach ER membranes from mitochondria.

Therefore, it will be important to further investigate the mechanisms regulating VAPB proteolysis, its involvement in modulating VAPB-PTPIP51 interactions and ultimately the association of ER to mitochondria. Finally, considering that ER-mitochondria contact sites are disrupted in a number of neurodegenerative diseases (Area-Gomez et

al., 2012; Cali et al., 2012; Zampese et al., 2011) and see also results Chapter 4), deciphering the mechanisms that regulate VAPB-PTPIP51 control of ER-mitochondria associations has direct relevance to human neurodegenerative disease mechanisms.

CHAPTER 6: SUMMARY AND FUTURE DIRECTIONS

6.1 Summary

The studies in this thesis sought to gain insight into the role of VAPB and PTPIP51 in mediating ER-mitochondria associations. This was achieved by modulating VAPB and/or PTPIP51 expression and monitoring ER-mitochondria contacts by electron microscopy and confocal microscopy. Knockdown of VAPB or PTPIP51 using siRNA caused a decrease in ER-mitochondria associations, while overexpression of VAPB and/or PTPIP51 via transfection induced a significant increase in ER-mitochondria associations. The increase was particularly striking after co-expressing VAPB and PTPIP51 which caused ER and mitochondria to redistribute and form close associations over approximately 60% of the mitochondrial surface. These results, together with the finding that VAPB and PTPIP51 mediate Ca^{2+} transmission at the ER-mitochondria interface (De Vos et al., 2012) strongly support a role for VAPB and PTPIP51 in tethering ER to mitochondria.

TDP-43 is a major component of pathological inclusions in most ALS and FTD cases (Arai et al., 2006; Neumann et al., 2006) and has also been linked to other neurodegenerative diseases (Chen-Plotkin et al., 2010). Moreover, mutations in *TARDBP* are responsible for a subset of familial ALS cases (Sreedharan et al., 2008). In this thesis, a variety of experimental approaches were used to explore the effect of wild-type and ALS mutant TDP-43 on ER-mitochondria associations. This was initially achieved by overexpressing TDP-43 in cell lines and monitoring the ER-mitochondria contacts using electron and confocal microscopy. Interestingly, both wild-type and mutant TDP-43 reduced the amount of ER-mitochondria associations. Since diminished contact between the two organelles could be a consequence of reduced molecular tether expression, the levels of VAPB, PTPIP51 and mitofusin-2 were assessed in the presence

of wild-type and mutant TDP-43. However, TDP-43 did not change the expression of these proteins on immunoblots.

TDP-43 toxicity could also target the interaction between VAPB and PTPIP51 to reduce ER-mitochondria contacts. Therefore, the VAPB-PTPIP51 interaction was investigated after overexpressing wild-type or four different ALS associated mutants of TDP-43 (M337V, Q331K, A382T and G348C). Both wild-type and all TDP-43 mutants used decreased the VAPB-PTPIP51 interaction as assessed by proximity ligation and immunoprecipitation assays. To test whether other ALS-related insults target the VAPB-PTPIP51 interaction, immunoprecipitation experiments were also performed in the presence of wild-type or mutant FUS and SOD1. Similar to TDP-43, both wild-type and mutant FUS produced a decrease in the VAPB-PTPIP51 interaction. However, wild-type and mutant SOD1 did not have an effect on VAPB binding to PTPIP51. Thus, both TDP-43 and FUS disrupt the VAPB-PTPIP51 interaction and this could be the mechanism underlying the TDP-43-induced reduction in ER-mitochondria associations.

It is likely that ER-mitochondria interactions are dynamic and change in response to physiological stimuli. To explore possible mechanisms regulating the VAPB-PTPIP51 interactions, studies in this thesis sought to determine whether phosphorylation of VAPB and/or PTPIP51 influences their binding. This involved identifying phosphorylation sites via mass spectrometry. A number of serine and threonine phosphorylation sites in both VAPB and PTPIP51 were identified. Interestingly, treating the cells with the tyrosine phosphatase inhibitor pervanadate indicated that PTPIP51 was also phosphorylated on tyrosines, although no specific phosphotyrosine residues were identified. The VAPB-PTPIP51 interaction was investigated after

mutating these phosphorylated serine and threonine residues to preclude phosphorylation or to mimic permanent phosphorylation. However, none of the phosphorylation mutants altered VAPB binding to PTPIP51.

6.2 Future directions

The results presented in this thesis highlight VAPB and PTPIP51 as proteins that control ER-mitochondria associations and reveal a novel pathogenic mechanism for TDP-43 in disrupting ER-mitochondria contacts via the VAPB-PTPIP51 interaction. Some suggestions for future research directions are listed below.

1. The effects of ALS-associated FUS and SOD1 on the VAPB-PTPIP51 interaction were investigated using biochemical approaches. The studies revealed that FUS but not SOD1 decreased binding of VAPB to PTPIP51. It would thus be useful to determine whether FUS and SOD1 affected ER-mitochondria association using the confocal and electron microscopy assays described in this thesis. Monitoring the ER-mitochondria associations in transgenic mouse models of TDP-43, FUS and SOD1 mediated ALS by electron microscopy would further support the data presented in this thesis.

2. A mutation in VAPB involving a proline to serine substitution at position 56 (VAB P56S) causes familial ALS type-8 and this alters its binding to PTPIP51 (De Vos et al., 2012). It would thus be interesting to compare ER-mitochondria associations in VAPB and VAPB P56S expressing cells using the assays described in this thesis.

3. Alzheimer's disease associated presenilins and Parkinson's disease associated α-synuclein have been shown to increase ER-mitochondria associations (Area-Gomez

et al., 2012; Cali et al., 2012; Zampese et al., 2011). However, these results were generated using mainly confocal light microscopy studies. Using such light microscopy analyses to monitor ER-mitochondria interactions involving approximate 25 nm tethers has been criticized recently and shown to generate artefactual results (Cosson et al., 2012). Indeed, a major review on MAM and ER-mitochondria interactions has suggested that electron microscopy analyses should be the preferred method for analyzing ER-mitochondria contacts (Rowland and Voeltz, 2012). The effects of presenilins and α-synuclein on ER-mitochondria contacts thus need to be re-evaluated using the sensitive electron microscopy assays described in this thesis.

4. Expression of TDP-43 was shown to decrease ER-mitochondria interactions. Since these contacts regulate Ca^{2+} handling and Ca^{2+} exchange between ER and mitochondria, the effects of TDP-43 on cellular Ca^{2+} homeostasis need to be investigated. This would involve Fura-2 measurement of Ca^{2+} levels in appropriately transfected cells and also monitoring Ca^{2+} exchange between ER and mitochondria using approaches similar to those described in other studies (De Vos et al., 2012; Morotz et al., 2012).

5. ER-mitochondria associations are believed to be involved in regulating ER stress and the UPR (Malhotra and Kaufman, 2011). It is also possible that ER-mitochondria associations impact upon the mitochondrial stress response (Malhotra and Kaufman, 2011; Pellegrino et al., 2013). Moreover, VAPB is involved in mediating ER stress and the UPR (Amarilio et al., 2005; Chen et al., 2010; Gkogkas et al., 2008; Kanekura et al., 2006; Langou et al., 2010; Suzuki et al., 2009). Thus, the effects of insults targeting VAPB-PTPIP51 interactions and ER-mitochondria associations (e.g. TDP-43) on ER and mitochondrial stress and the UPR should be investigated.

6. Finally, the findings reported here and in other studies (Area-Gomez et al., 2012; Cali et al., 2012; Zampese et al., 2011) which show that insults associated with neurodegenerative diseases disrupt ER-mitochondria associations, highlight the ER-mitochondria axis as a possible target for therapeutic intervention. Identifying small molecules that modulate the interaction may represent a new type of treatment for these diseases. The demonstration that VAPB and PTPIP51 represent some of the tethers that connect ER with mitochondria will facilitate the discovery of such molecules.

REFERENCES

Acharya, U., Jacobs, R., Peters, J.M., Watson, N., Farquhar, M.G., and Malhotra, V. (1995). The formation of Golgi stacks from vesiculated Golgi membranes requires two distinct fusion events. Cell 82, 895-904.

Ackerley, S., Grierson, A.J., Banner, S., Perkinton, M.S., Brownlees, J., Byers, H.L., Ward, M., Thornhill, P., Hussain, K., Waby, J.S., et al. (2004). p38α stress-activated protein kinase phosphorylates neurofilaments and is associated with neurofilament pathology in amyotrophic lateral sclerosis. Mol Cell Neurosci 26, 354-364.

Ackerley, S., Grierson, A.J., Brownlees, J., Thornhill, P., Anderton, B.H., Leigh, P.N., Shaw, C.E., and Miller, C.C.J. (2000). Glutamate slows axonal transport of neurofilaments in transfected neurons. J Cell Biol 150, 165-175.

Ackerley, S., Thornhill, P., Grierson, A.J., Brownlees, J., Anderton, B.H., Leigh, P.N., Shaw, C.E., and Miller, C.C.J. (2003). Neurofilament heavy chain side-arm phosphorylation regulates axonal transport of neurofilaments. J Cell Biol 161, 489-495.

Aggarwal, S.P., Zinman, L., Simpson, E., McKinley, J., Jackson, K.E., Pinto, H., Kaufman, P., Conwit, R.A., Schoenfeld, D., Shefner, J., et al. (2010). Safety and efficacy of lithium in combination with riluzole for treatment of amyotrophic lateral sclerosis: a randomised, double-blind, placebo-controlled trial. Lancet Neurol 9, 481-488.

Al-Chalabi, A., Andersen, P.M., Nilsson, P., Chioza, B., Andersson, J.L., Russ, C.R., Shaw, C.E., Powell, J.F., and Leigh, P.N. (1999). Deletions of the heavy neurofilament subunit tail in amyotrophic lateral sclerosis. Hum Mol Genet 8, 157-164.

Al-Chalabi, A., and Miller, C.C. (2003). Neurofilaments and neurological disease. BioEssays 25, 346-355.

Al-Sarraj, S., King, A., Troakes, C., Smith, B., Maekawa, S., Bodi, I., Rogelj, B., Al-Chalabi, A., Hortobagyi, T., and Shaw, C.E. (2011). p62 positive, TDP-43 negative, neuronal cytoplasmic and intranuclear inclusions in the cerebellum and hippocampus define the pathology of C9orf72-linked FTLD and MND/ALS. Acta Neuropathol 122, 691-702.

Albo, F., Pieri, M., and Zona, C. (2004). Modulation of AMPA receptors in spinal motor neurons by the neuroprotective agent riluzole. J Neurosci Res 78, 200-207.

Alexianu, M.E., Ho, B.K., Mohamed, A.H., La Bella, V., Smith, R.G., and Appel, S.H. (1994). The role of calcium-binding proteins in selective motoneuron vulnerability in amyotrophic lateral sclerosis. Ann Neurol 36, 846-858.

Alonso, A., Logroscino, G., Jick, S.S., and Hernan, M.A. (2009). Incidence and lifetime risk of motor neuron disease in the United Kingdom: a population-based study. Eur J Neurol 16, 745-751.

Amador-Ortiz, C., Lin, W.L., Ahmed, Z., Personett, D., Davies, P., Duara, R., Graff-Radford, N.R., Hutton, M.L., and Dickson, D.W. (2007). TDP-43 immunoreactivity in hippocampal sclerosis and Alzheimer's disease. Ann Neurol 61, 435-445.

Amarilio, R., Ramachandran, S., Sabanay, H., and Lev, S. (2005). Differential regulation of endoplasmic reticulum structure through VAP-Nir protein interaction. J Biol Chem 280, 5934-5944.

Anagnostou, G., Akbar, M.T., Paul, P., Angelinetta, C., Steiner, T.J., and de Belleroche, J. (2010). Vesicle associated membrane protein B (VAPB) is decreased in ALS spinal cord. Neurobiol Aging 31, 969-985.

Andersen, P.M., and Al-Chalabi, A. (2011). Clinical genetics of amyotrophic lateral sclerosis: what do we really know? Nat Rev Neurol 7, 603-615.

Andrus, P.K., Fleck, T.J., Gurney, M.E., and Hall, E.D. (1998). Protein oxidative damage in a transgenic mouse model of familial amyotrophic lateral sclerosis. J Neurochem 71, 2041-2048.

Arai, T., Hasegawa, M., Akiyama, H., Ikeda, K., Nonaka, T., Mori, H., Mann, D., Tsuchiya, K., Yoshida, M., Hashizume, Y., et al. (2006). TDP-43 is a component of ubiquitin-positive tau-negative inclusions in frontotemporal lobar degeneration and amyotrophic lateral sclerosis. Biochem Biophys Res Commun 351, 602-611.

Area-Gomez, E., de Groof, A.J., Boldogh, I., Bird, T.D., Gibson, G.E., Koehler, C.M., Yu, W.H., Duff, K.E., Yaffe, M.P., Pon, L.A., et al. (2009). Presenilins are enriched in endoplasmic reticulum membranes associated with mitochondria. Am J Pathol 175, 1810-1816.

Area-Gomez, E., Del Carmen Lara Castillo, M., Tambini, M.D., Guardia-Laguarta, C., de Groof, A.J., Madra, M., Ikenouchi, J., Umeda, M., Bird, T.D., Sturley, S.L., et al. (2012). Upregulated function of mitochondria-associated ER membranes in Alzheimer disease. EMBO J 31, 4106-4123.

Arnaudeau, S., Kelley, W.L., Walsh, J.V., Jr., and Demaurex, N. (2001). Mitochondria recycle Ca(2+) to the endoplasmic reticulum and prevent the depletion of neighboring endoplasmic reticulum regions. J Biol Chem 276, 29430-29439.

Atkin, J.D., Farg, M.A., Turner, B.J., Tomas, D., Lysaght, J.A., Nunan, J., Rembach, A., Nagley, P., Beart, P.M., Cheema, S.S., et al. (2006). Induction of the unfolded protein response in familial amyotrophic lateral sclerosis and association of protein-disulfide isomerase with superoxide dismutase 1. J Biol Chem 281, 30152-30165.

Atkin, J.D., Farg, M.A., Walker, A.K., McLean, C., Tomas, D., and Horne, M.K. (2008). Endoplasmic reticulum stress and induction of the unfolded protein response in human sporadic amyotrophic lateral sclerosis. Neurobiol Dis 30, 400-407.

Ayala, Y.M., Misteli, T., and Baralle, F.E. (2008). TDP-43 regulates retinoblastoma protein phosphorylation through the repression of cyclin-dependent kinase 6 expression. Proc Natl Acad Sci USA 105, 3785-3789.

Bar-Lavan, Y., Kosolapov, L., Frumkin, A., and Ben-Zvi, A. (2012). Regulation of cellular protein quality control networks in a multicellular organism. FEBS J 279, 526-531.

Barber, S.C., and Shaw, P.J. (2010). Oxidative stress in ALS: key role in motor neuron injury and therapeutic target. Free Radic Biol Med 48, 629-641.

Barisic, N., Claeys, K.G., Sirotkovic-Skerlev, M., Lofgren, A., Nelis, E., De Jonghe, P., and Timmerman, V. (2008). Charcot-Marie-Tooth disease: a clinico-genetic confrontation. Ann Hum Genet 72, 416-441.

Barlowe, C., Orci, L., Yeung, T., Hosobuchi, M., Hamamoto, S., Salama, N., Rexach, M.F., Ravazzola, M., Amherdt, M., and Schekman, R. (1994). COPII: a membrane coat formed by Sec proteins that drive vesicle budding from the endoplasmic reticulum. Cell 77, 895-907.

Bedard, K., and Krause, K.H. (2007). The NOX family of ROS-generating NADPH oxidases: physiology and pathophysiology. Physiol Rev 87, 245-313.

Beers, D.R., Henkel, J.S., Xiao, Q., Zhao, W., Wang, J., Yen, A.A., Siklos, L., McKercher, S.R., and Appel, S.H. (2006). Wild-type microglia extend survival in PU.1 knockout mice with familial amyotrophic lateral sclerosis. Proc Natl Acad Sci USA 103, 16021-16026.

Bensimon, G., Lacomblez, L., and Meininger, V. (1994). A controlled trial of riluzole in amyotrophic lateral sclerosis. ALS/Riluzole Study Group. N Engl J Med 330, 585-591.

Berliocchi, L., Bano, D., and Nicotera, P. (2005). Ca2+ signals and death programmes in neurons. Philosophical transactions of the Royal Society of London Series B, Biological sciences 360, 2255-2258.

Bernales, S., Papa, F.R., and Walter, P. (2006). Intracellular signaling by the unfolded protein response. Annu Rev Cell Dev Biol 22, 487-508.

Bilsland, L.G., Sahai, E., Kelly, G., Golding, M., Greensmith, L., and Schiavo, G. (2010). Deficits in axonal transport precede ALS symptoms in vivo. Proc Natl Acad Sci USA 107, 20523-20528.

BIPM (2006). The International System of Units (http://www.bipm.org/en/si/si_brochure/general.html).

Bogdanov, M., Brown, R.H., Jr., Matson, W., Smart, R., Hayden, D., O'Donnell, H., Beal, M.F., and Cudkowicz, M. (2000). Increased oxidative damage to DNA in ALS patients. Free RadicBiolMed 29, 652-658.

Boillee, S., Yamanaka, K., Lobsiger, C.S., Copeland, N.G., Jenkins, N.A., Kassiotis, G., Kollias, G., and Cleveland, D.W. (2006). Onset and Progression in Inherited ALS Determined by Motor Neurons and Microglia. Science 312, 1389-1392.

Borchelt, D.R., Lee, M.K., Slunt, H.S., Guarnieri, M., Xu, Z.-S., Wong, P.C., Brown Jr, R.H., Price, D.L., Sisodia, S.S., and Cleveland, D.L. (1994). Superoxide dismutase 1

with mutations linked to familial amyotrophic lateral sclerosis possesses significant activity. Proc Natl Acad Sci USA 91, 8292-8296.

Bosco, D.A., Morfini, G., Karabacak, N.M., Song, Y., Gros-Louis, F., Pasinelli, P., Goolsby, H., Fontaine, B.A., Lemay, N., McKenna-Yasek, D., et al. (2010). Wild-type and mutant SOD1 share an aberrant conformation and a common pathogenic pathway in ALS. Nat Neurosci 13, 1396-1403.

Boussif, O., Lezoualc'h, F., Zanta, M.A., Mergny, M.D., Scherman, D., Demeneix, B., and Behr, J.P. (1995). A versatile vector for gene and oligonucleotide transfer into cells in culture and in vivo: polyethylenimine. Proc Natl Acad Sci USA 92, 7297-7301.

Bradford, M.M. (1976). A rapid and sensitive method for the quantitation of microgram quantities of protein utilizing the principle of protein-dye binding. Anal Biochem 72, 248-254.

Braun, R.J., Sommer, C., Carmona-Gutierrez, D., Khoury, C.M., Ring, J., Buttner, S., and Madeo, F. (2011). Neurotoxic 43-kDa TAR DNA-binding protein (TDP-43) triggers mitochondrion-dependent programmed cell death in yeast. J Biol Chem 286, 19958-19972.

Bravo, R., Vicencio, J.M., Parra, V., Troncoso, R., Munoz, J.P., Bui, M., Quiroga, C., Rodriguez, A.E., Verdejo, H.E., Ferreira, J., et al. (2011). Increased ER-mitochondrial coupling promotes mitochondrial respiration and bioenergetics during early phases of ER stress. J Cell Sci 124, 2143-2152.

Brobeil, A., Bobrich, M., Tag, C., and Wimmer, M. (2012). PTPIP51 in protein interactions: regulation and in situ interacting partners. Cell Biochem Biophys 63, 211-222.

Brobeil, A., Bobrich, M., and Wimmer, M. (2011). Protein tyrosine phosphatase interacting protein 51--a jack-of-all-trades protein. Cell Tissue Res 344, 189-205.

Brobeil, A., Graf, M., Oeschger, S., Steger, K., and Wimmer, M. (2010). PTPIP51-a myeloid lineage specific protein interacts with PTP1B in neutrophil granulocytes. Blood Cells Mol Dis 45, 159-168.

Brooks, B.R. (1994). El Escorial World Federation of Neurology criteria for the diagnosis of amyotrophic lateral sclerosis. Subcommittee on Motor Neuron Diseases/Amyotrophic Lateral Sclerosis of the World Federation of Neurology Research Group on Neuromuscular Diseases and the El Escorial "Clinical limits of amyotrophic lateral sclerosis" workshop contributors. J Neurol Sci 124 Suppl, 96-107.

Brooks, B.R., Miller, R.G., Swash, M., and Munsat, T.L. (2000). El Escorial revisited: revised criteria for the diagnosis of amyotrophic lateral sclerosis. Amyotroph Lateral Scler Other Motor Neuron Disord 1, 293-299.

Bruijn, L.I., and Cleveland, D.W. (1996). Mechanisms of selective motor neuron death in ALS: Insights from transgenic mouse models of motor neuron disease. NeuropatholApplNeurobiol 22, 373-387.

Bruijn, L.I., Houseweart, M.K., Kato, S., Anderson, K.L., Anderson, S.D., Ohama, E., Reaume, A.G., Scott, R.W., and Cleveland, D.L. (1998). Aggregation and motor neuron toxicity of an ALS-linked SOD1 mutant independent from wild-type SOD1. Science 281, 1851-1854.

Bunina, T.L. (1962). [On intracellular inclusions in familial amyotrophic lateral sclerosis]. Zh Nevropatol Psikhiatr Im S S Korsakova 62, 1293-1299.

Buratti, E., and Baralle, F.E. (2008). Multiple roles of TDP-43 in gene expression, splicing regulation, and human disease. Front Biosci 13, 867-878.

Buratti, E., and Baralle, F.E. (2012). TDP-43: gumming up neurons through protein-protein and protein-RNA interactions. Trends Biochem Sci 37, 237-247.

Byrne, S., Walsh, C., Lynch, C., Bede, P., Elamin, M., Kenna, K., McLaughlin, R., and Hardiman, O. (2011). Rate of familial amyotrophic lateral sclerosis: a systematic review and meta-analysis. J Neurol Neurosurg Psychiatry 82, 623-627.

Cali, T., Ottolini, D., and Brini, M. (2011). Mitochondria, calcium, and endoplasmic reticulum stress in Parkinson's disease. Biofactors 37, 228-240.

Cali, T., Ottolini, D., Negro, A., and Brini, M. (2012). alpha-Synuclein controls mitochondrial calcium homeostasis by enhancing endoplasmic reticulum-mitochondria interactions. J Biol Chem 287, 17914-17929.

Campbell, J.L., and Schekman, R. (1997). Selective packaging of cargo molecules into endoplasmic reticulum-derived COPII vesicles. Proc Natl Acad Sci USA 94, 837-842.

Cao, K., Nakajima, R., Meyer, H.H., and Zheng, Y. (2003). The AAA-ATPase Cdc48/p97 regulates spindle disassembly at the end of mitosis. Cell 115, 355-367.

Carpenter, S. (1968). Proximal axonal enlargement in motor neuron disease. Neurology 18, 841-851.

Carrì, M.T., Ferri, A., Battistoni, A., Famhy, L., Gabbianelli, R., Poccia, F., and Rotilio, G. (1997). Expression of a Cu,Zn superoxide dismutase typical of familial amyotrophic lateral sclerosis induces mitochondrial alteration and increase of cytosolic Ca^{2+} concentration in transfected neuroblastoma SH-SY5Y cells. FEBS Lett 414, 365-368.

Carriedo, S.G., Sensi, S.L., Yin, H.Z., and Weiss, J.H. (2000). AMPA exposures induce mitochondrial Ca(2+) overload and ROS generation in spinal motor neurons in vitro. J Neurosci 20, 240-250.

Carriedo, S.G., Yin, H.Z., and Weiss, J.H. (1996). Motor neurons are selectively vulnerable to AMPA/kainate receptor-mediated injury in vitro. J Neurosci 16, 4069-4079.

Cashman, N.R., Durham, H.D., Blusztajn, J.K., Oda, K., Tabira, T., Shaw, I.T., Dahrouge, S., and Antel, J.P. (1992). Neuroblastoma x spinal cord (NSC) hybrid cell lines resemble developing motor neurons. Dev Dyn 194, 209-221.

Casoni, F., Basso, M., Massignan, T., Gianazza, E., Cheroni, C., Salmona, M., Bendotti, C., and Bonetto, V. (2005). Protein nitration in a mouse model of familial amyotrophic lateral sclerosis: possible multifunctional role in the pathogenesis. J Biol Chem 280, 16295-16304.

Chang, C., Yu, T.W., Bargmann, C.I., and Tessier-Lavigne, M. (2004). Inhibition of netrin-mediated axon attraction by a receptor protein tyrosine phosphatase. Science 305, 103-106.

Chang, D.T., Honick, A.S., and Reynolds, I.J. (2006). Mitochondrial trafficking to synapses in cultured primary cortical neurons. J Neurosci 26, 7035-7045.

Chang, Y., Kong, Q., Shan, X., Tian, G., Ilieva, H., Cleveland, D.W., Rothstein, J.D., Borchelt, D.R., Wong, P.C., and Lin, C.L. (2008). Messenger RNA oxidation occurs early in disease pathogenesis and promotes motor neuron degeneration in ALS. PLoS ONE 3, e2849.

Chen-Plotkin, A.S., Lee, V.M., and Trojanowski, J.Q. (2010). TAR DNA-binding protein 43 in neurodegenerative disease. Nat Rev Neurol 6, 211-220.

Chen, H.J., Anagnostou, G., Chai, A., Withers, J., Morris, A., Adhikaree, J., Pennetta, G., and de Belleroche, J.S. (2010). Characterization of the properties of a novel mutation in VAPB in familial amyotrophic lateral sclerosis. J Biol Chem 285, 40266-40281.

Chen, R.Q., Yang, Q.K., Lu, B.W., Yi, W., Cantin, G., Chen, Y.L., Fearns, C., Yates, J.R., 3rd, and Lee, J.D. (2009). CDC25B mediates rapamycin-induced oncogenic responses in cancer cells. Cancer Res 69, 2663-2668.

Chen, Y.Z., Bennett, C.L., Huynh, H.M., Blair, I.P., Puls, I., Irobi, J., Dierick, I., Abel, A., Kennerson, M.L., Rabin, B.A., et al. (2004). DNA/RNA helicase gene mutations in a form of juvenile amyotrophic lateral sclerosis (ALS4). Am J Hum Genet 74, 1128-1135.

Christensen, G.L., Kelstrup, C.D., Lyngso, C., Sarwar, U., Bogebo, R., Sheikh, S.P., Gammeltoft, S., Olsen, J.V., and Hansen, J.L. (2010). Quantitative phosphoproteomics dissection of seven-transmembrane receptor signaling using full and biased agonists. Mol Cell Proteomics 9, 1540-1553.

Clement, A.M., Nguyen, M.D., Roberts, E.A., Garcia, M.L., Boillee, S., Rule, M., McMahon, A.P., Doucette, W., Siwek, D., Ferrante, R.J., et al. (2003). Wild-type nonneuronal cells extend survival of SOD1 mutant motor neurons in ALS mice. Science 302, 113-117.

Cohen, T.J., Lee, V.M., and Trojanowski, J.Q. (2011). TDP-43 functions and pathogenic mechanisms implicated in TDP-43 proteinopathies. Trends Mol Med 17, 659-667.

Cole, N.B., Dieuliis, D., Leo, P., Mitchell, D.C., and Nussbaum, R.L. (2008). Mitochondrial translocation of alpha-synuclein is promoted by intracellular acidification. Exp Cell Res 314, 2076-2089.

Collard, J.-F., Cote, F., and Julien, J.-P. (1995). Defective axonal transport in a transgenic mouse model of amyotrophic lateral sclerosis. Nature 375, 61-64.

Colombrita, C., Zennaro, E., Fallini, C., Weber, M., Sommacal, A., Buratti, E., Silani, V., and Ratti, A. (2009). TDP-43 is recruited to stress granules in conditions of oxidative insult. J Neurochem 111, 1051-1061.

Cooper-Knock, J., Hewitt, C., Highley, J.R., Brockington, A., Milano, A., Man, S., Martindale, J., Hartley, J., Walsh, T., Gelsthorpe, C., et al. (2012). Clinico-pathological features in amyotrophic lateral sclerosis with expansions in C9ORF72. Brain 135, 751-764.

Corbo, M., and Hays, A.P. (1992). Peripherin and neurofilament protein coexist in spinal spheroids of motor neuron disease. J Neuropathol Exp Neurol 51, 531-537.

Corcia, P., Valdmanis, P., Millecamps, S., Lionnet, C., Blasco, H., Mouzat, K., Daoud, H., Belzil, V., Morales, R., Pageot, N., et al. (2012). Phenotype and genotype analysis in amyotrophic lateral sclerosis with TARDBP gene mutations. Neurology 78, 1519-2156.

Cosson, P., Marchetti, A., Ravazzola, M., and Orci, L. (2012). Mitofusin-2 independent juxtaposition of endoplasmic reticulum and mitochondria: an ultrastructural study. PLoS ONE 7, e46293.

Csordas, G., Renken, C., Varnai, P., Walter, L., Weaver, D., Buttle, K.F., Balla, T., Mannella, C.A., and Hajnoczky, G. (2006). Structural and functional features and significance of the physical linkage between ER and mitochondria. J Cell Biol 174, 915-921.

Csordas, G., Varnai, P., Golenar, T., Roy, S., Purkins, G., Schneider, T.G., Balla, T., and Hajnoczky, G. (2010). Imaging interorganelle contacts and local calcium dynamics at the ER-mitochondrial interface. Mol Cell 39, 121-132.

Cudkowicz, M.E., Shefner, J.M., Schoenfeld, D.A., Brown, R.H., Jr., Johnson, H., Qureshi, M., Jacobs, M., Rothstein, J.D., Appel, S.H., Pascuzzi, R.M., et al. (2003). A randomized, placebo-controlled trial of topiramate in amyotrophic lateral sclerosis. Neurology 61, 456-464.

d'Ydewalle, C., Bogaert, E., and Van Den Bosch, L. (2012). HDAC6 at the Intersection of Neuroprotection and Neurodegeneration. Traffic 13, 771-779.

Da Cruz, S., and Cleveland, D.W. (2011). Understanding the role of TDP-43 and FUS/TLS in ALS and beyond. Curr Opin Neurobiol 21, 904-919.

Dadon-Nachum, M., Melamed, E., and Offen, D. (2011). The "dying-back" phenomenon of motor neurons in ALS. J Mol Neurosci 43, 470-477.

Dai, R.M., and Li, C.C. (2001). Valosin-containing protein is a multi-ubiquitin chain-targeting factor required in ubiquitin-proteasome degradation. Nat Cell Biol 3, 740-744.

Dal Canto, M.C., and Gurney, M.E. (1995). Neuropathological changes in two lines of mice carrying a transgene for mutant human Cu,Zn SOD, and in mice overexpressing

wild type human SOD: A model of familial amyotrophic lateral sclerosis (FALS). Brain Res 676, 25-40.

Damiano, M., Starkov, A.A., Petri, S., Kipiani, K., Kiaei, M., Mattiazzi, M., Flint Beal, M., and Manfredi, G. (2006). Neural mitochondrial Ca2+ capacity impairment precedes the onset of motor symptoms in G93A Cu/Zn-superoxide dismutase mutant mice. J Neurochem 96, 1349-1361.

Danbolt, N.C. (2001). Glutamate uptake. Prog Neurobiol 65, 1-105.

de Brito, O.M., and Scorrano, L. (2008). Mitofusin 2 tethers endoplasmic reticulum to mitochondria. Nature 456, 605-610.

de Brito, O.M., and Scorrano, L. (2009). Mitofusin-2 regulates mitochondrial and endoplasmic reticulum morphology and tethering: The role of Ras. Mitochondrion 9, 222-226.

de Carvalho, M., Dengler, R., Eisen, A., England, J.D., Kaji, R., Kimura, J., Mills, K., Mitsumoto, H., Nodera, H., Shefner, J., et al. (2008). Electrodiagnostic criteria for diagnosis of ALS. Clin Neurophysiol 119, 497-503.

De Strooper, B., and Annaert, W. (2010). Novel research horizons for presenilins and gamma-secretases in cell biology and disease. Annu Rev Cell Dev Biol 26, 235-260.

De Vos, K.J., Chapman, A.L., Tennant, M.E., Manser, C., Tudor, E.L., Lau, K.F., Brownlees, J., Ackerley, S., Shaw, P.J., McLoughlin, D.M., et al. (2007). Familial amyotrophic lateral sclerosis-linked SOD1 mutants perturb fast axonal transport to reduce axonal mitochondria content. Hum Mol Genet 16, 2720-2728.

De Vos, K.J., Grierson, A.J., Ackerley, S., and Miller, C.C.J. (2008). Role of axonal transport in neurodegenerative diseases. Annu Rev Neurosci 31, 151-173.

De Vos, K.J., Morotz, G.M., Stoica, R., Tudor, E.L., Lau, K.F., Ackerley, S., Warley, A., Shaw, C.E., and Miller, C.C. (2012). VAPB interacts with the mitochondrial protein PTPIP51 to regulate calcium homeostasis. Hum Mol Genet 21, 1299-1311.

Debono, M.W., Le Guern, J., Canton, T., Doble, A., and Pradier, L. (1993). Inhibition by riluzole of electrophysiological responses mediated by rat kainate and NMDA receptors expressed in Xenopus oocytes. Eur J Pharmacol 235, 283-289.

DeJesus-Hernandez, M., Mackenzie, I.R., Boeve, B.F., Boxer, A.L., Baker, M., Rutherford, N.J., Nicholson, A.M., Finch, N.A., Flynn, H., Adamson, J., et al. (2011). Expanded GGGGCC hexanucleotide repeat in noncoding region of C9ORF72 causes chromosome 9p-linked FTD and ALS. Neuron 72, 245-256.

Deng, H.X., Chen, W., Hong, S.T., Boycott, K.M., Gorrie, G.H., Siddique, N., Yang, Y., Fecto, F., Shi, Y., Zhai, H., et al. (2011). Mutations in UBQLN2 cause dominant X-linked juvenile and adult-onset ALS and ALS/dementia. Nature 477, 211-215.

Deng, H.X., Zhai, H., Bigio, E.H., Yan, J., Fecto, F., Ajroud, K., Mishra, M., Ajroud-Driss, S., Heller, S., Sufit, R., et al. (2010). FUS-immunoreactive inclusions are a

common feature in sporadic and non-SOD1 familial amyotrophic lateral sclerosis. Ann Neurol 67, 739-748.

Derkinderen, P., Scales, T.M., Hanger, D.P., Leung, K.Y., Byers, H.L., Ward, M.A., Lenz, C., Price, C., Bird, I.N., Perera, T., et al. (2005). Tyrosine 394 is phosphorylated in Alzheimer's paired helical filament tau and in fetal tau with c-Abl as the candidate tyrosine kinase. J Neurosci 25, 6584-6593.

Devi, L., Raghavendran, V., Prabhu, B.M., Avadhani, N.G., and Anandatheerthavarada, H.K. (2008). Mitochondrial import and accumulation of alpha-synuclein impair complex I in human dopaminergic neuronal cultures and Parkinson disease brain. J Biol Chem 283, 9089-9100.

Dion, P.A., Daoud, H., and Rouleau, G.A. (2009). Genetics of motor neuron disorders: new insights into pathogenic mechanisms. Nat Rev Genet 10, 769-782.

Dobrowolny, G., Aucello, M., Rizzuto, E., Beccafico, S., Mammucari, C., Bonconpagni, S., Belia, S., Wannenes, F., Nicoletti, C., Del Prete, Z., et al. (2008). Skeletal Muscle Is a Primary Target of SOD1(G93A)-Mediated Toxicity. Cell Metab 8, 425-436.

Dormann, D., Rodde, R., Edbauer, D., Bentmann, E., Fischer, I., Hruscha, A., Than, M.E., Mackenzie, I.R., Capell, A., Schmid, B., et al. (2010). ALS-associated fused in sarcoma (FUS) mutations disrupt Transportin-mediated nuclear import. EMBO J 29, 2841-2857.

Duan, W., Li, X., Shi, J., Guo, Y., Li, Z., and Li, C. (2010). Mutant TAR DNA-binding protein-43 induces oxidative injury in motor neuron-like cell. Neuroscience 169, 1621-1629.

Eidenmuller, J., Fath, T., Hellwig, A., Reed, J., Sontag, E., and Brandt, R. (2000). Structural and functional implications of tau hyperphosphorylation: information from phosphorylation-mimicking mutated tau proteins. Biochemistry 39, 13166-13175.

Ekblom, J., Jossan, S.S., Bergström, M., Oreland, L., Walum, E., and Aquilonius, S.-M. (1993). Monoamine oxidase-B in astrocytes. Glia 8, 122-132.

Exner, N., Lutz, A.K., Haass, C., and Winklhofer, K.F. (2012). Mitochondrial dysfunction in Parkinson's disease: molecular mechanisms and pathophysiological consequences. EMBO J 31, 3038-3062.

Eymard-Pierre, E., Lesca, G., Dollet, S., Santorelli, F.M., di Capua, M., Bertini, E., and Boespflug-Tanguy, O. (2002). Infantile-onset ascending hereditary spastic paralysis is associated with mutations in the alsin gene. Am J Hum Genet 71, 518-527.

Farg, M.A., Soo, K.Y., Walker, A.K., Pham, H., Orian, J., Horne, M.K., Warraich, S.T., Williams, K.L., Blair, I.P., and Atkin, J.D. (2012). Mutant FUS induces endoplasmic reticulum stress in amyotrophic lateral sclerosis and interacts with protein disulfide-isomerase. Neurobiol Aging 33, 2855-2868.

Fasana, E., Fossati, M., Ruggiano, A., Brambillasca, S., Hoogenraad, C.C., Navone, F., Francolini, M., and Borgese, N. (2010). A VAPB mutant linked to amyotrophic lateral

sclerosis generates a novel form of organized smooth endoplasmic reticulum. FASEB J 24, 1419-1430.

Ferraiuolo, L., Kirby, J., Grierson, A.J., Sendtner, M., and Shaw, P.J. (2011). Molecular pathways of motor neuron injury in amyotrophic lateral sclerosis. Nat Rev Neurol 7, 616-630.

Ferrante, R.J., Browne, S.E., Shinobu, L.A., Bowling, A.C., Baik, M.J., MacGarvey, U., Kowall, N.W., Brown, R.H., Jr., and Beal, M.F. (1997). Evidence of increased oxidative damage in both sporadic and familial amyotrophic lateral sclerosis. J Neurochem 69, 2064-2074.

Figlewicz, D.A., Krizus, A., Martinoli, M.G., Meininger, V., Dib, M., Rouleau, G.A., and Julien, J.-P. (1994). Variants of the heavy neurofilament subunit are associated with the development of amyotrophic lateral sclerosis. Hum Mol Genet 3, 1757-1761.

Foran, E., and Trotti, D. (2009). Glutamate transporters and the excitotoxic path to motor neuron degeneration in amyotrophic lateral sclerosis. Antioxid Redox Signal 11, 1587-1602.

Fransson, S., Ruusala, A., and Aspenstrom, P. (2006). The atypical Rho GTPases Miro-1 and Miro-2 have essential roles in mitochondrial trafficking. Biochem Biophys Res Commun 344, 500-510.

Friedman, J.R., Lackner, L.L., West, M., DiBenedetto, J.R., Nunnari, J., and Voeltz, G.K. (2011). ER tubules mark sites of mitochondrial division. Science 334, 358-362.

Fujita, K., Yamauchi, M., Shibayama, K., Ando, M., Honda, M., and Nagata, Y. (1996). Decreased cytochrome c oxidase activity but unchanged superoxide dismutase and glutathione peroxidase activities in the spinal cords of patients with amyotrophic lateral sclerosis. J Neurosci Res 45, 276-281.

Gavin, A.C., Bosche, M., Krause, R., Grandi, P., Marzioch, M., Bauer, A., Schultz, J., Rick, J.M., Michon, A.M., Cruciat, C.M., et al. (2002). Functional organization of the yeast proteome by systematic analysis of protein complexes. Nature 415, 141-147.

Giorgi, C., Baldassari, F., Bononi, A., Bonora, M., De Marchi, E., Marchi, S., Missiroli, S., Patergnani, S., Rimessi, A., Suski, J.M., et al. (2012). Mitochondrial Ca(2+) and apoptosis. Cell calcium 52, 36-43.

Giorgi, C., De Stefani, D., Bononi, A., Rizzuto, R., and Pinton, P. (2009). Structural and functional link between the mitochondrial network and the endoplasmic reticulum. Int J Biochem Cell Biol 41, 1817-1827.

Giorgi, C., Ito, K., Lin, H.K., Santangelo, C., Wieckowski, M.R., Lebiedzinska, M., Bononi, A., Bonora, M., Duszynski, J., Bernardi, R., et al. (2010). PML regulates apoptosis at endoplasmic reticulum by modulating calcium release. Science 330, 1247-1251.

Gkogkas, C., Middleton, S., Kremer, A.M., Wardrope, C., Hannah, M., Gillingwater, T.H., and Skehel, P. (2008). VAPB interacts with and modulates the activity of ATF6. Hum Mol Genet 17, 1517-1526.

Gkogkas, C., Wardrope, C., Hannah, M., and Skehel, P. (2011). The ALS8-associated mutant VAPB(P56S) is resistant to proteolysis in neurons. J Neurochem 117, 286-294.

Goedert, M., Spillantini, M.G., Del Tredici, K., and Braak, H. (2012). 100 years of Lewy pathology. Nat Rev Neurol 9, 13-24.

Gong, Y.H., Parsadanian, A.S., Andreeva, A., Snider, W.D., and Elliot, J.L. (2000). Restricted expression of G86R Cu/Zn superoxide dismutase in astrocytes results in astrocytosis but does not cause motoneuron degeneration. J Neuroscience 20, 660-665.

Greenway, M.J., Andersen, P.M., Russ, C., Ennis, S., Cashman, S., Donaghy, C., Patterson, V., Swingler, R., Kieran, D., Prehn, J., et al. (2006). ANG mutations segregate with familial and 'sporadic' amyotrophic lateral sclerosis. Nat Genet 38, 411-413.

Gros-Louis, F., Meijer, I.A., Hand, C.K., Dube, M.P., MacGregor, D.L., Seni, M.H., Devon, R.S., Hayden, M.R., Andermann, F., Andermann, E., et al. (2003). An ALS2 gene mutation causes hereditary spastic paraplegia in a Pakistani kindred. Ann Neurol 53, 144-145.

Grosskreutz, J., Haastert, K., Dewil, M., Van Damme, P., Callewaert, G., Robberecht, W., Dengler, R., and Van Den Bosch, L. (2007). Role of mitochondria in kainate-induced fast Ca2+ transients in cultured spinal motor neurons. Cell calcium 42, 59-69.

Gurney, M.E., Pu, H., Chiu, A.Y., Dal Canto, M.C., Polchow, C.Y., Alexander, D.D., Caliendo, J., Hentati, A., Kwon, Y.W., Deng, H.-X., et al. (1994). Motor neuron degeneration in mice that express a human Cu,Zn superoxide dismutase mutation. Science 264, 1772-1775.

Hafezparast, M., Klocke, R., Ruhrberg, C., Marquardt, A., Ahmad-Annuar, A., Bowen, S., Lalli, G., Witherden, A.S., Hummerich, H., Nicholson, S., et al. (2003). Mutations in dynein link motor neuron degeneration to defects in retrograde transport. Science 300, 808-812.

Hajnoczky, G., Csordas, G., Das, S., Garcia-Perez, C., Saotome, M., Sinha Roy, S., and Yi, M. (2006). Mitochondrial calcium signalling and cell death: approaches for assessing the role of mitochondrial Ca2+ uptake in apoptosis. Cell calcium 40, 553-560.

Halliwell, B. (1994). Free radicals and antioxidants: a personal view. Nutr Rev 52, 253-265.

Hamamoto, I., Nishimura, Y., Okamoto, T., Aizaki, H., Liu, M., Mori, Y., Abe, T., Suzuki, T., Lai, M.M., Miyamura, T., et al. (2005). Human VAP-B is involved in hepatitis C virus replication through interaction with NS5A and NS5B. J Virol 79, 13473-13482.

Hammer, R.P., Jr., Tomiyasu, U., and Scheibel, A.B. (1979). Degeneration of the human Betz cell due to amyotrophic lateral sclerosis. Exp Neurol 63, 336-346.

Han, S.M., Tsuda, H., Yang, Y., Vibbert, J., Cottee, P., Lee, S.J., Winek, J., Haueter, C., Bellen, H.J., and Miller, M.A. (2012). Secreted VAPB/ALS8 major sperm protein

domains modulate mitochondrial localization and morphology via growth cone guidance receptors. Dev Cell 22, 348-362.

Hardiman, O., van den Berg, L.H., and Kiernan, M.C. (2011). Clinical diagnosis and management of amyotrophic lateral sclerosis. Nat Rev Neurol 7, 639-649.

Harraz, M.M., Marden, J.J., Zhou, W., Zhang, Y., Williams, A., Sharov, V.S., Nelson, K., Luo, M., Paulson, H., Schoneich, C., et al. (2008). SOD1 mutations disrupt redox-sensitive Rac regulation of NADPH oxidase in a familial ALS model. J Clin Invest 118, 659-670.

Hartl, F.U., Bracher, A., and Hayer-Hartl, M. (2011). Molecular chaperones in protein folding and proteostasis. Nature 475, 324-332.

Hayashi, T., Rizzuto, R., Hajnoczky, G., and Su, T.P. (2009). MAM: more than just a housekeeper. Trends Cell Biol 19, 81-88.

Hetz, C. (2012). The unfolded protein response: controlling cell fate decisions under ER stress and beyond. Nat Rev Mol Cell Biol 13, 89-102.

Hicks, G.G., Singh, N., Nashabi, A., Mai, S., Bozek, G., Klewes, L., Arapovic, D., White, E.K., Koury, M.J., Oltz, E.M., et al. (2000). Fus deficiency in mice results in defective B-lymphocyte development and activation, high levels of chromosomal instability and perinatal death. Nat Genet 24, 175-179.

Higgins, C.M., Jung, C., Ding, H., and Xu, Z. (2002). Mutant Cu, Zn superoxide dismutase that causes motoneuron degeneration is present in mitochondria in the CNS. J Neurosci 22, RC215.

Hirano, A., Donnenfeld, H., Sasaki, S., and Nakano, I. (1984). Fine structural observations of neurofilamentous changes in amyotrophic lateral sclerosis. J Neuropathol Exp Neurol 43, 461-470.

Hirokawa, N., and Noda, Y. (2008). Intracellular transport and kinesin superfamily proteins, KIFs: structure, function, and dynamics. Physiol Rev 88, 1089-1118.

Ho, A., and Shen, J. (2011). Presenilins in synaptic function and disease. Trends Mol Med 17, 617-624.

Holasek, S.S., Wengenack, T.M., Kandimalla, K.K., Montano, C., Gregor, D.M., Curran, G.L., and Poduslo, J.F. (2005). Activation of the stress-activated MAP kinase, p38, but not JNK in cortical motor neurons during early presymptomatic stages of amyotrophic lateral sclerosis in transgenic mice. Brain Res 1045, 185-198.

Hortobagyi, T., Troakes, C., Nishimura, A.L., Vance, C., van Swieten, J.C., Seelaar, H., King, A., Al-Sarraj, S., Rogelj, B., and Shaw, C.E. (2012). Optineurin inclusions occur in a minority of TDP-43 positive ALS and FTLD-TDP cases and are rarely observed in other neurodegenerative disorders. Acta Neuropathol 121, 519-527.

Huang, C., Tong, J., Bi, F., Wu, Q., Huang, B., Zhou, H., and Xia, X.G. (2012). Entorhinal cortical neurons are the primary targets of FUS mislocalization and ubiquitin aggregation in FUS transgenic rats. Hum Mol Genet 21, 4602-4614.

Huang, C., Zhou, H., Tong, J., Chen, H., Liu, Y.J., Wang, D., Wei, X., and Xia, X.G. (2011). FUS transgenic rats develop the phenotypes of amyotrophic lateral sclerosis and frontotemporal lobar degeneration. PLoS Genet 7, e1002011.

Huyer, G., Liu, S., Kelly, J., Moffat, J., Payette, P., Kennedy, B., Tsaprailis, G., Gresser, M.J., and Ramachandran, C. (1997). Mechanism of inhibition of protein-tyrosine phosphatases by vanadate and pervanadate. J Biol Chem 272, 843-851.

Ince, P., Stout, N., Shaw, P., Slade, J., Hunziker, W., Heizmann, C.W., and Baimbridge, K.G. (1993). Parvalbumin and calbindin D-28k in the human motor system and in motor neuron disease. Neuropathol Appl Neurobiol 19, 291-299.

Ince, P.G., Highley, J.R., Kirby, J., Wharton, S.B., Takahashi, H., Strong, M.J., and Shaw, P.J. (2011). Molecular pathology and genetic advances in amyotrophic lateral sclerosis: an emerging molecular pathway and the significance of glial pathology. Acta Neuropathol 122, 657-671.

Ince, P.G., Tomkins, J., Slade, J.Y., Thatcher, N.M., and Shaw, P.J. (1998). Amyotrophic lateral sclerosis associated with genetic abnormalities in the gene encoding Cu/Zn superoxide dismutase: molecular pathology of five new cases, and comparison with previous reports and 73 sporadic cases of ALS. J Neuropath Exp Neurol 57, 895-904.

Ishigaki, S., Masuda, A., Fujioka, Y., Iguchi, Y., Katsuno, M., Shibata, A., Urano, F., Sobue, G., and Ohno, K. (2012). Position-dependent FUS-RNA interactions regulate alternative splicing events and transcriptions. Sci Rep 2, 529.

Israelson, A., Arbel, N., Da Cruz, S., Ilieva, H., Yamanaka, K., Shoshan-Barmatz, V., and Cleveland, D.W. (2010). Misfolded mutant SOD1 directly inhibits VDAC1 conductance in a mouse model of inherited ALS. Neuron 67, 575-587.

Ito, D., Seki, M., Tsunoda, Y., Uchiyama, H., and Suzuki, N. (2011a). Nuclear transport impairment of amyotrophic lateral sclerosis-linked mutations in FUS/TLS. Ann Neurol 69, 152-162.

Ito, H., Fujita, K., Nakamura, M., Wate, R., Kaneko, S., Sasaki, S., Yamane, K., Suzuki, N., Aoki, M., Shibata, N., et al. (2011b). Optineurin is co-localized with FUS in basophilic inclusions of ALS with FUS mutation and in basophilic inclusion body disease. Acta Neuropathol 121, 555-557.

Jaiswal, M.K., and Keller, B.U. (2009). Cu/Zn superoxide dismutase typical for familial amyotrophic lateral sclerosis increases the vulnerability of mitochondria and perturbs Ca2+ homeostasis in SOD1G93A mice. Mol Pharmacol 75, 478-489.

Janknecht, R. (2005). EWS-ETS oncoproteins: the linchpins of Ewing tumors. Gene 363, 1-14.

Jensen, F.C., Girardi, A.J., Gilden, R.V., and Koprowski, H. (1964). Infection of Human and Simian Tissue Cultures with Rous Sarcoma Virus. Proc Natl Acad Sci USA 52, 53-59.

Johnson, J.O., Mandrioli, J., Benatar, M., Abramzon, Y., Van Deerlin, V.M., Trojanowski, J.Q., Gibbs, J.R., Brunetti, M., Gronka, S., Wuu, J., et al. (2010). Exome sequencing reveals VCP mutations as a cause of familial ALS. Neuron 68, 857-864.

Ju, J.S., Fuentealba, R.A., Miller, S.E., Jackson, E., Piwnica-Worms, D., Baloh, R.H., and Weihl, C.C. (2009). Valosin-containing protein (VCP) is required for autophagy and is disrupted in VCP disease. J Cell Biol 187, 875-888.

Ju, J.S., Miller, S.E., Hanson, P.I., and Weihl, C.C. (2008). Impaired protein aggregate handling and clearance underlie the pathogenesis of p97/VCP-associated disease. J Biol Chem 283, 30289-30299.

Kabashi, E., Valdmanis, P.N., Dion, P., Spiegelman, D., McConkey, B.J., Velde, C.V., Bouchard, J.P., Lacomblez, L., Pochigaeva, K., Salachas, F., et al. (2008). TARDBP mutations in individuals with sporadic and familial amyotrophic lateral sclerosis. Nat Genet 40, 572-574.

Kagiwada, S., Hosaka, K., Murata, M., Nikawa, J., and Takatsuki, A. (1998). The Saccharomyces cerevisiae SCS2 gene product, a homolog of a synaptobrevin-associated protein, is an integral membrane protein of the endoplasmic reticulum and is required for inositol metabolism. J Bacteriol 180, 1700-1708.

Kamo, H., Haebara, H., Akiguchi, I., Kameyama, M., Kimura, H., and McGeer, P.L. (1987). A distinctive distribution of reactive astroglia in the precentral cortex in amyotrophic lateral sclerosis. Acta Neuropathol 74, 33-38.

Kanai, Y., Dohmae, N., and Hirokawa, N. (2004). Kinesin transports RNA: isolation and characterization of an RNA-transporting granule. Neuron 43, 513-525.

Kanai, Y., and Hediger, M.A. (2004). The glutamate/neutral amino acid transporter family SLC1: molecular, physiological and pharmacological aspects. Pflugers Arch 447, 469-479.

Kanekura, K., Nishimoto, I., Aiso, S., and Matsuoka, M. (2006). Characterization of amyotrophic lateral sclerosis-linked P56S mutation of vesicle-associated membrane protein-associated protein B (VAPB/ALS8). J Biol Chem 28, 30223-30232.

Kanekura, K., Suzuki, H., Aiso, S., and Matsuoka, M. (2009). ER stress and unfolded protein response in amyotrophic lateral sclerosis. Mol Neurobiol 39, 81-89.

Kang, J.S., Tian, J.H., Pan, P.Y., Zald, P., Li, C., Deng, C., and Sheng, Z.H. (2008). Docking of axonal mitochondria by syntaphilin controls their mobility and affects short-term facilitation. Cell 132, 137-148.

Kasai, T., Tokuda, T., Ishigami, N., Sasayama, H., Foulds, P., Mitchell, D.J., Mann, D.M., Allsop, D., and Nakagawa, M. (2009). Increased TDP-43 protein in cerebrospinal fluid of patients with amyotrophic lateral sclerosis. Acta Neuropathol 117, 55-62.

Kawano, M., Kumagai, K., Nishijima, M., and Hanada, K. (2006). Efficient trafficking of ceramide from the endoplasmic reticulum to the Golgi apparatus requires a VAMP-associated protein-interacting FFAT motif of CERT. J Biol Chem 281, 30279-30288.

Kieran, D., Hafezparast, M., Bohnert, S., Dick, J.R., Martin, J., Schiavo, G., Fisher, E.M., and Greensmith, L. (2005). A mutation in dynein rescues axonal transport defects and extends the life span of ALS mice. J Cell Biol 169, 561-567.

Kikuchi, H., Almer, G., Yamashita, S., Guegan, C., Nagai, M., Xu, Z., Sosunov, A.A., McKhann, G.M., 2nd, and Przedborski, S. (2006). Spinal cord endoplasmic reticulum stress associated with a microsomal accumulation of mutant superoxide dismutase-1 in an ALS model. Proc Natl Acad Sci USA 103, 6025-6030.

Kim, S., Leal, S.S., Ben Halevy, D., Gomes, C.M., and Lev, S. (2010a). Structural requirements for VAP-B oligomerization and their implication in amyotrophic lateral sclerosis-associated VAP-B(P56S) neurotoxicity. J Biol Chem 285, 13839-13849.

Kim, S.H., Shanware, N.P., Bowler, M.J., and Tibbetts, R.S. (2010b). Amyotrophic lateral sclerosis-associated proteins TDP-43 and FUS/TLS function in a common biochemical complex to co-regulate HDAC6 mRNA. J Biol Chem 285, 34097-34105.

Kirby, J., Halligan, E., Baptista, M.J., Allen, S., Heath, P.R., Holden, H., Barber, S.C., Loynes, C.A., Wood-Allum, C.A., Lunec, J., et al. (2005). Mutant SOD1 alters the motor neuronal transcriptome: implications for familial ALS. Brain 128, 1686-1706.

Kirkinezos, I.G., Bacman, S.R., Hernandez, D., Oca-Cossio, J., Arias, L.J., Perez-Pinzon, M.A., Bradley, W.G., and Moraes, C.T. (2005). Cytochrome c association with the inner mitochondrial membrane is impaired in the CNS of G93A-SOD1 mice. J Neurosci 25, 164-172.

Ko, H.S., Uehara, T., Tsuruma, K., and Nomura, Y. (2004). Ubiquilin interacts with ubiquitylated proteins and proteasome through its ubiquitin-associated and ubiquitin-like domains. FEBS Lett 566, 110-114.

Kong, J., and Xu, Z. (1998). Massive mitochondrial degeneration in motor neurons triggers the onset of amyotrophic lateral sclerosis in mice expressing a mutant SOD1. J Neurosci 18, 3241-3250.

Kornmann, B., Currie, E., Collins, S.R., Schuldiner, M., Nunnari, J., Weissman, J.S., and Walter, P. (2009). An ER-mitochondria tethering complex revealed by a synthetic biology screen. Science 325, 477-481.

Kornmann, B., Osman, C., and Walter, P. (2011). The conserved GTPase Gem1 regulates endoplasmic reticulum-mitochondria connections. Proc Natl Acad Sci USA 108, 14151-14156.

Kuroda, M., Sok, J., Webb, L., Baechtold, H., Urano, F., Yin, Y., Chung, P., de Rooij, D.G., Akhmedov, A., Ashley, T., et al. (2000). Male sterility and enhanced radiation sensitivity in TLS(-/-) mice. EMBO J 19, 453-462.

Kwiatkowski, T.J., Jr., Bosco, D.A., LeClerc, A.L., Tamrazian, E., Vanderburg, C.R., Russ, C., Davis, A., Gilchrist, J., Kasarskis, E.J., Munsat, T., et al. (2009). Mutations in the FUS/TLS Gene on Chromosome 16 Cause Familial Amyotrophic Lateral Sclerosis. Science 323, 1205-1208.

Lacomblez, L., Bensimon, G., Leigh, P.N., Guillet, P., and Meininger, V. (1996). Dose-ranging study of riluzole in amyotrophic lateral sclerosis. Amyotrophic Lateral Sclerosis/Riluzole Study Group II. Lancet 347, 1425-1431.

Lagier-Tourenne, C., and Cleveland, D.W. (2009). Rethinking ALS: the FUS about TDP-43. Cell 136, 1001-1004.

Lagier-Tourenne, C., Polymenidou, M., and Cleveland, D.W. (2010). TDP-43 and FUS/TLS: emerging roles in RNA processing and neurodegeneration. Hum Mol Genet 19, R46-64.

Lai, C., Xie, C., McCormack, S.G., Chiang, H.C., Michalak, M.K., Lin, X., Chandran, J., Shim, H., Shimoji, M., Cookson, M.R., et al. (2006). Amyotrophic lateral sclerosis 2-deficiency leads to neuronal degeneration in amyotrophic lateral sclerosis through altered AMPA receptor trafficking. J Neurosci 26, 11798-11806.

LaMonte, B.H., Wallace, K.E., Holloway, B.A., Shelly, S.S., Ascano, J., Tokito, M., Van Winkle, T., Howland, D.S., and Holzbaur, E.L. (2002). Disruption of dynein/dynactin inhibits axonal transport in motor neurons causing late-onset progressive degeneration. Neuron 34, 715-727.

Langou, K., Moumen, A., Pellegrino, C., Aebischer, J., Medina, I., Aebischer, P., and Raoul, C. (2010). AAV-mediated expression of wild-type and ALS-linked mutant VAPB selectively triggers death of motoneurons through a Ca2+-dependent ER-associated pathway. J Neurochem 114, 795-809.

Larsen, M.R., Trelle, M.B., Thingholm, T.E., and Jensen, O.N. (2006). Analysis of posttranslational modifications of proteins by tandem mass spectrometry. BioTechniques 40, 790-798.

Latterich, M., Frohlich, K.U., and Schekman, R. (1995). Membrane fusion and the cell cycle: Cdc48p participates in the fusion of ER membranes. Cell 82, 885-893.

Laughlin, S.B., de Ruyter van Steveninck, R.R., and Anderson, J.C. (1998). The metabolic cost of neural information. Nat Neurosci 1, 36-41.

Lautenschlaeger, J., Prell, T., and Grosskreutz, J. (2012). Endoplasmic reticulum stress and the ER mitochondrial calcium cycle in amyotrophic lateral sclerosis. Amyotroph Lateral Scler 13, 166-177.

Law, W.J., Cann, K.L., and Hicks, G.G. (2006). TLS, EWS and TAF15: a model for transcriptional integration of gene expression. Brief Funct Genomic Proteomic 5, 8-14.

Lebiedzinska, M., Szabadkai, G., Jones, A.W., Duszynski, J., and Wieckowski, M.R. (2009). Interactions between the endoplasmic reticulum, mitochondria, plasma membrane and other subcellular organelles. Int J Biochem Cell Biol 41, 1805-1816.

Lee, V.M., and Trojanowski, J.Q. (2006). Mechanisms of Parkinson's disease linked to pathological alpha-synuclein: new targets for drug discovery. Neuron 52, 33-38.

Leigh, P.N., Anderton, B.H., Dodson, A., Gallo, J.M., Swash, M., and Power, D.M. (1988). Ubiquitin deposits in anterior horn cells in motor neurone disease. Neurosci Lett 93, 197-203.

Letourneur, F., Gaynor, E.C., Hennecke, S., Demolliere, C., Duden, R., Emr, S.D., Riezman, H., and Cosson, P. (1994). Coatomer is essential for retrieval of dilysine-tagged proteins to the endoplasmic reticulum. Cell 79, 1199-1207.

Levy, J.R., Sumner, C.J., Caviston, J.P., Tokito, M.K., Ranganathan, S., Ligon, L.A., Wallace, K.E., LaMonte, B.H., Harmison, G.G., Puls, I., et al. (2006). A motor neuron disease-associated mutation in p150Glued perturbs dynactin function and induces protein aggregation. J Cell Biol 172, 733-745.

Li, Q., Lau, A., Morris, T.J., Guo, L., Fordyce, C.B., and Stanley, E.F. (2004). A syntaxin 1, Galpha(o), and N-type calcium channel complex at a presynaptic nerve terminal: analysis by quantitative immunocolocalization. J Neurosci 24, 4070-4081.

Lin, C.-L.G., Bristol, L.A., Jin, L., Dykes-Hoberg, M., Crawford, T., Clawson, L., and Rothstein, J.D. (1998). Aberrant RNA processing in a neurodegenerative disease: the cause of absent EAAT2, a glutamate transporter, in Amyotrophic Lateral Sclerosis. Neuron 20, 589-602.

Lin, J.H., Walter, P., and Yen, T.S. (2008). Endoplasmic reticulum stress in disease pathogenesis. Annu Rev Pathol 3, 399-425.

Liu-Yesucevitz, L., Bilgutay, A., Zhang, Y.J., Vanderweyde, T., Citro, A., Mehta, T., Zaarur, N., McKee, A., Bowser, R., Sherman, M., et al. (2010). Tar DNA binding protein-43 (TDP-43) associates with stress granules: analysis of cultured cells and pathological brain tissue. PLoS ONE 5, e13250.

Liu, J., Lillo, C., Jonsson, P.A., Velde, C.V., Ward, C.M., Miller, T.M., Subramaniam, J.R., Rothstein, J.D., Marklund, S., Andersen, P.M., et al. (2004). Toxicity of familial ALS-linked SOD1 mutants from selective recruitment to spinal mitochondria. Neuron 43, 5-17.

Liu, R.G., Althaus, J.S., Ellerbrock, B.R., Becker, D.A., and Gurney, M.E. (1998). Enhanced oxygen radical production in a transgenic mouse model of familial amyotrophic lateral sclerosis. AnnNeurol 44, 763-770.

Lobsiger, C.S., Boillee, S., McAlonis-Downes, M., Khan, A.M., Feltri, M.L., Yamanaka, K., and Cleveland, D.W. (2009). Schwann cells expressing dismutase active mutant SOD1 unexpectedly slow disease progression in ALS mice. Proc Natl Acad Sci USA 106, 4465-4470.

Lodish, H.F., and Kong, N. (1990). Perturbation of cellular calcium blocks exit of secretory proteins from the rough endoplasmic reticulum. J Biol Chem 265, 10893-10899.

Loewen, C.J., Roy, A., and Levine, T.P. (2003). A conserved ER targeting motif in three families of lipid binding proteins and in Opi1p binds VAP. EMBO J 22, 2025-2035.

Logroscino, G., Traynor, B.J., Hardiman, O., Chio, A., Mitchell, D., Swingler, R.J., Millul, A., Benn, E., and Beghi, E. (2011). Incidence of amyotrophic lateral sclerosis in Europe. J Neurol Neurosurg Psychiatry 81, 385-390.

Lomen-Hoerth, C., Murphy, J., Langmore, S., Kramer, J.H., Olney, R.K., and Miller, B. (2003). Are amyotrophic lateral sclerosis patients cognitively normal? Neurology 60, 1094-1097.

Lowe, J., Aldridge, F., Lennox, G., Doherty, F., Jefferson, D., Landon, M., and Mayer, R.J. (1989). Inclusion bodies in motor cortex and brainstem of patients with motor neurone disease are detected by immunocytochemical localisation of ubiquitin. Neurosci Lett 105, 7-13.

Lv, B.F., Yu, C.F., Chen, Y.Y., Lu, Y., Guo, J.H., Song, Q.S., Ma, D.L., Shi, T.P., and Wang, L. (2006). Protein tyrosine phosphatase interacting protein 51 (PTPIP51) is a novel mitochondria protein with an N-terminal mitochondrial targeting sequence and induces apoptosis. Apoptosis 11, 1489-1501.

MacAskill, A.F., and Kittler, J.T. (2010). Control of mitochondrial transport and localization in neurons. Trends Cell Biol 20, 102-a112.

Macaskill, A.F., Rinholm, J.E., Twelvetrees, A.E., Arancibia-Carcamo, I.L., Muir, J., Fransson, A., Aspenstrom, P., Attwell, D., and Kittler, J.T. (2009). Miro1 is a calcium sensor for glutamate receptor-dependent localization of mitochondria at synapses. Neuron 61, 541-555.

Mackenzie, I.R., Bigio, E.H., Ince, P.G., Geser, F., Neumann, M., Cairns, N.J., Kwong, L.K., Forman, M.S., Ravits, J., Stewart, H., et al. (2007). Pathological TDP-43 distinguishes sporadic amyotrophic lateral sclerosis from amyotrophic lateral sclerosis with SOD1 mutations. Ann Neurol 61, 427-434.

Mackenzie, I.R., Rademakers, R., and Neumann, M. (2010). TDP-43 and FUS in amyotrophic lateral sclerosis and frontotemporal dementia. Lancet Neurol 9, 995-1007.

Majounie, E., Renton, A.E., Mok, K., Dopper, E.G., Waite, A., Rollinson, S., Chio, A., Restagno, G., Nicolaou, N., Simon-Sanchez, J., et al. (2012). Frequency of the C9orf72 hexanucleotide repeat expansion in patients with amyotrophic lateral sclerosis and frontotemporal dementia: a cross-sectional study. Lancet Neurol 11, 323-330.

Malhotra, J.D., and Kaufman, R.J. (2011). ER stress and its functional link to mitochondria: role in cell survival and death. Cold Spring Harb Perspect Biol 3, a004424.

Manjaly, Z.R., Scott, K.M., Abhinav, K., Wijesekera, L., Ganesalingam, J., Goldstein, L.H., Janssen, A., Dougherty, A., Willey, E., Stanton, B.R., et al. (2010). The sex ratio in amyotrophic lateral sclerosis: A population based study. Amyotroph Lateral Scler 11, 439-442.

Marinkovic, P., Reuter, M.S., Brill, M.S., Godinho, L., Kerschensteiner, M., and Misgeld, T. (2012). Axonal transport deficits and degeneration can evolve independently in mouse models of amyotrophic lateral sclerosis. Proc Natl Acad Sci USA 109, 4296-4301.

Maruyama, H., Morino, H., Ito, H., Izumi, Y., Kato, H., Watanabe, Y., Kinoshita, Y., Kamada, M., Nodera, H., Suzuki, H., et al. (2010). Mutations of optineurin in amyotrophic lateral sclerosis. Nature 465, 223-226.

Mattiazzi, M., D'Aurelio, M., Gajewski, C.D., Martushova, K., Kiaei, M., Beal, M.F., and Manfredi, G. (2002). Mutated human SOD1 causes dysfunction of oxidative phosphorylation in mitochondria of transgenic mice. J Biol Chem 277, 29626-29633.

Matusica, D., Fenech, M.P., Rogers, M.L., and Rush, R.A. (2008). Characterization and use of the NSC-34 cell line for study of neurotrophin receptor trafficking. J Neurosci Res 86, 553-565.

McCommis, K.S., and Baines, C.P. (2012). The role of VDAC in cell death: Friend or foe? Biochim Biophys Acta 1818, 1444-1450.

Mersiyanova, I.V., Perepelov, A.V., Polyakov, A.V., Sitnikov, V.F., Dadali, E.L., Oparin, R.B., Petrin, A.N., and Evgrafov, O.V. (2000). A new variant of Charcot-Marie-Tooth disease type 2 is probably the result of a mutation in the neurofilament-light gene. Am J Hum Genet 67, 37-46.

Millecamps, S., Robertson, J., Lariviere, R., Mallet, J., and Julien, J.P. (2006). Defective axonal transport of neurofilament proteins in neurons overexpressing peripherin. J Neurochem 98, 926-938.

Millecamps, S., Salachas, F., Cazeneuve, C., Gordon, P., Bricka, B., Camuzat, A., Guillot-Noel, L., Russaouen, O., Bruneteau, G., Pradat, P.F., et al. (2010). SOD1, ANG, VAPB, TARDBP, and FUS mutations in familial amyotrophic lateral sclerosis: genotype-phenotype correlations. J Med Genet 47, 554-560.

Miller, R.G., Mitchell, J.D., and Moore, D.H. (2012). Riluzole for amyotrophic lateral sclerosis (ALS)/motor neuron disease (MND). Cochrane Database Syst Rev 3, CD001447.

Misko, A., Jiang, S., Wegorzewska, I., Milbrandt, J., and Baloh, R.H. (2010). Mitofusin 2 is necessary for transport of axonal mitochondria and interacts with the Miro/Milton complex. J Neurosci 30, 4232-4240.

Mitchell, J.C., McGoldrick, P., Vance, C., Hortobagyi, T., Sreedharan, J., Rogelj, B., Tudor, E.L., Smith, B.N., Klasen, C., Miller, C.C., et al. (2012). Overexpression of human wild-type FUS causes progressive motor neuron degeneration in an age- and dose-dependent fashion. Acta Neuropathol 125, 273-288.

Mitne-Neto, M., Ramos, C.R., Pimenta, D.C., Luz, J.S., Nishimura, A.L., Gonzales, F.A., Oliveira, C.C., and Zatz, M. (2007). A mutation in human VAP-B--MSP domain, present in ALS patients, affects the interaction with other cellular proteins. Protein Expr Purif 55, 139-146.

Mizuno, Y., Amari, M., Takatama, M., Aizawa, H., Mihara, B., and Okamoto, K. (2006). Transferrin localizes in Bunina bodies in amyotrophic lateral sclerosis. Acta Neuropathol 112, 597-603.

Mizuno, Y., Fujita, Y., Takatama, M., and Okamoto, K. (2011). Peripherin partially localizes in Bunina bodies in amyotrophic lateral sclerosis. J Neurol Sci 302, 14-18.

Morita, M., Al-Chalabi, A., Andersen, P.M., Hosler, B., Sapp, P., Englund, E., Mitchell, J.E., Habgood, J.J., de Belleroche, J., Xi, J., et al. (2006). A locus on chromosome 9p confers susceptibility to ALS and frontotemporal dementia. Neurology 66, 839-844.

Morotz, G.M., De Vos, K.J., Vagnoni, A., Ackerley, S., Shaw, C.E., and Miller, C.C. (2012). Amyotrophic lateral sclerosis-associated mutant VAPBP56S perturbs calcium homeostasis to disrupt axonal transport of mitochondria. Hum Mol Genet 21, 1979-1988.

Morris, H.R., Waite, A.J., Williams, N.M., Neal, J.W., and Blake, D.J. (2012). Recent advances in the genetics of the ALS-FTLD complex. Curr Neurol Neurosci Rep 12, 243-250.

Moumen, A., Virard, I., and Raoul, C. (2011). Accumulation of wildtype and ALS-linked mutated VAPB impairs activity of the proteasome. PLoS ONE 6, e26066.

Munch, C., Sedlmeier, R., Meyer, T., Homberg, V., Sperfeld, A.D., Kurt, A., Prudlo, J., Peraus, G., Hanemann, C.O., Stumm, G., et al. (2004). Point mutations of the p150 subunit of dynactin (DCTN1) gene in ALS. Neurology 63, 724-726.

Munoz, D.G., Greene, C., Perl, D.P., and Selkoe, D.J. (1988). Accumulation of phosphorylated neurofilaments in anterior horn motoneurons of amyotrophic lateral sclerosis patients. J Neuropathol Exp Neurol 47, 9-18.

Nakagawa, T., Zhu, H., Morishima, N., Li, E., Xu, J., Yankner, B.A., and Yuan, J.Y. (2000). Caspase-12 mediates endoplasmic-reticulum-specific apoptosis and cytotoxicity by amyloid-β. Nature 403, 98-103.

Neumann, M., Sampathu, D.M., Kwong, L.K., Truax, A.C., Micsenyi, M.C., Chou, T.T., Bruce, J., Schuck, T., Grossman, M., Clark, C.M., et al. (2006). Ubiquitinated TDP-43 in frontotemporal lobar degeneration and amyotrophic lateral sclerosis. Science 314, 130-113.

Nguyen, T., Nioi, P., and Pickett, C.B. (2009). The Nrf2-antioxidant response element signaling pathway and its activation by oxidative stress. J Biol Chem 284, 13291-13295.

Nicoletti, F., Bockaert, J., Collingridge, G.L., Conn, P.J., Ferraguti, F., Schoepp, D.D., Wroblewski, J.T., and Pin, J.P. (2011). Metabotropic glutamate receptors: from the workbench to the bedside. Neuropharmacology 60, 1017-1041.

Nishimura, A.L., Mitne-Neto, M., Silva, H.C., Richieri-Costa, A., Middleton, S., Cascio, D., Kok, F., Oliveira, J.R., Gillingwater, T., Webb, J., et al. (2004). A mutation in the vesicle-trafficking protein VAPB causes late-onset spinal muscular atrophy and amyotrophic lateral sclerosis. Am J Hum Genet 75, 822-831.

Nishimura, Y., Hayashi, M., Inada, H., and Tanaka, T. (1999). Molecular cloning and characterization of mammalian homologues of vesicle-associated membrane protein-associated (VAMP-associated) proteins. Biochem Biophys Res Commun 254, 21-26.

Nishitoh, H., Kadowaki, H., Nagai, A., Maruyama, T., Yokota, T., Fukutomi, H., Noguchi, T., Matsuzawa, A., Takeda, K., and Ichijo, H. (2008). ALS-linked mutant SOD1 induces ER stress- and ASK1-dependent motor neuron death by targeting Derlin-1. Genes Dev 22, 1451-1464.

Nishitoh, H., Matsuzawa, A., Tobiume, K., Saegusa, K., Takeda, K., Inoue, K., Hori, S., Kakizuka, A., and Ichijo, H. (2002). ASK1 is essential for endoplasmic reticulum stress-induced neuronal cell death triggered by expanded polyglutamine repeats. Genes Dev 16, 1345-1355.

Oakes, S.A., Scorrano, L., Opferman, J.T., Bassik, M.C., Nishino, M., Pozzan, T., and Korsmeyer, S.J. (2005). Proapoptotic BAX and BAK regulate the type 1 inositol trisphosphate receptor and calcium leak from the endoplasmic reticulum. Proc Natl Acad Sci USA 102, 105-110.

Oishi, K., Okano, H., and Sawa, H. (2007). RMD-1, a novel microtubule-associated protein, functions in chromosome segregation in Caenorhabditis elegans. J Cell Biol 179, 1149-1162.

Okamoto, K., Hirai, S., Amari, M., Watanabe, M., and Sakurai, A. (1993). Bunina bodies in amyotrophic lateral sclerosis immunostained with rabbit anti-cystatin C serum. Neurosci Lett 162, 125-128.

Okamoto, K., Mizuno, Y., and Fujita, Y. (2008). Bunina bodies in amyotrophic lateral sclerosis. Neuropathology 28, 109-115.

Olsen, J.V., Blagoev, B., Gnad, F., Macek, B., Kumar, C., Mortensen, P., and Mann, M. (2006). Global, in vivo, and site-specific phosphorylation dynamics in signaling networks. Cell 127, 635-648.

Olsen, J.V., Vermeulen, M., Santamaria, A., Kumar, C., Miller, M.L., Jensen, L.J., Gnad, F., Cox, J., Jensen, T.S., Nigg, E.A., et al. (2010). Quantitative phosphoproteomics reveals widespread full phosphorylation site occupancy during mitosis. Sci Signal 3, ra3.

Omasa, T., Onitsuka, M., and Kim, W.D. (2010). Cell engineering and cultivation of chinese hamster ovary (CHO) cells. Curr Pharm Biotechnol 11, 233-240.

Orci, L., Stamnes, M., Ravazzola, M., Amherdt, M., Perrelet, A., Sollner, T.H., and Rothman, J.E. (1997). Bidirectional transport by distinct populations of COPI-coated vesicles. Cell 90, 335-349.

Orrell, R.W. (2009). Motor neuron disease: systematic reviews of treatment for ALS and SMA. Br Med Bull 93, 145-159.

Osawa, T., Mizuno, Y., Fujita, Y., Takatama, M., Nakazato, Y., and Okamoto, K. (2011). Optineurin in neurodegenerative diseases. Neuropathology 31, 569-574.

Otomo, A., Hadano, S., Okada, T., Mizumura, H., Kunita, R., Nishijima, H., Showguchi-Miyata, J., Yanagisawa, Y., Kohiki, E., Suga, E., et al. (2003). ALS2, a novel guanine nucleotide exchange factor for the small GTPase Rab5, is implicated in endosomal dynamics. Hum Mol Genet 12, 1671-1687.

Ou, S.H., Wu, F., Harrich, D., Garcia-Martinez, L.F., and Gaynor, R.B. (1995). Cloning and characterization of a novel cellular protein, TDP-43, that binds to human immunodeficiency virus type 1 TAR DNA sequence motifs. J Virol 69, 3584-3596.

Oyanagi, K., Makifuchi, T., and Ikuta, F. (1995). The anterolateral funiculus in the spinal cord in amyotrophic lateral sclerosis. Acta Neuropathol 90, 221-227.

Panico, R., Powell, W.H. & Richer, J.-C. (1993). A Guide to IUPAC Nomenclature of Organic Compounds (recommendations 1993) (Oxford, UK, Blackwell Scientific Publications [International Union of Pure and Applied Chemistry. Division of Organic Chemistry. Commission on Nomenclature of Organic Chemistry]).

Pasinelli, P., Belford, M.E., Lennon, N., Bacskai, B.J., Hyman, B.T., Trotti, D., and Brown, R.H., Jr. (2004). Amyotrophic lateral sclerosis-associated SOD1 mutant proteins bind and aggregate with Bcl-2 in spinal cord mitochondria. Neuron 43, 19-30.

Pellegrino, M.W., Nargund, A.M., and Haynes, C.M. (2013). Signaling the mitochondrial unfolded protein response. Biochim Biophys Acta 1833, 410-416.

Pennetta, G., Hiesinger, P., Fabian-Fine, R., Meinertzhagen, I., and Bellen, H. (2002). Drosophila VAP-33A directs bouton formation at neuromuscular junctions in a dosage-dependent manner. Neuron 35, 291-306.

Peretti, D., Dahan, N., Shimoni, E., Hirschberg, K., and Lev, S. (2008). Coordinated lipid transfer between the endoplasmic reticulum and the Golgi complex requires the VAP Proteins and is essential for Golgi-mediated transport. Mol Biol Cell 19, 3871-3884.

Petri, M.K., Koch, P., Stenzinger, A., Kuchelmeister, K., Nestler, U., Paradowska, A., Steger, K., Brobeil, A., Viard, M., and Wimmer, M. (2011). PTPIP51, a positive modulator of the MAPK/Erk pathway, is upregulated in glioblastoma and interacts with 14-3-3beta and PTP1B in situ. Histol Histopathol 26, 1531-1543.

Piao, Y.S., Wakabayashi, K., Kakita, A., Yamada, M., Hayashi, S., Morita, T., Ikuta, F., Oyanagi, K., and Takahashi, H. (2003). Neuropathology with clinical correlations of sporadic amyotrophic lateral sclerosis: 102 autopsy cases examined between 1962 and 2000. Brain Pathol 13, 10-22.

Pinton, P., Giorgi, C., Siviero, R., Zecchini, E., and Rizzuto, R. (2008). Calcium and apoptosis: ER-mitochondria Ca2+ transfer in the control of apoptosis. Oncogene 27, 6407-6418.

Pitts, K.R., Yoon, Y., Krueger, E.W., and McNiven, M.A. (1999). The dynamin-like protein DLP1 is essential for normal distribution and morphology of the endoplasmic reticulum and mitochondria in mammalian cells. Mol Biol Cell 10, 4403-4417.

Polymenidou, M., Lagier-Tourenne, C., Hutt, K.R., Huelga, S.C., Moran, J., Liang, T.Y., Ling, S.C., Sun, E., Wancewicz, E., Mazur, C., et al. (2011). Long pre-mRNA depletion and RNA missplicing contribute to neuronal vulnerability from loss of TDP-43. Nat Neurosci 14, 459-468.

Pramatarova, A., Laganière, J., Roussel, J., Brisebois, K., and Rouleau, G.A. (2001). Neuron-specific expression of mutant superoxide dismutase 1 in transgenic mice does not lead to motor impairment. JNeurosci 21, 3369-3374.

Puls, I., Jonnakuty, C., LaMonte, B.H., Holzbaur, E.L., Tokito, M., Mann, E., Floeter, M.K., Bidus, K., Drayna, D., Oh, S.J., et al. (2003). Mutant dynactin in motor neuron disease. Nat Genet 33, 455-456.

Rabbitts, T.H., Forster, A., Larson, R., and Nathan, P. (1993). Fusion of the dominant negative transcription regulator CHOP with a novel gene FUS by translocation t(12;16) in malignant liposarcoma. Nat Genet 4, 175-180.

Rabouille, C., Levine, T.P., Peters, J.M., and Warren, G. (1995). An NSF-like ATPase, p97, and NSF mediate cisternal regrowth from mitotic Golgi fragments. Cell 82, 905-914.

Rademakers, R., Neumann, M., and Mackenzie, I.R. (2012). Advances in understanding the molecular basis of frontotemporal dementia. Nat Rev Neurol 8, 423-434.

Raingeaud, J., Whitmarsh, A.J., Barrett, T., Derijard, B., and Davis, R.J. (1996). MKK3- and MKK6-regulated gene expression is mediated by the p38 mitogen-activated protein kinase signal transduction pathway. Mol Cell Biol 16, 1247-1255.

Rakhit, R., Robertson, J., Vande Velde, C., Horne, P., Ruth, D.M., Griffin, J., Cleveland, D.W., Cashman, N.R., and Chakrabartty, A. (2007). An immunological epitope selective for pathological monomer-misfolded SOD1 in ALS. Nat Med 13, 754-759.

Rapizzi, E., Pinton, P., Szabadkai, G., Wieckowski, M.R., Vandecasteele, G., Baird, G., Tuft, R.A., Fogarty, K.E., and Rizzuto, R. (2002). Recombinant expression of the voltage-dependent anion channel enhances the transfer of Ca2+ microdomains to mitochondria. J Cell Biol 159, 613-624.

Ratnaparkhi, A., Lawless, G.M., Schweizer, F.E., Golshani, P., and Jackson, G.R. (2008). A Drosophila model of ALS: human ALS-associated mutation in VAP33A suggests a dominant negative mechanism. PLoS ONE 3, e2334.

Ravits, J.M., and La Spada, A.R. (2009). ALS motor phenotype heterogeneity, focality, and spread: deconstructing motor neuron degeneration. Neurology 73, 805-811.

Renton, A.E., Majounie, E., Waite, A., Simon-Sanchez, J., Rollinson, S., Gibbs, J.R., Schymick, J.C., Laaksovirta, H., van Swieten, J.C., Myllykangas, L., et al. (2011). A hexanucleotide repeat expansion in C9ORF72 is the cause of chromosome 9p21-linked ALS-FTD. Neuron 72, 257-268.

Ringholz, G.M., Appel, S.H., Bradshaw, M., Cooke, N.A., Mosnik, D.M., and Schulz, P.E. (2005). Prevalence and patterns of cognitive impairment in sporadic ALS. Neurology 65, 586-590.

Rintoul, G.L., Filiano, A.J., Brocard, J.B., Kress, G.J., and Reynolds, I.J. (2003). Glutamate decreases mitochondrial size and movement in primary forebrain neurons. J Neurosci 23, 7881-7888.

Ritz, D., Vuk, M., Kirchner, P., Bug, M., Schutz, S., Hayer, A., Bremer, S., Lusk, C., Baloh, R.H., Lee, H., et al. (2011). Endolysosomal sorting of ubiquitylated caveolin-1 is regulated by VCP and UBXD1 and impaired by VCP disease mutations. Nat Cell Biol 13, 1116-1123.

Rizzuto, R., Marchi, S., Bonora, M., Aguiari, P., Bononi, A., De Stefani, D., Giorgi, C., Leo, S., Rimessi, A., Siviero, R., et al. (2009). Ca(2+) transfer from the ER to mitochondria: when, how and why. Biochim Biophys Acta 1787, 1342-1351.

Rizzuto, R., Pinton, P., Carrington, W., Fay, F.S., Fogarty, K.E., Lifshitz, L.M., Tuft, R.A., and Pozzan, T. (1998). Close contacts with the endoplasmic reticulum as determinants of mitochondrial Ca2+ responses. Science 280, 1763-1766.

Rosen, D.R., Siddique, T., Patterson, D., Figlewicz, D.A., Sapp, P., Hentati, A., Donaldson, D., Goto, J., O'Regan, J.P., Deng, H.X., et al. (1993). Mutations in the Cu/Zn superoxide dismutase gene are associated with familial amyotrophic lateral sclerosis. Nature 362, 59-62.

Rothstein, J.D. (2009). Current hypotheses for the underlying biology of amyotrophic lateral sclerosis. Ann Neurol 65 Suppl 1, S3-9.

Rothstein, J.D., Martin, L.J., and Kuncl, R.W. (1992). Decreased glutamate transport in the brain and spinal cord in amyotrophic lateral sclerosis. New England J Med 326, 1464-1468.

Rothstein, J.D., Tsai, G., Kuncl, R.W., Clawson, L., Cornblath, D.R., Drachman, D.B., Pestronk, A., Stauch, B.L., and Coyle, J.T. (1990). Abnormal excitatory amino acid metabolism in amyotrophic lateral sclerosis. AnnNeurol 28, 18-25.

Rowland, A.A., and Voeltz, G.K. (2012). Endoplasmic reticulum-mitochondria contacts: function of the junction. Nat Rev Mol Cell Biol 13, 607-625.

Rusinol, A.E., Cui, Z., Chen, M.H., and Vance, J.E. (1994). A unique mitochondria-associated membrane fraction from rat liver has a high capacity for lipid synthesis and contains pre-Golgi secretory proteins including nascent lipoproteins. J Biol Chem 269, 27494-27502.

Ryberg, H., Askmark, H., and Persson, L.I. (2003). A double-blind randomized clinical trial in amyotrophic lateral sclerosis using lamotrigine: effects on CSF glutamate, aspartate, branched-chain amino acid levels and clinical parameters. Acta Neurol Scand 108, 1-8.

Sambrook, J., Fritsch, E.F., and Maniatis, T. (1989). Molecular cloning. A laboratory Manual. (Cold Spring Harbor, Cold Spring Harbor Laboratory Press).

Saotome, M., Safiulina, D., Szabadkai, G., Das, S., Fransson, A., Aspenstrom, P., Rizzuto, R., and Hajnoczky, G. (2008). Bidirectional Ca2+-dependent control of mitochondrial dynamics by the Miro GTPase. Proc Natl Acad Sci USA 105, 20728-20733.

Sarlette, A., Krampfl, K., Grothe, C., Neuhoff, N., Dengler, R., and Petri, S. (2008). Nuclear erythroid 2-related factor 2-antioxidative response element signaling pathway

in motor cortex and spinal cord in amyotrophic lateral sclerosis. J Neuropathol Exp Neurol 67, 1055-1062.

Sasaki, S. (2010). Endoplasmic reticulum stress in motor neurons of the spinal cord in sporadic amyotrophic lateral sclerosis. J Neuropathol Exp Neurol 69, 346-355.

Sasaki, S., and Iwata, M. (2007). Mitochondrial alterations in the spinal cord of patients with sporadic amyotrophic lateral sclerosis. J Neuropathol Exp Neurol 66, 10-16.

Saxena, S., Cabuy, E., and Caroni, P. (2009). A role for motoneuron subtype-selective ER stress in disease manifestations of FALS mice. Nat Neurosci 12, 627-636.

Schon, E.A., and Area-Gomez, E. (2010). Is Alzheimer's disease a disorder of mitochondria-associated membranes? J Alzheimers Dis 20 Suppl 2, S281-292.

Schon, E.A., and Area-Gomez, E. (2012). Mitochondria-associated ER membranes in Alzheimer disease. Mol Cell Neurosci.-in press

Seelaar, H., Schelhaas, H.J., Azmani, A., Kusters, B., Rosso, S., Majoor-Krakauer, D., de Rijik, M.C., Rizzu, P., ten Brummelhuis, M., van Doorn, P.A., et al. (2007). TDP-43 pathology in familial frontotemporal dementia and motor neuron disease without Progranulin mutations. Brain 130, 1375-1385.

Selkoe, D.J., and Wolfe, M.S. (2007). Presenilin: running with scissors in the membrane. Cell 131, 215-221.

Sephton, C.F., Cenik, C., Kucukural, A., Dammer, E.B., Cenik, B., Han, Y., Dewey, C.M., Roth, F.P., Herz, J., Peng, J., et al. (2011). Identification of neuronal RNA targets of TDP-43-containing ribonucleoprotein complexes. J Biol Chem 286, 1204-1215.

Sephton, C.F., Good, S.K., Atkin, S., Dewey, C.M., Mayer, P., 3rd, Herz, J., and Yu, G. (2010). TDP-43 is a developmentally regulated protein essential for early embryonic development. J Biol Chem 285, 6826-6834.

Shan, X., Chiang, P.M., Price, D.L., and Wong, P.C. (2010). Altered distributions of Gemini of coiled bodies and mitochondria in motor neurons of TDP-43 transgenic mice. Proc Natl Acad Sci USA 107, 16325-16330.

Shavali, S., Brown-Borg, H.M., Ebadi, M., and Porter, J. (2008). Mitochondrial localization of alpha-synuclein protein in alpha-synuclein overexpressing cells. Neurosci Lett 439, 125-128.

Shaw, P.J., Ince, P.G., Falkous, G., and Mantle, D. (1995). Oxidative damage to protein in sporadic motor neuron disease spinal cord. Ann Neurol 38, 691-695.

Shi, J., Shaw, C.L., Du Plessis, D., Richardson, A.M., Bailey, K.L., Julien, C., Stopford, C., Thompson, J., Varma, A., Craufurd, D., et al. (2005). Histopathological changes underlying frontotemporal lobar degeneration with clinicopathological correlation. Acta Neuropathol 110, 501-512.

Shibata, N., Asayama, K., Hirano, A., and Kobayashi, M. (1996). Immunohistochemical study on superoxide dismutases in spinal cords from autopsied patients with amyotrophic lateral sclerosis. DevNeurosci 18, 492-498.

Siklos, L., Engelhardt, J., Harati, Y., Smith, R.G., Joo, F., and Appel, S.H. (1996). Ultrastructural evidence for altered calcium in motor nerve terminals in amyotropic lateral sclerosis. Ann Neurol 39, 203-216.

Simmen, T., Aslan, J.E., Blagoveshchenskaya, A.D., Thomas, L., Wan, L., Xiang, Y., Feliciangeli, S.F., Hung, C.H., Crump, C.M., and Thomas, G. (2005). PACS-2 controls endoplasmic reticulum-mitochondria communication and Bid-mediated apoptosis. EMBO J 24, 717-729.

Simmen, T., Lynes, E.M., Gesson, K., and Thomas, G. (2010). Oxidative protein folding in the endoplasmic reticulum: tight links to the mitochondria-associated membrane (MAM). Biochim Biophys Acta 1798, 1465-1473.

Simpson, E.P., Henry, Y.K., Henkel, J.S., Smith, R.G., and Appel, S.H. (2004). Increased lipid peroxidation in sera of ALS patients: a potential biomarker of disease burden. Neurology 62, 1758-1765.

Skehel, P.A., Fabian-Fine, R., and Kandel, E.R. (2000). Mouse VAP33 is associated with the endoplasmic reticulum and microtubules. Proc Natl Acad Sci USA 97, 1101-1106.

Skehel, P.A., Martin, K.C., Kandel, E.R., and Bartsch, D. (1995). A VAMP-binding protein from Aplysia required for neurotransmitter release. Science 269, 1580-1583.

Smith, R.G., Henry, Y.K., Mattson, M.P., and Appel, S.H. (1998). Presence of 4-hydroxynonenal in cerebrospinal fluid of patients with sporadic amyotrophic lateral sclerosis. Ann Neurol 44, 696-699.

Soderberg, O., Gullberg, M., Jarvius, M., Ridderstrale, K., Leuchowius, K.J., Jarvius, J., Wester, K., Hydbring, P., Bahram, F., Larsson, L.G., et al. (2006). Direct observation of individual endogenous protein complexes in situ by proximity ligation. Nat Methods 3, 995-1000.

Sonawane, N.D., Szoka, F.C., Jr., and Verkman, A.S. (2003). Chloride accumulation and swelling in endosomes enhances DNA transfer by polyamine-DNA polyplexes. J Biol Chem 278, 44826-44831.

Sotelo-Silveira, J.R., Lepanto, P., Elizondo, V., Horjales, S., Palacios, F., Martinez-Palma, L., Marin, M., Beckman, J.S., and Barbeito, L. (2009). Axonal mitochondrial clusters containing mutant SOD1 in transgenic models of ALS. Antioxid Redox Signal 11, 1535-1545.

Soussan, L., Burakov, D., Daniels, M.P., Toister-Achituv, M., Porat, A., Yarden, Y., and Elazar, Z. (1999). ERG30, a VAP-33-related protein, functions in protein transport mediated by COPI vesicles. J Cell Biol 146, 301-311.

Sreedharan, J., Blair, I.P., Tripathi, V.B., Hu, X., Vance, C., Rogelj, B., Ackerley, S., Durnall, J.C., Williams, K.L., Buratti, E., et al. (2008). TDP-43 Mutations in Familial and Sporadic Amyotrophic Lateral Sclerosis. Science 319, 1688-1672.

Staal, J., Abramoff, M.D., Niemeijer, M., Viergever, M.A., and van Ginneken, B. (2004). Ridge-based vessel segmentation in color images of the retina. IEEE Trans Med Imaging 23, 501-509.

Stallings, N.R., Puttaparthi, K., Luther, C.M., Burns, D.K., and Elliott, J.L. (2010). Progressive motor weakness in transgenic mice expressing human TDP-43. Neurobiol Dis 40, 404-414.

Standen, C.L., Perkinton, M.S., Byers, H.L., Kesavapany, S., Lau, K.F., Ward, M., McLoughlin, D., and Miller, C.C. (2003). The neuronal adaptor protein Fe65 is phosphorylated by mitogen-activated protein kinase (ERK1/2). Mol Cell Neurosci 24, 851-857.

Stenzinger, A., Kajosch, T., Tag, C., Porsche, A., Welte, I., Hofer, H.W., Steger, K., and Wimmer, M. (2005). The novel protein PTPIP51 exhibits tissue- and cell-specific expression. Histochem Cell Biol 123, 19-28.

Stevenson, A., Yates, D.M., Manser, C., De Vos, K.J., Vagnoni, A., Leigh, P.N., McLoughlin, D.M., and Miller, C.C. (2009). Riluzole protects against glutamate-induced slowing of neurofilament axonal transport. Neurosci Lett 454, 161-164.

Stewart, H., Rutherford, N.J., Briemberg, H., Krieger, C., Cashman, N., Fabros, M., Baker, M., Fok, A., DeJesus-Hernandez, M., Eisen, A., et al. (2012). Clinical and pathological features of amyotrophic lateral sclerosis caused by mutation in the C9ORF72 gene on chromosome 9p. Acta Neuropathol 123, 409-417.

Sun, Q., Bahri, S., Schmid, A., Chia, W., and Zinn, K. (2000). Receptor tyrosine phosphatases regulate axon guidance across the midline of the Drosophila embryo. Development 127, 801-812.

Suzuki, H., Kanekura, K., Levine, T.P., Kohno, K., Olkkonen, V.M., Aiso, S., and Matsuoka, M. (2009). ALS-linked P56S-VAPB, an aggregated loss-of-function mutant of VAPB, predisposes motor neurons to ER stress-related death by inducing aggregation of co-expressed wild-type VAPB. J Neurochem 108, 973-985.

Suzuki, H., Lee, K., and Matsuoka, M. (2011). TDP-43-induced death is associated with altered regulation of BIM and Bcl-xL and attenuated by caspase-mediated TDP-43 cleavage. J Biol Chem 286, 13171-13183.

Suzuki, H., and Matsuoka, M. (2012). TDP-43 toxicity is mediated by the unfolded protein response-unrelated induction of C/EBP homologous protein expression. J Neurosci Res 90, 641-647.

Suzuki, H., and Matsuoka, M. (2013). The JNK/c-Jun signaling axis contributes to the TDP-43-induced cell death. Mol Cell Biochem 372, 241-248.

Suzuki, M., Mikami, H., Watanabe, T., Yamano, T., Yamazaki, T., Nomura, M., Yasui, K., Ishikawa, H., and Ono, S. (2010). Increased expression of TDP-43 in the skin of amyotrophic lateral sclerosis. Acta Neurol Scand 122, 367-372.

Suzuki, N., Kato, S., Kato, M., Warita, H., Mizuno, H., Shimakura, N., Akiyama, H., Kobayashi, Z., Konno, H., and Aoki, M. (2012). FUS/TLS-Immunoreactive Neuronal and Glial Cell Inclusions Increase With Disease Duration in Familial Amyotrophic Lateral Sclerosis With an R521C FUS/TLS Mutation. J Neuropathol Exp Neurol 71, 779-788.

Swarup, V., Phaneuf, D., Dupre, N., Petri, S., Strong, M., Kriz, J., and Julien, J.P. (2011). Deregulation of TDP-43 in amyotrophic lateral sclerosis triggers nuclear factor kappaB-mediated pathogenic pathways. J Exp Med 208, 2429-2447.

Szabadkai, G., Bianchi, K., Varnai, P., De Stefani, D., Wieckowski, M.R., Cavagna, D., Nagy, A.I., Balla, T., and Rizzuto, R. (2006). Chaperone-mediated coupling of endoplasmic reticulum and mitochondrial Ca2+ channels. J Cell Biol 175, 901-911.

Szabadkai, G., Simoni, A.M., Chami, M., Wieckowski, M.R., Youle, R.J., and Rizzuto, R. (2004). Drp-1-dependent division of the mitochondrial network blocks intraorganellar Ca2+ waves and protects against Ca2+-mediated apoptosis. Mol Cell 16, 59-68.

Takeuchi, H., Kobayashi, Y., Ishigaki, S., Doyu, M., and Sobue, G. (2002). Mitochondrial localization of mutant SOD1 triggers caspase-dependent cell death in a cellular model of familial amyotrophic lateral sclerosis. J Biol Chem 277, 50966-50972.

Tang, T.S., Tu, H., Chan, E.Y., Maximov, A., Wang, Z., Wellington, C.L., Hayden, M.R., and Bezprozvanny, I. (2003). Huntingtin and huntingtin-associated protein 1 influence neuronal calcium signaling mediated by inositol-(1,4,5) triphosphate receptor type 1. Neuron 39, 227-239.

Tateishi, T., Hokonohara, T., Yamasaki, R., Miura, S., Kikuchi, H., Iwaki, A., Tashiro, H., Furuya, H., Nagara, Y., Ohyagi, Y., et al. (2010). Multiple system degeneration with basophilic inclusions in Japanese ALS patients with FUS mutation. Acta Neuropathol 119, 355-364.

Teuling, E., Ahmed, S., Haasdijk, E., Demmers, J., Steinmetz, M.O., Akhmanova, A., Jaarsma, D., and Hoogenraad, C.C. (2007). Motor neuron disease-associated mutant vesicle-associated membrane protein-associated protein (VAP) B recruits wild-type VAPs into endoplasmic reticulum-derived tubular aggregates. J Neurosci 27, 9801-9815.

Teuling, E., van Dis, V., Wulf, P.S., Haasdijk, E.D., Akhmanova, A., Hoogenraad, C.C., and Jaarsma, D. (2008). A novel mouse model with impaired dynein/dynactin function develops amyotrophic lateral sclerosis (ALS)-like features in motor neurons and improves lifespan in SOD1-ALS mice. Hum Mol Genet 17, 2849-2862.

Thomas, M.G., Loschi, M., Desbats, M.A., and Boccaccio, G.L. (2011). RNA granules: the good, the bad and the ugly. Cell Signal 23, 324-334.

Tobisawa, S., Hozumi, Y., Arawaka, S., Koyama, S., Wada, M., Nagai, M., Aoki, M., Itoyama, Y., Goto, K., and Kato, T. (2003). Mutant SOD1 linked to familial amyotrophic lateral sclerosis, but not wild-type SOD1, induces ER stress in COS7 cells and transgenic mice. Biochem Biophys Res Commun 303, 496-503.

Todd, P.K., and Paulson, H.L. (2010). RNA-mediated neurodegeneration in repeat expansion disorders. Ann Neurol 67, 291-300.

Tollervey, J.R., Curk, T., Rogelj, B., Briese, M., Cereda, M., Kayikci, M., Konig, J., Hortobagyi, T., Nishimura, A.L., Zupunski, V., et al. (2011). Characterizing the RNA targets and position-dependent splicing regulation by TDP-43. Nat Neurosci 14, 452-458.

Tomkins, J., Usher, P., Slade, J.Y., Ince, P.G., Curtis, A., Bushby, K., and Shaw, P.J. (1998). Novel insertion in the KSP region of the neurofilament heavy gene in amyotrophic lateral sclerosis (ALS). Neuroreport 9, 3967-3970.

Tong, J., Huang, C., Bi, F., Wu, Q., Huang, B., and Zhou, H. (2012). XBP1 depletion precedes ubiquitin aggregation and Golgi fragmentation in TDP-43 transgenic rats. J Neurochem 123, 406-416.

Tran, D., Chalhoub, A., Schooley, A., Zhang, W., and Ngsee, J.K. (2012). A mutation in VAPB that causes amyotrophic lateral sclerosis also causes a nuclear envelope defect. J Cell Sci 125, 2831-2836.

Traynelis, S.F., Wollmuth, L.P., McBain, C.J., Menniti, F.S., Vance, K.M., Ogden, K.K., Hansen, K.B., Yuan, H., Myers, S.J., and Dingledine, R. (2010). Glutamate receptor ion channels: structure, regulation, and function. Pharmacological reviews 62, 405-496.

Tsai, K.J., Yang, C.H., Fang, Y.H., Cho, K.H., Chien, W.L., Wang, W.T., Wu, T.W., Lin, C.P., Fu, W.M., and Shen, C.K. (2010). Elevated expression of TDP-43 in the forebrain of mice is sufficient to cause neurological and pathological phenotypes mimicking FTLD-U. J Exp Med 207, 1661-1673.

Tsuda, H., Han, S.M., Yang, Y., Tong, C., Lin, Y.Q., Mohan, K., Haueter, C., Zoghbi, A., Harati, Y., Kwan, J., et al. (2008). The amyotrophic lateral sclerosis 8 protein VAPB is cleaved, secreted, and acts as a ligand for Eph receptors. Cell 133, 963-977.

Tsukagoshi, H., Yanagisawa, N., Oguchi, K., Nagashima, K., and Murakami, T. (1979). Morphometric quantification of the cervical limb motor cells in controls and in amyotrophic lateral sclerosis. J Neurol Sci 41, 287-297.

Tudor, E.L., Galtrey, C.M., Perkinton, M.S., Lau, K.F., De Vos, K.J., Mitchell, J.C., Ackerley, S., Hortobagyi, T., Vamos, E., Leigh, P.N., et al. (2010). Amyotrophic lateral sclerosis mutant vesicle-associated membrane protein-associated protein-B transgenic mice develop TAR-DNA-binding protein-43 pathology. Neuroscience 167, 774-785.

Turner, B.J., and Talbot, K. (2008). Transgenics, toxicity and therapeutics in rodent models of mutant SOD1-mediated familial ALS. Prog Neurobiol 85, 94-134.

Urushitani, M., Sik, A., Sakurai, T., Nukina, N., Takahashi, R., and Julien, J.P. (2006). Chromogranin-mediated secretion of mutant superoxide dismutase proteins linked to amyotrophic lateral sclerosis. Nat Neurosci 9, 108-118.

Valdmanis, P.N., Dupre, N., Bouchard, J.P., Camu, W., Salachas, F., Meininger, V., Strong, M., and Rouleau, G.A. (2007). Three families with amyotrophic lateral sclerosis and frontotemporal dementia with evidence of linkage to chromosome 9p. Arch Neurol 64, 240-245.

Van Damme, P., Van Den Bosch, L., Van Houtte, E., Callewaert, G., and Robberecht, W. (2002). GluR2-dependent properties of AMPA receptors determine the selective vulnerability of motor neurons to excitotoxicity. J Neurophysiol 88, 1279-1287.

van de Leemput, J., Chandran, J., Knight, M.A., Holtzclaw, L.A., Scholz, S., Cookson, M.R., Houlden, H., Gwinn-Hardy, K., Fung, H.C., Lin, X., et al. (2007). Deletion at ITPR1 underlies ataxia in mice and spinocerebellar ataxia 15 in humans. PLoS Genet 3, e108.

Van Den Bosch, L., Vandenberghe, W., Klaassen, H., Van Houtte, E., and Robberecht, W. (2000). Ca(2+)-permeable AMPA receptors and selective vulnerability of motor neurons. J Neurol Sci 180, 29-34.

Vance, C., Al-Chalabi, A., Ruddy, D., Smith, B.N., Hu, X., Sreedharan, J., Siddique, T., Schelhaas, H.J., Kusters, B., Troost, D., et al. (2006). Familial amyotrophic lateral sclerosis with frontotemporal dementia is linked to a locus on chromosome 9p13.2-21.3. Brain 129, 868-876.

Vance, C., Rogelj, B., Hortobagyi, T., De Vos, K.J., Nishimura, A.L., Sreedharan, J., Hu, X., Smith, B., Ruddy, D., Wright, P., et al. (2009). Mutations in FUS, an RNA Processing Protein, Cause Familial Amyotrophic Lateral Sclerosis Type 6. Science 323, 1208-1211.

Vande Velde, C., McDonald, K.K., Boukhedimi, Y., McAlonis-Downes, M., Lobsiger, C.S., Bel Hadj, S., Zandona, A., Julien, J.P., Shah, S.B., and Cleveland, D.W. (2011). Misfolded SOD1 associated with motor neuron mitochondria alters mitochondrial shape and distribution prior to clinical onset. PLoS ONE 6, e22031.

Vande Velde, C., Miller, T.M., Cashman, N.R., and Cleveland, D.W. (2008). Selective association of misfolded ALS-linked mutant SOD1 with the cytoplasmic face of mitochondria. Proc Natl Acad Sci USA 105, 4022-4027.

Verfaillie, T., Rubio, N., Garg, A.D., Bultynck, G., Rizzuto, R., Decuypere, J.P., Piette, J., Linehan, C., Gupta, S., Samali, A., et al. (2012). PERK is required at the ER-mitochondrial contact sites to convey apoptosis after ROS-based ER stress. Cell Death Differ 19, 1880-1891.

Vijayvergiya, C., Beal, M.F., Buck, J., and Manfredi, G. (2005). Mutant superoxide dismutase 1 forms aggregates in the brain mitochondrial matrix of amyotrophic lateral sclerosis mice. J Neurosci 25, 2463-2470.

Volkening, K., Leystra-Lantz, C., Yang, W., Jaffee, H., and Strong, M.J. (2009). Tar DNA binding protein of 43 kDa (TDP-43), 14-3-3 proteins and copper/zinc superoxide

dismutase (SOD1) interact to modulate NFL mRNA stability. Implications for altered RNA processing in amyotrophic lateral sclerosis (ALS). Brain Res 1305, 168-182.

von Lewinski, F., and Keller, B.U. (2005). Ca2+, mitochondria and selective motoneuron vulnerability: implications for ALS. Trends Neurosci 28, 494-500.

Wang, H.U., and Anderson, D.J. (1997). Eph family transmembrane ligands can mediate repulsive guidance of trunk neural crest migration and motor axon outgrowth. Neuron 18, 383-396.

Wang, H.Y., Wang, I.F., Bose, J., and Shen, C.K. (2004). Structural diversity and functional implications of the eukaryotic TDP gene family. Genomics 83, 130-139.

Wang, X., and Schwarz, T.L. (2009). The mechanism of Ca2+ -dependent regulation of kinesin-mediated mitochondrial motility. Cell 136, 163-174.

Weber, C., Schreiber, T.B., and Daub, H. (2012). Dual phosphoproteomics and chemical proteomics analysis of erlotinib and gefitinib interference in acute myeloid leukemia cells. J Proteomics 75, 1343-1356.

Wegorzewska, I., Bell, S., Cairns, N.J., Miller, T.M., and Baloh, R.H. (2009). TDP-43 mutant transgenic mice develop features of ALS and frontotemporal lobar degeneration. Proc Natl Acad Sci USA 106, 18809-18814.

Wengenack, T.M., Holasek, S.S., Montano, C.M., Gregor, D., Curran, G.L., and Poduslo, J.F. (2004). Activation of programmed cell death markers in ventral horn motor neurons during early presymptomatic stages of amyotrophic lateral sclerosis in a transgenic mouse model. Brain Res 1027, 73-86.

White, C., Li, C., Yang, J., Petrenko, N.B., Madesh, M., Thompson, C.B., and Foskett, J.K. (2005). The endoplasmic reticulum gateway to apoptosis by Bcl-X(L) modulation of the InsP3R. Nat Cell Biol 7, 1021-1028.

Whitehead, T.P., Kricka, L.J., Carter, T.J., and Thorpe, G.H. (1979). Analytical luminescence: its potential in the clinical laboratory. Clin Chem 25, 1531-1546.

Wiedemann, F.R., Manfredi, G., Mawrin, C., Beal, M.F., and Schon, E.A. (2002). Mitochondrial DNA and respiratory chain function in spinal cords of ALS patients. J Neurochem 80, 616-625.

Wightman, G., Anderson, V.E., Martin, J., Swash, M., Anderton, B.H., Neary, D., Mann, D., Luthert, P., and Leigh, P.N. (1992). Hippocampal and neocortical ubiquitin-immunoreactive inclusions in amyotrophic lateral sclerosis with dementia. Neurosci Lett 139, 269-274.

Williamson, T.L., and Cleveland, D.W. (1999). Slowing of axonal transport is a very early event in the toxicity of ALS-linked SOD1 mutants to motor neurons. Nature Neurosci 2, 50-56.

Wils, H., Kleinberger, G., Janssens, J., Pereson, S., Joris, G., Cuijt, I., Smits, V., Ceuterick-de Groote, C., Van Broeckhoven, C., and Kumar-Singh, S. (2010). TDP-43

transgenic mice develop spastic paralysis and neuronal inclusions characteristic of ALS and frontotemporal lobar degeneration. Proc Natl Acad Sci USA 107, 3858-3863.

Wolfson, C., Kilborn, S., Oskoui, M., and Genge, A. (2009). Incidence and prevalence of amyotrophic lateral sclerosis in Canada: a systematic review of the literature. Neuroepidemiology 33, 79-88.

Wong, E., and Cuervo, A.M. (2010). Integration of clearance mechanisms: the proteasome and autophagy. Cold Spring Harb Perspect Biol 2, a006734.

Wong, M., and Martin, L.J. (2010). Skeletal muscle-restricted expression of human SOD1 causes motor neuron degeneration in transgenic mice. Hum Mol Genet 19, 2284-2302.

Wong, P.C., Pardo, C., Borchelt, D.R., Lee, M.K., Copeland, N.G., Jenkins, N.A., Sisodia, S.S., Cleveland, D.W., and Price, D.L. (1995). An adverse property of a familial ALS-linked SOD1 mutation causes motor neuron disease characterised by vacuolar degeneration of mitochondria. Neuron 14, 1105-1116.

Wootz, H., Hansson, I., Korhonen, L., Napankangas, U., and Lindholm, D. (2004). Caspase-12 cleavage and increased oxidative stress during motoneuron degeneration in transgenic mouse model of ALS. Biochem Biophys Res Commun 322, 281-286.

Wu, D.C., Re, D.B., Nagai, M., Ischiropoulos, H., and Przedborski, S. (2006). The inflammatory NADPH oxidase enzyme modulates motor neuron degeneration in amyotrophic lateral sclerosis mice. Proc Natl Acad Sci USA 103, 12132-12137.

Wu, F., Wang, P., Zhang, J., Young, L.C., Lai, R., and Li, L. (2010). Studies of phosphoproteomic changes induced by nucleophosmin-anaplastic lymphoma kinase (ALK) highlight deregulation of tumor necrosis factor (TNF)/Fas/TNF-related apoptosis-induced ligand signaling pathway in ALK-positive anaplastic large cell lymphoma. Mol Cell Proteomics 9, 1616-1632.

Wu, L.S., Cheng, W.C., and Shen, C.K. (2012). Targeted depletion of TDP-43 expression in the spinal cord motor neurons leads to the development of amyotrophic lateral sclerosis-like phenotypes in mice. J Biol Chem 287, 27335-27344.

Xu, S., Peng, G., Wang, Y., Fang, S., and Karbowski, M. (2011a). The AAA-ATPase p97 is essential for outer mitochondrial membrane protein turnover. Mol Biol Cell 22, 291-300.

Xu, Y.F., Gendron, T.F., Zhang, Y.J., Lin, W.L., D'Alton, S., Sheng, H., Casey, M.C., Tong, J., Knight, J., Yu, X., et al. (2010). Wild-type human TDP-43 expression causes TDP-43 phosphorylation, mitochondrial aggregation, motor deficits, and early mortality in transgenic mice. J Neurosci 30, 10851-10859.

Xu, Y.F., Zhang, Y.J., Lin, W.L., Cao, X., Stetler, C., Dickson, D.W., Lewis, J., and Petrucelli, L. (2011b). Expression of mutant TDP-43 induces neuronal dysfunction in transgenic mice. Mol Neurodegener 6, 73.

Yamanaka, K., Chun, S.J., Boillee, S., Fujimori-Tonou, N., Yamashita, H., Gutmann, D.H., Takahashi, R., Misawa, H., and Cleveland, D.W. (2008). Astrocytes as

determinants of disease progression in inherited amyotrophic lateral sclerosis. Nat Neurosci 11, 251-253.

Ye, Y., Shibata, Y., Kikkert, M., van Voorden, S., Wiertz, E., and Rapoport, T.A. (2005). Recruitment of the p97 ATPase and ubiquitin ligases to the site of retrotranslocation at the endoplasmic reticulum membrane. Proc Natl Acad Sci USA 102, 14132-14138.

Yoshida, M. (2006). Cellular tau pathology and immunohistochemical study of tau isoforms in sporadic tauopathies. Neuropathology 26, 457-470.

Youle, R.J., and van der Bliek, A.M. (2012). Mitochondrial fission, fusion, and stress. Science 337, 1062-1065.

Yu, C., Han, W., Shi, T., Lv, B., He, Q., Zhang, Y., Li, T., Song, Q., Wang, L., and Ma, D. (2008). PTPIP51, a novel 14-3-3 binding protein, regulates cell morphology and motility via Raf-ERK pathway. Cell Signal 20, 2208-2220.

Zakaryan, R.P., and Gehring, H. (2006). Identification and characterization of the nuclear localization/retention signal in the EWS proto-oncoprotein. J Mol Biol 363, 27-38.

Zampese, E., Fasolato, C., Kipanyula, M.J., Bortolozzi, M., Pozzan, T., and Pizzo, P. (2011). Presenilin 2 modulates endoplasmic reticulum (ER)-mitochondria interactions and Ca2+ cross-talk. Proc Natl Acad Sci USA 108, 2777-2782.

Zhang, B., Tu, P., Abtahian, F., Trojanowski, J.Q., and Lee, V.M. (1997). Neurofilaments and orthograde transport are reduced in ventral root axons of transgenic mice that express human SOD1 with a G93A mutation. J Cell Biol 139, 1307-1315.

Zhang, K., and Kaufman, R.J. (2008). From endoplasmic-reticulum stress to the inflammatory response. Nature 454, 455-462.

Zhao, W., Beers, D.R., Henkel, J.S., Zhang, W., Urushitani, M., Julien, J.P., and Appel, S.H. (2010). Extracellular mutant SOD1 induces microglial-mediated motoneuron injury. Glia 58, 231-243.

Zhou, H., Huang, C., Chen, H., Wang, D., Landel, C.P., Xia, P.Y., Bowser, R., Liu, Y.J., and Xia, X.G. (2010). Transgenic rat model of neurodegeneration caused by mutation in the TDP gene. PLoS Genet 6, e1000887.

Zhu, Y.B., and Sheng, Z.H. (2011). Increased axonal mitochondrial mobility does not slow amyotrophic lateral sclerosis (ALS)-like disease in mutant SOD1 mice. J Biol Chem 286, 23432-23440.

Zimmerman, M.C., Oberley, L.W., and Flanagan, S.W. (2007). Mutant SOD1-induced neuronal toxicity is mediated by increased mitochondrial superoxide levels. J Neurochem 102, 609-618.

Zinszner, H., Sok, J., Immanuel, D., Yin, Y., and Ron, D. (1997). TLS (FUS) binds RNA in vivo and engages in nucleo-cytoplasmic shuttling. J Cell Sci 110 (Pt 15), 1741-1750.